Physics of laser-driven plasma-based electron accelerators

E. Esarey, C. B. Schroeder, and W. P. Leemans

Lawrence Berkeley National Laboratory, Berkeley, California 94720, USA

(Dated: September 21, 2007)

The physics of plasma-based accelerators driven by short-pulse lasers in underdense plasma is reviewed. This includes the laser wakefield accelerator, the plasma beat wave accelerator, the self-modulated laser wakefield accelerator, plasma waves driven by multiple laser pulses, and highly-nonlinear regimes. The properties of linear and nonlinear plasma waves are discussed, as well as electron acceleration in plasma waves. Methods for injecting and trapping plasma electrons in plasma waves are also discussed. Limits to the electron energy gain are summarized, including laser pulse diffraction, electron dephasing, laser pulse energy depletion, and beam loading limitations. The basic physics of laser pulse evolution in underdense plasmas is also reviewed. This includes the propagation, self-focusing, and guiding of laser pulses in uniform plasmas and plasmas with preformed density channels. Instabilities relevant to intense short-pulse laser-plasma interactions, such as Raman, self-modulation, and hose instabilities, are discussed. Recent experimental results are summarized.

CONTENTS

I. INTRODUCTION

Laser-driven plasma-based accelerators were originally proposed by Tajima and Dawson (1979). John Dawson, who passed away in 2001, was responsible for many of the key developments in this field, including the plasma beat wave accelerator, the laser wakefield accelerator, and the photon accelerator (Joshi *et al.*, 1984; Tajima and Dawson, 1979; Wilks *et al.*, 1989). In addition, he was one of the early pioneers of particle-in-cell simulation of plasmas (Birdsall *et al.*, 1991; Dawson, 1983; Mori *et al.*, 1988), which is now a widely-used tool in the study of plasma-based accelerators. During his lifetime, the field of plasma-based accelerators has grown into a world-wide research effort with ongoing experimental programs in France, Germany, Korea, Japan, Taiwan, the UK, and the United States, to name a few [see, e.g., the proceedings of the Advanced Accelerator Concepts Workshop (Conde and Eyberger, 2006)]. Much of this growth is due to the rapid development of chirp-pulse amplification (CPA) laser technology, pioneered by G. Mourou and his colleagues (Maine *et al.*, 1988; Mourou and Umstadter, 1992; Perry and Mourou, 1994; Strickland and Mourou, 1985), making readily available compact sources of intense, high power, ultrashort laser pulses.

Laser-plasma accelerator experiments have demonstrated acceleration gradients > 100 GV/m, accelerated electron energies > 100 MeV, and accelerated charge > 1 nC (Gahn *et al.*, 1999; Leemans *et al.*, 2002; Malka *et al.*, 2002; Modena *et al.*, 1995; Nakajima *et al.*, 1995; Ting *et al.*, 1997; Umstadter *et al.*, 1996a). Prior to 2004, however, the quality of the accelerated electron bunch was less than desired. Typically, the accelerated bunch was characterized by an exponential energy distribution, with most of the electrons at low energy (< 10 MeV) and

a long, exponentially small tail extending out to high energy (> 100 MeV). This dramatically changed in 2004, when three groups reported (Faure *et al.*, 2004; Geddes *et al.*, 2004; Mangles *et al.*, 2004) the production of high quality electron bunches characterized by a significant charge ($\gtrsim 100$ pC) at high mean energy (~ 100 MeV) with a small energy spread ($\sim$ few percent) and a low divergence ($\sim$ few degrees). The normalized transverse emittance has also been measured and shown to be a few μm-rad at 55 MeV (Fritzler *et al.*, 2004). These high quality electron beams were a result of a higher degree of control of the laser and plasma parameters, an improvement of diagnostic techniques, an extension of the laser propagation distance through the plasma, and a greater understanding of the underlying physics, in particular, the importance of matching the acceleration length to the dephasing length. Recently, using a plasma-channel-guided laser, high-quality electron beams up to 1 GeV have been experimentally demonstrated (Leemans *et al.*, 2006). High quality, GeV-class, electron bunches will enable a variety of applications of laser-plasma accelerators, such as front end injectors for conventional accelerators or drivers for compact, short-pulse radiation sources.

This review provides an overview of the physics and issues relevant to laser-driven plasma-based accelerators, including the plasma beat wave accelerator (PBWA) (Amiranoff *et al.*, 1995; Clayton *et al.*, 1994; Ebrahim, 1994; Joshi *et al.*, 1984; Kitagawa *et al.*, 1992; Tajima and Dawson, 1979), the laser wakefield accelerator (LWFA) (Amiranoff *et al.*, 1998; Dewa *et al.*, 1998; Gorbunov and Kirsanov, 1987; Sprangle *et al.*, 1988; Tajima and Dawson, 1979), the self-modulated LWFA (Andreev *et al.*, 1992; Antonsen, Jr. and Mora, 1992; Coverdale *et al.*, 1995; Gordon *et al.*, 1998; Joshi *et al.*, 1981; Leemans *et al.*, 2001; Malka *et al.*, 2001; Modena *et al.*, 1995; Moore *et al.*, 1997; Sprangle *et al.*, 1992; Wagner *et al.*, 1997), LWFAs driven by multiple laser pulses (Berezhiani and Murusidze, 1992; Bonnaud *et al.*, 1994; Dalla and Lontano, 1994; Nakajima, 1992; Umstadter *et al.*, 1994), as well as other highly-nonlinear LWFA regimes (Faure *et al.*, 2004; Geddes *et al.*, 2004; Malka *et al.*, 2002; Mangles *et al.*, 2004; Pukhov and Meyer-ter-Vehn, 2002; Tsung *et al.*, 2004). These configurations are shown schematically in Fig. 1. The remainder of the introduction discusses the basic principles and limitations of laser-driven acceleration in vacuum and gases. Section II discusses the basic models used to describe plasma wave generation. Included is a discussion of nonlinear plasma waves, wavebreaking, and plasma wave phase velocity, as well as the trapping and acceleration of electrons by the plasma wave. Section III describes the various laser-driven plasma-based acceleration configurations, specifically, the LWFA, the PBWA, the self-modulated LWFA, wakefields driven by multiple pulses, and the regime of electron cavitation. Included is a brief discussion of diffraction, dephasing, and pump depletion, which can limit the single-stage energy gain. The injection of ultrashort electron bunches into plasma waves using laser triggered injection or density gradients is discussed in Sec. IV. Methods for optically guiding laser pulses in plasmas are discussed in Sec. V, including relativistic self-focusing, preformed density channels, ponderomotive self-channel, and plasma wave effects. Section VI describes a few of the more relevant laser-plasma instabilities, including backward and forward Raman scattering, self-modulation, and laser-hosing. Throughout this report recent experimental results are mentioned. A summary is presented in Sec. VIII, as well as a discussion of future prospects for laser-driven plasma-based accelerators.

A. Acceleration in plasma

Plasma-based accelerators are of great interest because of their ability to sustain extremely large acceleration gradients. The accelerating gradients in conventional radio-frequency linear accelerators (linacs) are currently limited to approximately 100 MV/m, partly due to breakdown that occurs on the walls of the structure. Ionized plasmas, however, can sustain electron plasma waves with electric fields in excess of $E_0 = cm_e\omega_p/e$, or

$$E_0(\mathrm{V/m}) \simeq 96\sqrt{n_0(\mathrm{cm^{-3}})}, \tag{1}$$

where $\omega_p = (4\pi n_0 e^2/m_e)^{1/2}$ is the electron plasma frequency, n_0 is the ambient electron number density, m_e and e are the electron rest mass and charge, respectively, and c is the speed of light in vacuum. Equation (1) is referred to as the cold nonrelativistic wavebreaking field (Dawson, 1959). For example, a plasma density of $n_0 = 10^{18}\,\mathrm{cm^{-3}}$ yields $E_0 \simeq 100\,\mathrm{GV/m}$, which is approximately three orders of magnitude greater than that obtained in conventional linacs. Accelerating gradients on the order of 100 GV/m have been inferred in plasma-based accelerator experiments (Gordon *et al.*, 1998; Malka *et al.*, 2002).

In addition to extremely large accelerating gradients, plasma-based accelerators have the potential to produce extremely short electron bunches. The length of the accelerating wave in a plasma-based accelerator is approximately the plasma wavelength $\lambda_p = 2\pi c/\omega_p = 2\pi/k_p$, or

$$\lambda_p(\mu\mathrm{m}) \simeq 3.3\times 10^{10}/\sqrt{n_0(\mathrm{cm^{-3}})}, \tag{2}$$

e.g., $\lambda_p \simeq 30\,\mu$m for $n_0 = 10^{18}\,\mathrm{cm^{-3}}$. A high-quality electron bunch produced by a plasma-based accelerator would have a bunch duration $\tau_b < \lambda_p/c$, i.e., a duration $\tau_b < 100$ fs for $n_0 = 10^{18}\,\mathrm{cm^{-3}}$ (Banerjee *et al.*, 2005; Leemans *et al.*, 2003; van Tilborg *et al.*, 2006). Laser-driven, plasma-based accelerators, which are typically driven by femtosecond laser pulses, are intrinsically sources of femtosecond electron bunches.

An important parameter in the discussion of intense laser-plasma interactions is the laser strength parameter a_0, defined as the peak amplitude of the normalized vector potential of the laser field, $\boldsymbol{a} = e\boldsymbol{A}/m_e c^2$. The laser

strength parameter is related to the peak laser intensity I_0 and power $P = \pi r_0^2 I_0/2$ by $I_0 = (\pi c/2)(m_e c^2 a_0/e\lambda)^2$, which yields

$$a_0^2 \simeq 7.3 \times 10^{-19} [\lambda(\mu\mathrm{m})]^2 I_0(\mathrm{W/cm^2}), \tag{3}$$

and $P(\mathrm{GW}) \simeq 21.5(a_0 r_0/\lambda)^2$, where a linearly polarized laser field with a Gaussian radial profile is assumed, e.g., $\boldsymbol{a} = a_0 \exp(-r^2/r_0^2)\cos(kz - \omega t)\boldsymbol{e}_x$ with r_0 the laser spot size at focus, $\lambda = 2\pi/k$ the laser wavelength, and $\omega = ck$ the laser frequency in vacuum. Furthermore, the peak laser electric field amplitude is given by $E_L = m_e c\omega a_0/e$, i.e., $E_L(\mathrm{TV/m}) \simeq 3.21 a_0/\lambda(\mu\mathrm{m})$. Physically, $\boldsymbol{a} = \boldsymbol{p}_\perp/m_e c$ is the normalized transverse "quiver" momentum of a plasma electron in the laser field, as indicated by conservation of transverse canonical momentum in the broad laser pulse [or one-dimensional (1D)] limit ($r_0 \gg \lambda$). When $a_0 \gtrsim 1$, the electron quiver motion is highly relativistic and the laser-plasma interaction is nonlinear. Highly relativistic electron motion ($a_0 \gtrsim 1$) requires laser intensities $I \gtrsim 10^{18}\,\mathrm{W/cm^2}$ for wavelengths of $\lambda \simeq 1\,\mu$m. Such intensities are routinely produced by compact, solid-state laser systems based on the technique of CPA.

B. Acceleration in vacuum and gases

The laser acceleration of electrons in vacuum and gases is intrinsically limited by diffraction, electron slippage, ionization, and the smallness of the laser wavelength (Esarey *et al.*, 1995; Sprangle *et al.*, 1996a). In vacuum, the motion of an electron in a laser field is determined by the Lorentz force equation

$$d\tilde{\boldsymbol{p}}/dct = \partial \boldsymbol{a}/\partial ct - (\tilde{\boldsymbol{p}}/\tilde{\gamma}) \times (\nabla \times \boldsymbol{a}), \tag{4}$$

where $\tilde{\boldsymbol{p}}$ is the electron momentum normalized to $m_e c$ and $\tilde{\gamma} = (1 + \tilde{p}^2)^{1/2}$ is the relativistic Lorentz factor. Roughly speaking, the first term on the right-hand side of the above equation describes the linear response of the electron to the electric field $\boldsymbol{E}$ of the laser and is responsible for "direct" laser acceleration; whereas the second term describes the nonlinear response to the $\boldsymbol{v} \times \boldsymbol{B}$ force and is responsible for "ponderomotive" laser acceleration. Typically, the axial (in the z-direction of laser propagation) ponderomotive force is written as $F_{pz} \simeq -(m_e c^2/\tilde{\gamma})(\partial/\partial z)a^2/2$, assuming $\tilde{\boldsymbol{p}}_\perp = \boldsymbol{a}_\perp$, which is exact in 1D (i.e., $r_0 \gg \lambda$).

When a laser field propagating along the z-axis is focused in vacuum, the laser spot size and intensity evolve via $r_s = r_0(1 + z^2/Z_R^2)^{1/2}$ and $I = I_0(r_0^2/r_s^2)\exp(-2r^2/r_s^2)$, respectively, where $Z_R = kr_0^2/2$ is the Rayleigh length, and a fundamental Gaussian mode is assumed. The finite laser spot size implies the existence of an axial component of the electric field of the laser via $\nabla \cdot \boldsymbol{E} = 0$, i.e., $E_z \sim (1/kr_0)E_\perp$. The amplitude of this axial field can be very large, which suggests using the axial field directly for laser acceleration, with an energy gain for a relativistic ($\tilde{\gamma} \gg 1$) electron propagating along the axis scaling as $\int dz(v_z E_z)$. The phase velocity, however, of the optical field along the axis is greater than c and is approximately $v_p/c \simeq 1 + 1/(kZ_R)$ near the focus. Since $v_p > c$, electrons with $v_z \lesssim c$ will phase slip with respect to the accelerating field and decelerate. This will occur over a dephasing length L_d, which for highly relativistic electrons is $\sim Z_R$, i.e., the dephasing length is on order of the diffraction length.

This phase slippage argument forms the basis for the so-called Lawson-Woodward (LW) theorem (Lawson, 1979; Palmer, 1980; Woodward, 1947), which states that under certain restrictive conditions no net electron energy gain is possible using laser fields. The LW theorem assumes (i) the region of interaction is infinite, (ii) the laser fields are in vacuum with no walls or boundaries present, (iii) the electron is highly relativistic ($v_z \simeq c$) along the acceleration path, (iv) no static electric or magnetic fields are present, and (v) nonlinear effects (e.g., ponderomotive and radiation reaction forces) are neglected.

One or more of the assumptions of LW theorem must be violated in order to achieve a nonzero net energy gain. For example, one can introduce optics to limit the laser-electron interaction to approximately a region of length $2Z_R$ about the focus, such that minimal phase slippage occurs (Esarey *et al.*, 1995; Huang and Byer, 1996; Plettner *et al.*, 2005). The maximum energy gain due to direct acceleration by the E_z field is then given by $\Delta W(\mathrm{MeV}) \simeq 31\sqrt{P(\mathrm{TW})}$, where a first-order Laguerre-Gaussian mode has been assumed (Esarey *et al.*, 1995). Although substantial energy gains are possible with high laser power, this is problematic in practice, since this method requires that optics be placed near the focus and are susceptible to laser damage at high intensity. Furthermore, the electron beam must pass through a small aperture in the optics, which can limit the amount of charge that can be accelerated (Sprangle *et al.*, 1996a).

Alternatively, finite energy gains can be achieved by introducing a background of gas into the interaction region, as in the inverse Cherenkov accelerator (Kimura *et al.*, 1995). The gas can reduce the phase velocity of the laser field to less than c, reducing the slippage. Furthermore, in principle, diffraction can be overcome by relying on optical guiding (self-focusing) in the gas (Sprangle *et al.*, 1996b). Nevertheless, ionization of the gas, which occurs at a relatively low laser intensity $\sim 10^{14}$ W/cm^2 (for $\lambda \approx 1$ μm) and increases the phase velocity, remains a fundamental limitation to the accelerating field in gas-filled devices.

In addition to direct laser acceleration, finite energy gains can also result from the nonlinear or ponderomotive force. Since the ponderomotive force scales inversely with electron energy and proportional to the laser intensity, $F_p \sim (1/\tilde{\gamma})\nabla a^2$, this mechanism is most efficient at low electron energies and high laser intensities. Simulations (Quesnel and Mora, 1998; Stupakov and Zolotorev, 2001) and experiments (Malka *et al.*, 1997) have

shown that by focusing a high intensity laser pulse onto a low density gas jet (essentially, a source of electrons at rest), ponderomotive acceleration can result in the production of electrons with energies in the range of a few MeV with a large energy spread and a high degree of scattering. Simulations (Pang *et al.*, 2002) indicate that when a moderate energy electron beam intersects with a very intense laser pulse at a small angle, a signification fraction of the electrons can be accelerated to energies in excess of 100 MeV (for $a \sim 10$) through a combination of direct and ponderomotive acceleration. Other ponderomotive acceleration schemes include the vacuum beat wave accelerator (Esarey *et al.*, 1995), which relies on the ponderomotive force of the beat wave produced by two co-propagating laser pulses, and the inverse free-electron laser (Kimura *et al.*, 2001; Liu *et al.*, 1998; Musumeci *et al.*, 2005), which relies on the beat wave produced by a laser pulse propagating through a magnetic wiggler field. Again, a major limitation to these schemes is the $1/\tilde{\gamma}$ scaling of the ponderomotive force.

A fundamental limitation to all concepts that rely on electron acceleration through the direct interaction (linear or nonlinear) with the laser field is the smallness of the laser wavelength, typically on the order of a micron. For example, a first-order Laguerre-Gaussian mode has a quarter wavelength phase region for which the laser field is both accelerating and focusing. To accelerate an electron bunch while maintaining a small energy spread and emittance, it is desirable that a high quality bunch be injected into the proper phase region of the laser field with a bunch length small compared to a $\lambda/4$ (corresponding to 0.8 fs for $\lambda = 1$ μm). Conventional accelerators typically produce electron bunches with durations $\gtrsim 1$ ps. One possibility may be to pre-bunch a conventional electron bunch at the laser wavelength using an inverse free-electron laser, as has been experimentally demonstrated (Liu *et al.*, 1998), and use this as an injector into a second stage of a laser accelerator (Kimura *et al.*, 2001).

Plasma-based accelerators can overcome many of the fundamental limitations that restrict laser acceleration in vacuum and gases. For example, ionization and breakdown is not a limitation, since the plasma can be fully pre-ionized. Diffraction can be overcome through self-focusing and with preformed plasma channels. In plasma-based accelerators, acceleration is the result of the axial field of the plasma wave and not the laser field directly. The phase velocity of the plasma wave is typically equal to the group velocity of the laser pulse and is less than c. Although the plasma wave is excited by the ponderomotive force of the laser field, the $1/\tilde{\gamma}$ scaling of the ponderomotive force is not a limitation, since for the plasma electrons $\tilde{\gamma} \sim 1$. In effect, the plasma acts as a transformer, converting the transverse laser field into the axial electric field of the plasma wave. Furthermore, the accelerating wavelength is the plasma wavelength λ_p, which is typically 10–1000 times larger than the laser wavelength, and in many cases equal to the laser pulse length. The injection of ultrashort electron bunches into a single period of a plasma wave is possible using laser injection methods (see Sec. IV.C.2). Plasma-based acceleration methods are, however, subject to their own intrinsic limitations, such as restrictions arising from electron dephasing, pump depletion, and, in some cases, laser-plasma instabilities.

II. PLASMA WAVES AND ACCELERATION

Calculation of the plasma wakefields (driven electron plasma waves) generated by nonevolving drive laser beams is straightforward. Analytical solutions exist in the three-dimensional (3D) linear regime and in the 1D nonlinear regime. In the 3D nonlinear regime, the use of numerical codes is usually required. The full problem, which includes the self-consistent evolution of the drive laser beams, is sufficiently complicated to require numerical calculation. Various aspects of the propagation and transport of the drive beams will be discussed in subsequent sections. Before discussing specific laser-plasma-based accelerator configurations (e.g., PBWA, LWFA, self-modulated LWFA, etc.), the physical forces that drive wakefields (i.e., space charge and ponderomotive forces) and the mathematical models used to describe wakefield generation will be briefly discussed. In the following, it is convenient to use the normalized electrostatic $\phi = e\Phi/m_e c^2$ and vector $\boldsymbol{a} = e\boldsymbol{A}/m_e c^2$ potentials.

A. Ponderomotive force

In laser-driven plasma-based accelerators, wakefields are driven via the ponderomotive force. The ponderomotive force (Kruer, 1988) can be derived by considering the electron fluid momentum equation in the cold fluid limit,

$$d\boldsymbol{p}/dt = -e[\boldsymbol{E} + (\boldsymbol{v} \times \boldsymbol{B})/c], \tag{5}$$

where $\boldsymbol{p}$ and $\boldsymbol{v}$ are the plasma fluid element momentum and velocity, respectively, and $d/dt = \partial/\partial t + (\boldsymbol{v} \cdot \nabla)$. The electric and magnetic fields of the laser can be written as $\boldsymbol{E} = -\partial \boldsymbol{A}/\partial ct$ and $\boldsymbol{B} = \nabla \times \boldsymbol{A}$, where the vector potential of the laser is polarized predominately in the transverse direction, e.g., $\boldsymbol{A} = A_0 \cos(kz - \omega t)\boldsymbol{e}_\perp$. In the linear limit $|a| = e|A|/m_e c^2 \ll 1$, the leading order electron fluid motion is the quiver momentum $\boldsymbol{p}_q = m_e c\boldsymbol{a}$, as indicated by $\partial \boldsymbol{p}_q/\partial t = -e\boldsymbol{E}$. Letting $\boldsymbol{p} = \boldsymbol{p}_q + \delta\boldsymbol{p}$, the second order motion is given by

$$\begin{aligned} d\delta\boldsymbol{p}/dt &= -[(\boldsymbol{p}_q/m_e) \cdot \nabla]\boldsymbol{p}_q - \boldsymbol{p}_q \times (c\nabla \times \boldsymbol{a}) \\ &= -m_e c^2 \nabla(a^2/2). \end{aligned} \tag{6}$$

Hence, $\boldsymbol{F}_p = -m_e c^2 \nabla(a^2/2)$ is the 3D ponderomotive force in the linear limit ($a^2 \ll 1$). The ponderomotive force can also be viewed as the radiation pressure (i.e., the gradient of the electromagnetic energy density).

In the 1D nonlinear regime, conservation of canonical momentum implies $\boldsymbol{u}_\perp = \boldsymbol{a}_\perp$, i.e., $\boldsymbol{a}_\perp$ is the normalized quiver momentum. Hence, in 1D, the nonlinear ponderomotive force is given by $F_{pz} = -(m_e c^2/2\gamma)\partial a_\perp^2/\partial z$. In the 3D nonlinear regime, the leading order transverse motion of the electron fluid is still the quiver motion, $\boldsymbol{u}_\perp \simeq \boldsymbol{a}_\perp$, provided that the laser pulse is propagating in an underdense plasma and has a sufficiently broad spot size, $r_0 \gtrsim \lambda_p \gg \lambda$. Defining $\delta\boldsymbol{u} = \boldsymbol{u} - \boldsymbol{a}$, the fluid momentum equation can be written as (Chen and Sudan, 1993; Esarey *et al.*, 1993a; Sprangle *et al.*, 1992)

$$\partial \delta \boldsymbol{u}/\partial ct = \nabla(\phi - \gamma), \tag{7}$$

which is exact under the assumption that the quantity $\nabla \times \delta\boldsymbol{u}$ is initially (prior to the passage of the laser pulse) zero. Here, $\nabla\phi$ is the space-charge force and $\nabla\gamma$ represents the generalized nonlinear ponderomotive force, $\boldsymbol{F}_{pN} = -m_e c^2 \nabla\gamma$.

B. Linear plasma waves

In the linear ($a \ll 1$), 3D regime, wakefield generation can be examined using the cold fluid equations, i.e., the Poisson equation, the continuity equation, and the fluid momentum equation. For example, the plasma wave generated in an initially uniform plasma is described by (Esarey *et al.*, 1989; Gorbunov and Kirsanov, 1987; Sprangle *et al.*, 1988)

$$\left(\partial^2/\partial t^2 + \omega_p^2\right) \delta n/n_0 = c^2 \nabla^2 a^2/2, \tag{8}$$

$$(\partial^2/\partial t^2 + \omega_p^2)\phi = \omega_p^2 a^2/2, \tag{9}$$

where $\delta n/n_0 = (n - n_0)/n_0$ is the normalized density perturbation associated with the electrostatic wake ϕ in the limit $a^2 \ll 1$. The solutions for the density perturbation ($|\delta n/n_0| \ll 1$) and electric field of the wake are given by

$$\delta n/n_0 = (c^2/\omega_p) \int_0^t dt' \sin\omega_p(t - t') \nabla^2 a^2(\boldsymbol{r}, t')/2, \tag{10}$$

$$\boldsymbol{E}/E_0 = -c \int_0^t dt' \sin\omega_p(t - t') \nabla a^2(\boldsymbol{r}, t')/2. \tag{11}$$

Equations (10) and (11) describe plasma waves generated at the frequency ω_p and are valid for $E \ll E_0$, where $E_0 = m_e c\omega_p/e$ is the cold nonrelativistic wavebreaking field Eq. (1). Solutions to Eq. (10) indicate that wakefields will be generated most efficiently when the envelope scale length, which characterizes the axial gradient in the normalized laser intensity a^2, is on the order of the plasma wavelength $\lambda_p = 2\pi c/\omega_p$. The radial extent of the wake is on the order of the laser spot size r_s.

In addition to the axial wakefield E_z, transverse wakefields E_r and B_θ will be generated. The transverse wakefields are related to the axial wakefield by the Panofsky-Wenzel theorem (Keinings and Jones, 1987; Panofsky and Wenzel, 1956), $\partial E_z/\partial r = \partial(E_r - B_\theta)/\partial(z - ct)$. A relativistic particle with axial velocity $v_z \simeq c$ which is being accelerated by a wakefield with phase velocity $v_p \simeq c$ will experience a radial force proportional to $E_r - B_\theta$. Notice that if $E_z \sim \exp(-2r^2/r_s^2)\cos[k_p(z - ct)]$, then $E_r - B_\theta \sim (4r/k_p r_s^2)\exp(-2r^2/r_s^2)\sin[k_p(z - ct)]$ and the radial force is zero along the axis. Typically, for an electron displaced from the axis, there is a phase region of the wake of width $k_p|\Delta(z - ct)| = \pi/4$ for which a relativistic electron will experience simultaneous axial accelerating and radial focusing forces.

Equations (8)–(11) are valid to order $\sim a^2$ assuming $a \ll 1$. Applying a perturbation expansion of the fluid quantities in powers of a, higher-order corrections to the density and field may be computed (Gorbunov *et al.*, 1997). In particular a quasi-static (varying on the time scale $\sim \omega_p^{-1}$) magnetic field that scales as $\sim a^4$ is generated in an initially uniform plasma, given by (Gorbunov *et al.*, 1996, 1997)

$$\left(\partial_{ct}^2 - \nabla^2 + k_p^2\right) \boldsymbol{B}/E_0 = -k_p^{-3} \boldsymbol{\nabla} \times \left[(\boldsymbol{\nabla}\partial_{ct}\phi)\, \nabla^2\phi\right], \tag{12}$$

behind the drive laser, where ϕ is given by Eq. (9).

The linear response of plasma wave excitation in a plasma channel (transverse plasma inhomogeneity) has been investigated by Andreev *et al.* (1997). Wake excitation in a plasma channel also leads to damping of the plasma wave (Andreev *et al.*, 1997; Shvets and Li, 1999).

C. Nonlinear plasma waves

In the linear regime, $E \ll E_0$, the plasma wave is a simple sinusoidal oscillation with frequency ω_p and an arbitrary phase velocity v_p (the phase velocity is determined by the driver), e.g., $\phi = \phi_0 \cos[\omega_p(z/v_p - t)]$. When $E \gtrsim E_0$, the plasma wave becomes highly nonlinear. Wakefield generation in the nonlinear 1D regime can be examined by assuming that the drive beam is nonevolving, i.e., the drive beam is a function of only the coordinate $\xi = z - v_p t$, where $v_p \leq c$ is the phase velocity of the plasma wave. For laser drivers, $v_p \simeq v_g$, where v_g is the laser pulse group velocity. The quasi-static approximation (Sprangle *et al.*, 1990a,b) can be applied such that the plasma fluid quantities are also assumed to be functions only of the co-moving variable ξ. The 1D limit applies to broad drivers, $k_p r_\perp \gg 1$, where $r_\perp$ is the characteristic radial dimension of the drive beam. Using the fluid momentum and continuity equations,

$$\boldsymbol{u}_\perp - \boldsymbol{a}_\perp = 0, \tag{13}$$

$$\gamma - \beta_p u_z - \phi = 1, \tag{14}$$

$$n\,(\beta_p - \beta_z) = \beta_p n_0, \tag{15}$$

the Poisson equation $\partial^2\phi/\partial\xi^2 = k_p^2(n/n_0 - 1)$ can be written as (Berezhiani and Murusidze, 1992; Esarey *et al.*,

1993b; Teychenné *et al.*, 1993)

$$k_p^{-2}\frac{\partial^2\phi}{\partial\xi^2} = \gamma_p^2\left\{\beta_p\left[1-\frac{(1+a^2)}{\gamma_p^2(1+\phi)^2}\right]^{-1/2}-1\right\}, \quad (16)$$

where $\gamma_p = (1-\beta_p^2)^{-1/2}$ and $\beta_p = v_p/c$. The axial electric field of the wake is given by $E_z = -E_0\partial\phi/\partial\xi$. In the limit $\gamma_p^2 \gg 1$, Eq. (16) simplifies to (Berezhiani and Murusidze, 1990; Bulanov *et al.*, 1989; Sprangle *et al.*, 1990a,b)

$$k_p^{-2}\frac{\partial^2\phi}{\partial\xi^2} = \frac{(1+a^2)}{2(1+\phi)^2}-\frac{1}{2}. \quad (17)$$

Analytical solutions in terms of elliptic integrals can be found for square laser pulse profiles (Berezhiani and Murusidze, 1990; Bulanov *et al.*, 1989; Sprangle *et al.*, 1990a,b). As the plasma wave amplitude becomes nonlinear, the plasma wave steepens and its period lengthens.

In the region behind the drive beam, $a^2 = 0$, an analysis of Eq. (16) indicates that the electrostatic potential oscillates between $\phi_{\min} \le \phi \le \phi_{\max}$ and the axial electric field oscillates between $-E_{\max} \le E \le E_{\max}$. The values $\phi_{\min}$ and $\phi_{\max}$, denoted by ϕ_m, are given by (Esarey and Pilloff, 1995)

$$\phi_m = \hat{E}_{\max}^2/2 \pm \beta_p\left[(1+\hat{E}_{\max}^2/2)^2-1\right]^{1/2}, \quad (18)$$

where $\hat{E}_{\max} = E_{\max}/E_0$ and the $\pm$ give $\phi_{\max}$ and $\phi_{\min}$, respectively. For $E_{\max}/E_0 \gtrsim 1$, Eq. (16) indicates that the electric field departs from a simple sinusoidal form (Akhiezer and Polovin, 1956; Berezhiani and Murusidze, 1990; Bulanov *et al.*, 1989; Sprangle *et al.*, 1990a,b). In particular, the electric field exhibits the characteristic "sawtooth" profile associated with wave steepening and the density oscillations become highly peaked (as illustrated in Fig. 5 of Sec. III.A). Furthermore, the period of the nonlinear plasma wave increases as the amplitude increases. The nonlinear plasma wavelength in the limit $\gamma_p \gg 1$ is given by (Berezhiani and Murusidze, 1990; Bulanov *et al.*, 1989; Sprangle *et al.*, 1990a,b)

$$\lambda_{Np} = \lambda_p\begin{cases}1, & E_{\max}/E_0 \ll 1,\\ (2/\pi)E_{\max}/E_0, & E_{\max}/E_0 \gg 1\end{cases} \quad (19)$$

where $E_{\max}$ is the peak electric field of the plasma wave and $\lambda_p = 2\pi/k_p = 2\pi c/\omega_p$. For a square laser pulse profile of optimal length for plasma wave excitation ($L = \lambda_{Np}/2$), $E_{\max} = a^2/2/(1+a^2)^{1/2}$ for a linearly polarized laser.

The lengthening of the plasma wave period can be important in plasma-based accelerators. For example, in the PBWA, the plasma wave is driven at a constant beat frequency $\Delta\omega = \omega_1 - \omega_2 \simeq \omega_p$. As the wave grows, however, the effective plasma frequency decreases, $\omega_{p,\text{eff}} = 2\pi c/\lambda_{Np}$. Hence, the driver (i.e., the laser beat wave) becomes out of phase with the nonlinear plasma wave. This leads to saturation of the plasma wave amplitude in the PBWA (Rosenbluth and Liu, 1972; Tang *et al.*, 1985). Alternatively, if the plasma wave is to be driven to large amplitudes by a series of individual laser pulses, the change in the nonlinear plasma period can affect the optimal spacing between pulses as well as the optimal duration of the pulses (Umstadter *et al.*, 1994).

In the two-dimensional (2D) and 3D nonlinear regimes, numerical calculations are usually required. One possible approach is to use a full nonlinear plasma fluid model (Shadwick *et al.*, 2002) or a nonlinear quasi-static fluid model (Esarey *et al.*, 1993a; Sprangle *et al.*, 1992), which is discussed in Sec. V. An alternative (more computationally expensive) approach for wakefield calculation is to use 2D and 3D particle simulations (Mora and Antonsen, Jr., 1997; Pukhov and Meyer-ter-Vehn, 1996; Ren *et al.*, 2000; Tzeng *et al.*, 1996).

The increase in the plasma wavelength with increasing wave amplitude has an additional effect on nonlinear 2D plasma waves. Consider a plasma wave which is driven more strongly on-axis than it is off-axis, e.g., a laser driven accelerator, where the laser intensity peaks on-axis and typically has a Gaussian radial profile. On-axis, the plasma wave amplitude is maximum and, in the nonlinear regime, the plasma wavelength on-axis is larger than it is off-axis. Thus the plasma wavelength varies as a function of radius $\lambda_{Np}(r)$. This causes the wavefronts of the plasma wave to become curved and take on a "horseshoe" shape. For a plasma wave of fixed amplitude, the farther back within the plasma wave train, the more curved the plasma wave front, i.e., after ℓ periods, the phase front at large radii is located at $\ell\lambda_p$, whereas on-axis, the phase front is located at $\ell\lambda_{Np}(r=0)$. This effect has been observed in 2D nonlinear fluid simulations (Esarey *et al.*, 1993a; Krall *et al.*, 1993; Sprangle *et al.*, 1992) and 2D particle simulations (Bulanov *et al.*, 1995, 1997; Decker *et al.*, 1994). Curvature of the plasma wavefronts can lead to transverse wavebreaking, as discussed in Sec. II.D.

D. Wavebreaking

Plasmas are capable of supporting large amplitude, electrostatic waves with phase velocities near the speed of light. In the linear regime, the electric field of a plasma wave in a plasma-based accelerator has the form $E_z = E_{\max}\sin[\omega_p(z/v_p - t)]$, where $v_p \simeq c$ is the phase velocity. The peak field amplitude $E_{\max}$ of the plasma wave can be estimated from the Poisson equation $\nabla\cdot\boldsymbol{E} = 4\pi e(n_0 - n_e)$. A simple estimate for the maximum field amplitude is given by assuming all of the plasma electrons are oscillating with a wavenumber $k_p = \omega_p/c$. This gives $(\omega_p/c)E_{\max} = 4\pi e n_0$, or $E_{\max} = E_0$, where $E_0 = cm_e\omega_p/e$ is the cold nonrelativistic wavebreaking field (Dawson, 1959).

It is possible for the maximum amplitude of a nonlinear plasma wave to exceed the value E_0. Using the nonlinear, relativistic, cold fluid equations in 1D, it is possible to show that the maximum amplitude of a periodic plasma

wave is given by (Akhiezer and Polovin, 1956; Esarey and Pilloff, 1995)

$$E_{\rm WB} = \sqrt{2}(\gamma_p - 1)^{1/2} E_0, \tag{20}$$

which is referred to as the cold relativistic wavebreaking field, where $\gamma_p = (1 - v_p^2/c^2)^{-1/2}$ is the relativistic Lorentz factor associated with the phase velocity of the plasma wave. The plasma wave phase velocity is approximately the group velocity of the laser, $\gamma_p \simeq \omega/\omega_p$, where ω is the frequency of the laser. As an example, consider a laser-driven accelerator with a plasma density of $n_0 \simeq 10^{17}$ cm^{-3}. For a laser wavelength of 1 μm, $\gamma_p \simeq 100$ and $E_{\rm WB} \simeq 24 E_0$. Note that, when the plasma wave field amplitude approaches $E_{\rm WB}$, Eq. (18) implies $(1+\phi) \to 1/\gamma_p$, and, from Eq. (16), the cold plasma density becomes singular $n \to \infty$. This singularity indicates a breakdown of the cold fluid equations. Cold fluid theory will be a good approximation near the wavebreaking field in the limit $\gamma_p \beta_{\rm th} \ll 1$, where $c\beta_{\rm th} = (k_{\rm B} T_0/m)^{1/2}$ is the thermal velocity spread of the electrons, with T_0 the initial electron plasma temperature and $k_{\rm B}$ the Boltzmann constant. In a warm plasma, the electron distribution has a thermal spread about its mean fluid velocity, and thermal effects (i.e., pressure) will reduce the maximum plasma wave amplitude, or wavebreaking field.

In the limit of very slow phase velocity waves, $\beta_{\rm th} \ll \beta_p \ll 1$, corrections to the cold nonrelativistic wavebreaking field E_0 have been calculated using a warm fluid model by Coffey (1971). In the ultra-relativistic phase velocity $\beta_p = 1$ limit, the warm wavebreaking field was found (Katsouleas and Mori, 1989; Rosenzweig, 1988) to be $E_{\rm WB} \sim E_0/\beta_{\rm th}^{1/2}$. This expression for $E_{\rm WB}$ is valid for $\gamma_p \beta_{\rm th} \gg 1$, e.g., for an ultra-relativistic ($\beta_p = 1$) particle beam driver. For laser-driven plasma waves, however, typically plasma wave phase velocities are $\gamma_p \sim 10$–100 and initial plasma temperatures are $\beta_{\rm th}^2 mc^2 \sim 10$ eV (Durfee III *et al.*, 1995; Volfbeyn *et al.*, 1999). Therefore, a laser-plasma accelerator typically satisfies $\gamma_p \beta_{\rm th} \lesssim 1$, and, hence, the above expression for $E_{\rm th}$ does not apply.

A warm, relativistic fluid theory has been formulated to describe wavebreaking in all regimes of interest, including that of laser-plasma accelerators.(Schroeder *et al.*, 2005) This theory assumes the quasi-static approximation (i.e., a non-evolving wakefield driver) in 1D and assumes $k_{\rm B} T < mc^2$ (i.e., nonrelativistic temperatures). Using warm fluid momentum and continuity equations, the Poisson equation can be written as (Schroeder *et al.*, 2005)

$$\frac{\partial^2}{\partial \xi^2}\left[\frac{\gamma_\perp(1-\beta_\varphi w_z)}{(1-w_z^2)^{1/2}} + \frac{3}{2}\beta_{\rm th}^2 \frac{(1-\beta_\varphi w_z)(1-w_z^2)^{1/2}}{\gamma_\perp(1-\beta_\varphi^{-1} w_z)^2}\right] = \frac{k_p^2 w_z}{\beta_\varphi - w_z}, \tag{21}$$

where w_z is the warm fluid velocity. An example of this warm fluid theory is shown in Fig. 6, which plots the plasma density n/n_0 (dotted curve), plasma wave electric field E_z/E_0 (solid curve), and plasma temperature T/T_0 (dashed curve) as a function of $\xi = z - v_p t$ excited by a Gaussian laser pulse $a = a_0 \exp(-\xi^2/4L_{\rm RMS}^2)$ with normalized peak intensity $a_0 = 2$ and intensity RMS length $k_p L_{\rm RMS} = 1$ for $\gamma_p = 10$. The plasma temperature undergoes periodic oscillations in the wake owing to compression of the plasma density (Esarey *et al.*, 2007; Schroeder *et al.*, 2005; Shadwick *et al.*, 2004, 2005). The temperature evolution (to lowest order in the small parameter $k_{\rm B} T/mc^2 < 1$) is given by $T = [(n/n_0)^2(1 - w_z^2)]T_0$. The wavebreaking limit, defined as the maximum amplitude of an electrostatic standing wave (a function of only $\xi = z - v_p t$) allowed within the warm fluid model, can be calculated using Eq. (21). For example, the lowest-order corrections (in the limit $\gamma_p \beta_{\rm th} < 1$) to the cold relativistic wavebreaking field Eq. (20) are (Schroeder *et al.*, 2005)

$$(E_{\rm WB}/E_0)^2 \simeq 2\gamma_\perp(\gamma_p - 1) - 2\beta_p\gamma_p\left[\frac{4}{3}\left(3\beta_p^2\gamma_p^2\gamma_\perp^2\beta_{\rm th}^2\right)^{1/4} - \left(3\gamma_p^2\beta_{\rm th}^2\right)^{1/2}\right]. \tag{22}$$

Equation (22) includes the possible presence of an intense laser field (e.g., the self-modulated LWFA), with $\gamma_\perp^2 = 1 + a^2/2$. The wavebreaking field is larger in the presence of a laser field. For a plasma wave behind the drive laser pulse $\gamma_\perp = 1$. In the warm fluid theory of wavebreaking there is no shock formation (i.e., the density remains finite) at the wavebreaking limit. For fields larger that Eq. (22) no traveling wave solutions exist. Figure 7 shows the wavebreaking field, $\hat{E}_{\rm WB} = E_{\rm WB}/E_0$ (solid curve), versus initial temperature $\beta_{\rm th}$ with $\gamma_p = 10$ and $\gamma_\perp = 1$. The dotted curve is the ultra-relativistic result ($\beta_p = 1$), and the dashed line is the cold limit ($\beta_{\rm th} = 0$). Note that for typical short-pulse laser-plasma-interactions, $\beta_{\rm th}^2 \sim 10^{-4}$.

The above expressions for the wavebreaking field were based on 1D theories. Wavebreaking in 3D has not been thoroughly investigated and general expressions for the maximum field amplitude are not known. Particle-in-cell simulations (Bulanov *et al.*, 1995; Decker *et al.*, 1994; Pukhov and Meyer-ter-Vehn, 2002; Tsung *et al.*, 2004) in 2D and 3D in the highly-nonlinear cavitated regime have demonstrated the generation of plasma waves with amplitudes in excess of E_0. The wake generation in the blowout regime is discussed in Sec. III.E. Simulations (Krall *et al.*, 1993; Shadwick *et al.*, 2002) based on nonlinear, 2D fluid equations have shown wave amplitudes in excess of E_0.

The transverse structure of the plasma wave and curvature of the wake phase fronts, as described in Sec. II.C, can lead to 2D wavebreaking (Bulanov *et al.*, 1997). Specifically, when the curvature radius of the phase front is on the order of the electron fluid displacement, the regular structure of the plasma wave is destroyed (i.e., 2D wavebreaking) and particle trapping may occur. For a fixed amplitude nonlinear 2D wake (i.e., neglecting wake damping), 2D wavebreaking will always occur at a sufficiently long distance behind the driver. The larger

the wake amplitude, the shorter the distance behind the driver is the onset point of 2D wavebreaking. A similar effect can occur for linear (or nonlinear) plasma waves in a plasma channel. In a plasma channel, the plasma density is minimum on axis, hence the plasma wavelength is longer on-axis than off-axis. This leads to wake wavefront curvature, and the curvature increases with distance behind the driver until the point of 2D wavebreaking is reached.

E. Electron acceleration and dephasing

Consider an electron accelerated along the z-axis (laser-propagation axis) by a linear electrostatic plasma wave of the form $E_z = E_{\max} \sin \omega_p(z/v_p - t)$. As the electron is accelerated, its velocity will increase and approach the speed of light, $v_z \to c$. If the phase velocity of the plasma wave is constant with $v_p < c$, the electrons will eventually outrun the plasma wave and move into a phase region of the plasma wave which is decelerating. This limits the energy gain of the electron in the plasma wave and is commonly referred to as electron dephasing. The dephasing length L_d is defined as the length the electron must travel before it phase slips by one-half of a period with respect to the plasma wave. For a highly relativistic electron, $v_z \simeq c$, the dephasing time t_d is given by $\omega_p(c/v_p - 1)t_d = \pi$, i.e., $L_d = ct_d \simeq \gamma_p^2 \lambda_p$, assuming $\gamma_p \gg 1$. The maximum energy gain after a dephasing length (Joshi *et al.*, 1984; Tajima and Dawson, 1979) is given approximately by $W_{\max} \simeq eE_{\max}L_d \simeq 2\pi\gamma_p^2(E_{\max}/E_0)m_ec^2$, assuming $E < E_0$.

In a 1D plasma wave, electron trapping, acceleration, and dephasing can be studied by examining the electron orbits in phase space $(\tilde{p}, \psi)$, where $\tilde{p}$ is the normalized momentum and $\psi = k_p\xi = k_p(z - v_pt)$ is the phase. In the linear regime, the plasma wave is described by a sinusoidal electrostatic potential $\phi = \phi_0 \cos\psi$, where $\phi_0 = E_{\max}/E_0$ is the amplitude. The phase region $-\pi < \psi < 0$ is accelerating. Consider an electron injected into the plasma wave with $v_z < v_p$ at $\psi = 0$. Initially, the electron is slipping backward with respect to the plasma wave. If the initial electron velocity is too low, the electron does not gain sufficient energy and $v_z < v_p$ at $\psi = -\pi$. Hence, the electron would be untrapped and would continue to slip backward through the plasma wave. If, however, the electron has a sufficiently high initial velocity such that $v_z > v_p$ as the electron approaches $\psi \to -\pi$, the electron will be trapped and execute closed orbits in the $-\pi < \psi < \pi$ phase region. The separatrix, which separates the region of trapped and untrapped orbits in phase space, is shown schematically in Fig. 2 for a small amplitude plasma wave.

The motion of a test electron in a 1D nonlinear plasma wave is described by the Hamiltonian (Esarey and Pilloff, 1995)

$$H(\tilde{p}, \psi) = \tilde{\gamma} - \beta_p\tilde{p} - \phi(\psi), \tag{23}$$

where $H(\tilde{p}, \psi)$ = constant along a given electron orbit and $\phi = \phi(\psi)$ is the solution to Eq. (16), which oscillates between $\phi_{\min} \le \phi \le \phi_{\max}$ and is related to $E_{\max}$ by Eq. (18). In particular, the separatrix $\tilde{\gamma}_s(\psi)$ characterizing the test electron orbits in $(\tilde{\gamma}, \psi)$ phase space is given by $H(\tilde{\gamma}_s, \psi) = H(\gamma_p, \psi_{\min})$, where $\phi(\psi_{\min}) = \phi_{\min}$.

Figure 3 shows several separatrices for $\gamma_p = 20$ and for different values of the plasma wave amplitude, characterized by the parameter ϵ, where $\phi_{\max} = (2\gamma_p^2 - 1)\epsilon/\gamma_p - 1$, for $\epsilon = 0.03$, 0.04, 0.1, 0.3 and 0.9 ($\epsilon = 1$ corresponds to the cold wavebreaking limit). This corresponds to values of the peak electric field $E_{\max}$ given by $E_{\max}/E_0 = 0.18$, 0.47, 1.5, 3.2, and 5.8, respectively. The value $\epsilon = 0.03$ corresponds to the innermost curve and $\epsilon = 0.9$ corresponds to the outermost curve. These curves were obtained (Esarey and Pilloff, 1995) by plotting $H(\tilde{\gamma}_s, \psi) = H(\gamma_p, \psi_{\min})$ after numerically solving Eq. (16) for $\phi = \phi(\psi)$ with the initial conditions $\partial\phi/\partial\xi = 0$ and $\phi = \phi_{\max}$ at $\psi = 0$. The width of the separatrix $\Delta\psi_s$ corresponds to the nonlinear plasma wavelength, $\lambda_{Np} = \Delta\psi_s/k_p$, given by Eq. (19). As the plasma wave amplitude increases, the nonlinear wavelength increases.

The maximum energy $\tilde{\gamma}_{\max}$ and minimum energy $\tilde{\gamma}_{\min}$, denoted by $\tilde{\gamma}_m$, for an electron on the separatrix are given by (Esarey and Pilloff, 1995)

$$\tilde{\gamma}_m = \gamma_p(1 + \gamma_p\Delta\phi) \pm \gamma_p\beta_p\left[(1 + \gamma_p\Delta\phi)^2 - 1\right]^{1/2}, \tag{24}$$

where $\Delta\phi = \phi_{\max} - \phi_{\min}$, i.e., $\Delta\phi = 2\beta_p[(1 + \hat{E}_{\max}^2/2)^2 - 1]^{1/2}$, as indicated by Eq. (18). In the limits $\gamma_p\Delta\phi \gg 1$ and $\gamma_p^2 \gg 1$, $\gamma_{\max} \simeq 2\gamma_p^2\Delta\phi$ and $\gamma_{\min} \simeq \Delta\phi/2 + 1/(2\Delta\phi)$. In particular, the maximum energy of a trapped electron is given by (Esarey and Pilloff, 1995)

$$\tilde{\gamma}_{\max} \simeq 2\gamma_p^2 \begin{cases} \hat{E}_{\max}^2, & \text{for } \hat{E}_{\max}^2 \gg 2, \\ 2\hat{E}_{\max}, & \text{for } 2 \gg \hat{E}_{\max}^2 \gg 1/4\gamma_p^2, \end{cases} \tag{25}$$

where $\hat{E}_{\max} = E_{\max}/E_0$. The limit $\hat{E}_{\max}^2 \ll 2$ corresponds to the well-known limit for linear, sinusoidal plasma waves (Joshi *et al.*, 1984; Mora, 1992; Tajima and Dawson, 1979). When $\hat{E}_{\max}^2 \gg 2$, however, $\tilde{\gamma}_{\max} \simeq 2\gamma_p^2\hat{E}_{\max}^2$, which implies that higher electron energies can be obtained for electrons trapped in nonlinear plasma waves. The nonlinear regime where $\hat{E}_{\max} > 1$ has been observed in simulations of the self-modulated LWFA (Bulanov *et al.*, 1995; Decker *et al.*, 1994; Krall *et al.*, 1993) and laser wakefields driven by multiple pulses (Bonnaud *et al.*, 1994; Nakajima, 1992; Umstadter *et al.*, 1994). As for the maximum field in a cold plasma ($\epsilon = 1$, $E_{\max} = E_{\rm WB}$), Eq. (24) indicates that (Esarey and Pilloff, 1995) $\tilde{\gamma}_{\max} = 4\gamma_p^3 - 3\gamma_p$.

A rough estimate for the dephasing length is given by $W_{\max} = m_ec^2\tilde{\gamma}_{\max} = eE_{\max}L_d$. This yields

$$L_d = \gamma_p^2\lambda_{Np} \begin{cases} 2/\pi, & \hat{E}_{\max} \ll 1, \\ 1/2, & \hat{E}_{\max} \gg 1, \end{cases} \tag{26}$$

where λ_{Np} is given by Eq. (19). The actual dephasing length (Teychenné *et al.*, 1994b) requires the simultaneous solution of the equation of motion and Eq. (16).

As an example, consider a LWFA with $n_0 = 2.8 \times 10^{18}$ cm^{-3} and $\lambda = 1$ μm, i.e., $\gamma_g \simeq \gamma_p \simeq 20$ and $E_0 \simeq 160$ GV/m. In the limit $\hat{E}^2_{\max} \gg 2$, Eq. (25) yields $W_{\max} \simeq 400\hat{E}^2_{\max}$, where $W_{\max} \simeq m_e c^2 \tilde{\gamma}_{\max}$. At the maximum field in a cold plasma, $E_{\rm WB} \simeq 6.2E_0$ and $W_{\max} \simeq 16$ GeV. Notice that $\tilde{\gamma}_{\max} \simeq 4\gamma_p^3 E_{\max}/E_{\rm WB}$, assuming $\gamma_p^2 \gg 1$ and $\gamma_p(E_{\max}/E_{\rm WB})^2 \gg 1$. Hence, for a fixed value of $E_{\max}/E_{\rm WB}$, $\tilde{\gamma}_{\max} \propto n_0^{-3/2}$ and substantially higher single-stage energy gains can be achieved by operating at lower densities, albeit with longer acceleration stages.

Note that the above results are obtained from 1D theory and assume a constant amplitude plasma wave. An evolving plasma wave amplitude and 2D effects could alter these results. For example, Mora (1992) has shown that the effects of laser diffraction can lead to a more restrictive trapping condition for linear plasma waves.

F. Plasma wave phase velocity

The phase velocity of the plasma wave is important for determining the minimum injection energy, the maximum energy gain, and the dephasing length. Neglecting the evolution of the drive beam as it propagates, the phase velocity of the plasma wave is equal to the group velocity of the drive laser.

In the linear regime, the group velocity of a laser pulse in a plasma can be determined from the 1D dispersion relation, $\omega^2 = c^2k^2 + \omega_p^2$. This yields $v_g = c(1-\omega_p^2/\omega^2)^{1/2}$ and $\gamma_g = (1 - v_g^2/c^2)^{-1/2} = \omega/\omega_p$. Nonlinear corrections to the group velocity in 1D have been analyzed by Decker and Mori (1994). Note that, in the nonlinear regime the linear relation $v_g = c^2k/\omega$ is no longer valid. In the long pulse, underdense $\omega_p/\omega \ll 1$ limit, the nonlinear group velocity was found by Decker and Mori (1994) to be $(\omega/\omega_p)[(\gamma_\perp + 1)/2]^{1/2}$, where $\gamma_\perp = (1 + a_0^2/2)^{1/2}$ is the relativistic Lorentz factor associated with the quiver motion of the electrons in the laser field.

The group velocity of a laser pulse is also reduced by 3D effects. For example, consider a laser pulse in vacuum undergoing Rayleigh diffraction. The evolution of the spot size (or radius) of a Gaussian laser beam evolves according to $r_s = r_0(1 + z^2/Z_R^2)^{1/2}$, where r_0 is the minimum spot size at the focal point $z = 0$, and $Z_R = kr_0^2/2$ is the Rayleigh length. In effect, the photons are traveling at approximately a diffraction angle $\theta_d = r_0/Z_R$ with respect to the z-axis. Hence, the axial group velocity is reduced by $v_g \simeq c\cos\theta_d \simeq c(1 - \theta_d^2/2)$. A more detailed calculation indicates that, in the linear regime, the 3D group velocity is given by (Esarey and Leemans, 1999)

$$\gamma_g \simeq (\omega_p^2/\omega^2 + 2c^2/\omega^2 r_0^2)^{-1/2}. \qquad (27)$$

In effect, the linear 3D dispersion relation is given by $\omega^2 - c^2k^2 = \omega_p^2 + 2c^2/r_0^2$ (for a matched laser pulse in a plasma channel, $\omega^2 - c^2k^2 = \omega_p^2 + 4c^2/r_0^2$). For tightly focused laser pulses, this 3D correction can significantly limit the group velocity. As an example, consider a laser pulse with a $\lambda = 1$ μm wavelength and $r_0 = 10$ μm spot size, propagating in a plasma of density $n_0 = 10^{16}$ cm^{-3}; in 1D, $\gamma_g \simeq 330$, however, the finite spot size reduces the group velocity such that $\gamma_g \simeq 44$.

Distortions of the pulse driving the plasma wave can also affect the plasma wave phase velocity. In the LWFA in the 1D limit, it has been shown that the wake phase velocity is approximately equal to the group velocity associated with the position of the peak of intensity profile (Decker and Mori, 1994). Furthermore, the plasma wave can lead to locally enhanced diffraction and focusing, which distorts the pulse profile and reduces the plasma wave phase velocity (Leemans *et al.*, 1996).

G. Photon acceleration

In addition to accelerating electrons, a plasma wave can be used to upshift the frequency of a properly phased, low intensity, short laser pulse, as shown schematically in Fig. 4 (often referred to as photon acceleration) (Esarey *et al.*, 1990; Wilks *et al.*, 1989). Consider a plasma wave with an electron density perturbation of the form $\delta n = -\delta n_0 \sin k_p\zeta$, where $\zeta = z - ct$, and a low intensity, "witness" laser pulse centered about $\zeta = 0$ with a pulse length $L \ll \lambda_p$. The local density at the front of the pulse, $n(\zeta = L/2)$, will be less than that at the back of the pulse, $n(\zeta = -L/2)$. Since the local phase velocity of the laser pulse is given by $\beta_p = v_p/c \simeq 1 + \omega_p^2(\zeta)/2\omega^2$, where $\omega_p^2(\zeta) \propto n(\zeta)$, the phase velocity at the pulse front is less than that at the back of the pulse, i.e., $v_p(L/2) < v_p(-L/2)$. Hence, the phase peaks at the back move faster than those at the front and the pulse wavelength decreases (the pulse frequency increases). For small shifts, the laser wavelength will evolve according to $\lambda \simeq \lambda_0 + z\Delta\beta_p$, where $\Delta\beta_p = \lambda_0 d\beta_p/d\zeta < 0$ is the difference in phase velocity between adjacent phase peaks, z is the propagation distance, and $\lambda_0 = 2\pi c/\omega_0$ is the initial laser wavelength. Hence, the frequency shift is given by $\omega/\omega_0 \simeq 1 - zd\beta_p/d\zeta$, where $d\beta_p/d\zeta \simeq (\omega_p^2/2\omega_0^2)d(\delta n/n_0)/d\zeta$. A more detailed calculation indicates that the frequency will be upshifted according to (Esarey *et al.*, 1990)

$$\frac{\omega}{\omega_0} \simeq \left(1 + \frac{\omega_p^2}{\omega_0^2}\frac{\delta n_0}{n_0} k_p z \cos k_p\zeta\right)^{1/2}, \qquad (28)$$

where nonlinear effects and phase slippage between the laser pulse and plasma wave (i.e., dephasing) have been neglected.

Typically, the plasma wave induced frequency shifts are small. For example, consider a laser with $\lambda = 1$ μm and $r_0 = 30$ μm, propagating in a plasma of density $n_0 = 10^{18}$ cm^{-3} ($\lambda_p = 30$ μm). After propagating one

Rayleigh length $z = Z_R$, $\omega/\omega_0 \simeq 1 + \delta n_0/3n_0$. Small frequency shifts, however, can be detected and this process can be useful for diagnosing the wakefield (Marquès *et al.*, 1996; Siders *et al.*, 1996). Large frequency shifts require long propagation distances and large plasma wave amplitudes. For example, after one electron dephasing length $L_d = \lambda_p\omega^2/\omega_p^2$, $\omega/\omega_0 = (1 + 2\pi\delta n_0/n_0)^{1/2}$.

III. LASER-PLASMA ACCELERATORS

A. Laser wakefield accelerator

In the laser wakefield accelerator (LWFA) (Gorbunov and Kirsanov, 1987; Sprangle *et al.*, 1988; Tajima and Dawson, 1979), a single, short ($\lesssim$ 1 ps), high intensity ($\gtrsim 10^{17}$ W/cm^2) laser pulse drives a plasma wave. The wakefield is driven most efficiently when the laser pulse length is approximately the plasma period $L \sim \lambda_p$. The LWFA was first proposed by Tajima and Dawson (1979). Prior to 1985, the technology for generating ultra-intense, picosecond laser pulses did not exist and only the PBWA concept, described in Sec. III.B, appeared feasible (the PBWA concept relied on long pulses of modest intensity). The LWFA was later re-invented independently by Gorbunov and Kirsanov (1987) and by Sprangle *et al.* (1988). This roughly coincides to the time when CPA was applied to compact solid-state lasers and a table-top, terawatt laser system was first demonstrated by Mourou and co-workers (Maine *et al.*, 1988). The nonlinear theory of the LWFA in 1D was developed by Bulanov *et al.* (1989), Sprangle *et al.* (1990a,b), and Berezhiani and Murusidze (1990). The nonlinear theory of the LWFA in 2D, including the self-consistent evolution of the laser pulse, was analyzed by Esarey *et al.* (1993a); Sprangle *et al.* (1992).

As an intense laser pulse propagates through an underdense plasma, $(\lambda/\lambda_p)^2 \ll 1$, the ponderomotive force associated with the laser pulse envelope, $F_p \sim \nabla a^2$, expels electrons from the region of the laser pulse. If the length scale L_z of the axial gradient in the pulse profile is approximately equal to the plasma wavelength, $L_z \sim \lambda_p$, the ponderomotive force excites large amplitude plasma waves (wakefields) with phase velocities approximately equal to the laser pulse group velocity [see Fig. 1(a)]. For a typical axially symmetric laser pulse (e.g., a Gaussian profile), the wakefield amplitude will be maximum when $L \simeq \lambda_p/2$, where $L = c\tau_L$ is laser pulse length. The precise value of L which maximizes the wake amplitude will depend on the shape of the axial pulse profile. Following are some examples.

Linear regime, sine pulse. Consider a LWFA driven by a circularly polarized laser pulse with a normalized intensity $a^2 = a_0^2 \exp(-2r^2/r_s^2)\sin^2(\pi\zeta/L)$ for $0 < \zeta < L$, where $\zeta = z - ct$ and $a_0^2 \ll 1$. Solutions to Eq. (11) indicate that the wakefield amplitude is maximum for pulse lengths $L \simeq \lambda_p$. Behind the pulse, $\zeta < 0$, the axial electric field and density perturbation of the wake are given by (Esarey *et al.*, 1989)

$$\frac{E_z}{E_0} = \frac{\pi}{4} a_0^2 \exp\left(-\frac{2r^2}{r_s^2}\right)\cos k_p\zeta, \tag{29}$$

$$\frac{\delta n}{n_0} = \frac{\pi}{4} a_0^2 \left[1 + \frac{8}{k_p^2 r_s^2}\left(1 - \frac{2r^2}{r_s^2}\right)\right]\exp\left(-\frac{2r^2}{r_s^2}\right)\sin k_p\zeta, \tag{30}$$

for $L = \lambda_p$. For linear polarization, averaging over the fast oscillation yields Eqs. (29) and (30) with a_0^2 replaced with $a_0^2/2$. Notice that a tightly focused laser pulse with $k_p^2 r_s^2/8 < 1$ will result in a larger density perturbation $\delta n/n_0$ on-axis, whereas the axial electric field E_z on-axis is unchanged in comparison to the 1D values.

Linear regime, Gaussian pulse. For a circularly polarized, Gaussian pulse profile, $a^2 = a_0^2 \exp(-\zeta^2/L^2)$, the wakefield amplitude behind the pulse ($\zeta^2 \gg L^2$) is given by (Gorbunov and Kirsanov, 1987)

$$E_{\max}/E_0 = (\sqrt{\pi} a_0^2/2) k_p L \exp(-k_p^2 L^2/4), \tag{31}$$

assuming $a_0^2 \ll 1$. Equation (31) explicitly shows the dependence of the wake amplitude on the pulse length L. In particular, the wake amplitude achieves a maximum value of $E_{\max}/E_0 = a_0^2(\pi/2e)^{1/2} \simeq 0.76 a_0^2$ when $L = \lambda_p/\pi\sqrt{2}$.

Nonlinear regime, square pulse. Consider a circularly polarized laser pulse with a square axial profile in the 1D limit $r_0^2 \gg \lambda_p^2$. The wakefield amplitude is maximum when $L \simeq \lambda_{Np}/2$, where λ_{Np} is the nonlinear plasma wavelength Eq. (19), and is given by (Berezhiani and Murusidze, 1990; Bulanov *et al.*, 1989; Sprangle *et al.*, 1990a,b)

$$E_{\max}/E_0 = a_0^2(1 + a_0^2)^{-1/2}, \tag{32}$$

where $a_0^2 = 3.6 \times 10^{-19}\lambda^2(\mu\text{m})I_0(\text{W/cm}^2)$ (for linear polarization, replace a_0^2 with $a_0^2/2$). Notice that $E_{\max} \propto \lambda_p^{-1} \sim L^{-1}$. Hence, the wakefield amplitude can be increased by operating at high densities and shorter pulse lengths. At high densities, however, the laser pulse group velocity is reduced and electron dephasing can limit the energy gain, as discussed in Sects. II.E and III.G.

Nonlinear regime, sine pulse. As an example of nonlinear plasma wave behavior, Eq. (16) has been solved numerically (Sprangle *et al.*, 1990a,b) for a linearly polarized laser of the form $a^2 = a_0^2 \sin^2(\pi\zeta/L)\cos^2(k\zeta)$ for $-L < \zeta < 0$ (and zero otherwise), with $L = \lambda_p$ and $\lambda = 1$ μm. The ambient plasma density is $n_0 = 1.2 \times 10^{16}$ cm^{-3}, which yields $L = \lambda_p = 300$ μm ($\tau_L = L/c = 1$ ps). A mildly relativistic case $a_0 = 0.5$ ($I_0 = 3.5 \times 10^{17}$ W/cm^2) is shown in Fig. 5(a), and a highly relativistic case $a_0 = 2$

($I_0 = 5.6 \times 10^{18}$ W/cm^2) is shown in Fig. 5(b). Figure 5 shows the density variation $\delta n/n_0 = n/n_0 - 1$ and the axial electric field E_z, with $E_{\max} \simeq 1$ GV/m in Fig. 5(a) and $E_{\max} \simeq 10$ GV/m in Fig. 5(b). Note that the rapid oscillations in the plasma density at one-half the laser wavelength are due to a fast component of the ponderomotive force at twice the laser frequency, i.e., $a^2 \sim 1 + \cos(2k\zeta)$. The nonlinear effects of wave steepening and period lengthening are clearly evident in Fig. 5(b).

Because the plasma wave is driven by a single laser pulse with $L \simeq \lambda_p$, the wakefield amplitude is relatively insensitive to uncertainties in the pulse duration and the plasma uniformity. This is shown in Fig. 8, where the peak wakefield amplitude $E_{\max}$ is shown as a function of the pulse length L, at a fixed density and intensity. The parameters are identical to the sine profile laser pulse examples shown in Figs. 5(a) and 5(b) (i.e., for $a_0 = 0.5$ and $a_0 = 2$), only now the pulse length L is varied. Plotted in Fig. 8 is the wakefield amplitude normalized to $E_N = E_0(a_0^2/2)(1 + a_0^2/2)^{-1/2}$, which is the maximum wakefield amplitude for a square pulse profile. Notice that the electric field amplitude is maximum for $L \simeq 0.75\ \lambda_p$ and is fairly insensitive to changes in the pulse length. The curve for the $a_0 = 2$ case is also broader because of an increase in the nonlinear plasma wavelength.

The optimal pulse length conditions for the square, sine, and Gaussian pulse profiles discussed above may be summarized as follows. For the square pulse, the wakefield is maximum $E_{\max} = a_0^2 E_0$ when $L_{\rm FWHM} = 0.5\ \lambda_p$ ($k_p L_{\rm RMS} = 0.91$). For the sine pulse, the wakefield is maximum $E_{\max} = 0.82\ a_0^2 E_0$ when $L_{\rm FWHM} = 0.5\ \lambda_p$ ($k_p L_{\rm RMS} = 1.1$). For the Gaussian pulse, the wakefield is maximum $E_{\max} = 0.76\ a_0^2 E_0$ when $L_{\rm FWHM} = 0.37\ \lambda_p$ ($k_p L_{\rm RMS} = 1$). Here the pulse length is expressed in terms of the full-width-half-maximum (FWHM) length $L_{\rm FWHM}$ and the root-mean-square (RMS) length $L_{\rm RMS}$ of the pulse intensity profile. These results assume $a_0^2 \ll 1$ and circular polarization (Leemans *et al.*, 1996).

Furthermore, since the laser pulse in the LWFA is of short duration, $L \simeq \lambda_p$, various instabilities which can be detrimental to the propagation of long pulses can be reduced. Schemes that use long laser pulses, $L \gg \lambda_p$, such as the PBWA and the self-modulated LWFA, are subject to various instabilities, some of which are discussed in Sec. VI.

Perhaps the first experimental evidence for plasma wave generation by the LWFA mechanism was obtained by Hamster *et al.* (1993). In these experiments, the emission of terahertz radiation at the plasma frequency was observed when the plasma was driven by a laser pulse of length $L \simeq \lambda_p$. Specifically, $\omega_p/2\pi = 4.6$ THz radiation was observed for a 0.1 ps laser pulse propagating in a plasma of density 2×10^{17} cm^{-3}. This radiation is emitted presumably by the 2D electron plasma currents of the laser-induced wakefield. Direct measurement of plasma wave generated in the LWFA has been reported by researchers at Ecole Polytechnique (Marquès *et al.*, 1996) and at the University of Texas at Austin (Siders *et al.*, 1996) by using probe pulses and optical interferometry techniques. In the Ecole Polytechnique experiments (Marquès *et al.*, 1996), a 120 fs duration, 800 nm wavelength laser pulse with a maximum energy of 40 mJ was focused to a maximum intensity of 3×10^{17} W/cm^2 in a plasma of density 10^{17} cm^{-3}. A pair of probe pulses, separated from each other by 1.5 λ_p, were used to map out the wakefield by adjusting the delay between the pump and probe pulses. A plasma wave with a perturbed density of 30% to 100% was measured over several plasma periods behind the probe pulse. At the University of Texas (Siders *et al.*, 1996), three probe pulses were used to measure the density perturbation at a fixed delay behind the pump pulse. By varying the ambient plasma density, the plasma wave amplitude was observed to vary in good agreement with theory. Kotaki *et al.* (2002) measured laser wakefield excitation with field amplitude of 20 GeV/m using a a time-resolved frequency domain interferometer.

Dewa *et al.* (1998) have reported on the observation of electron acceleration in LFWA experiments, although with some controversy (Bernard *et al.*, 1999), with energies of 100 MeV (17 MeV injected from a linac) with a 2 TW laser system. Amiranoff *et al.* (1998) have observed LWFA accelerated electrons with an energy gain of 1.6 MeV (3 MeV injected) using a 3.5 TW laser system. The peak longitudinal electric field was estimated to be 1.5 GV/m. Kitagawa *et al.* (2004) observed electron acceleration using a 1 μm, ~ 0.5 ps duration laser exciting a plasma wave in a glass capillary with plasma density (plasma electrons created via ablation) of 10^{16} cm^{-3}.

B. Plasma beat wave accelerator

In the plasma beat wave accelerator (PBWA) (Clayton *et al.*, 1993; Everett *et al.*, 1994; Joshi *et al.*, 1984; Kitagawa *et al.*, 1992; Rosenbluth and Liu, 1972; Tajima and Dawson, 1979), two long pulse laser beams of frequencies ω_1 and ω_2 are used to resonantly excite a plasma wave. This is done by appropriately adjusting the laser frequencies and plasma density to satisfy the resonance condition $\Delta\omega \equiv \omega_1 - \omega_2 \simeq \omega_p$. When this is satisfied, large amplitude plasma waves can be generated. The PBWA was first proposed by Tajima and Dawson (1979) as an alternative to the laser wakefield accelerator, since compact, ultrashort pulse, ultrahigh power laser technology (Mourou and Umstadter, 1992; Perry and Mourou, 1994) was not available in 1979. The PBWA was subsequently analyzed by various researchers (Esarey *et al.*, 1988; Gibbon and Bell, 1988; Horton and Tajima, 1986; Joshi *et al.*, 1984; McKinstrie and Forslund, 1987; Mori *et al.*, 1988; Tang *et al.*, 1985). (Resonant excitation of a plasma wave using two laser beams had been previously analyzed by Rosenbluth and Liu (1972) for plasma

heating applications.) To overcome the problem of dephasing between the accelerated electrons and the plasma wave, Katsouleas and Dawson (1983) proposed the use of a transverse magnetic field. Tang *et al.* (1985) described how the plasma wave amplitude could be increased by operating at an optimal frequency mismatch $\Delta\omega_{\rm opt}$, such that $\omega_1 - \omega_2 = \omega_p + \Delta\omega_{\rm opt}$. Since this early work, various aspects of the PBWA have been analyzed and simulated, such as the self-focusing of the laser beams by relativistic, plasma wave, and cascading effects (Esarey and Ting, 1990; Esarey *et al.*, 1988; Gibbon and Bell, 1988; Mori *et al.*, 1988).

Consider two lasers beams with combined normalized vector potentials given by $a = a_1\cos(k_1 z - \omega_1 t) + a_2\cos(k_2 z - \omega_2 t)$, where $k_{1,2}$ are the laser wavenumbers. The ponderomotive force $\nabla a^2/2$ will have a resonant beat term $(a^2)_{\rm res} = a_1 a_2\cos(\Delta k z - \Delta\omega t)$, where $\Delta k \equiv k_1 - k_2$. In the linear regime, plasma wave generation is described by $(\partial^2/\partial t^2 + \omega_p^2)\phi = \omega_p^2(a^2/2)_{\rm res}$, and the ponderomotive beat term can resonantly drive a plasma wave when $\Delta\omega \simeq \omega_p$. When the resonance condition is exactly satisfied, $\Delta\omega = \omega_p$, secular growth of the plasma wave results, $\phi = -\phi_s\sin(\Delta k z - \Delta\omega t)$, where $\phi_s = a_1 a_2 k_p|\zeta|/4$ and $|\zeta| = |z - ct|$ is the distance behind the front of the laser beams. Hence, the amplitude of the plasma wave within the laser pulse is (Rosenbluth and Liu, 1972)

$$E_{\rm max}/E_0 = a_1 a_2 k_p|\zeta|/4. \tag{33}$$

Furthermore, notice that the phase velocity of the plasma, $v_p = \Delta\omega/\Delta k$, is given by $v_p/c \simeq 1 - \omega_p^2/(2\omega_1\omega_2)$ in the limit $\omega_p^2/\omega_1^2 \sim \omega_p^2/\omega_2^2 \ll 1$, i.e., the phase velocity of the plasma wave is approximately equal to the group velocity of the driving lasers.

In effect, the laser beat wave acts as a series of laser pulses, each of amplitude $a_1 a_2$ and of duration $\Delta\tau = 2\pi/\Delta\omega$. Each of these pulses generates a wake of amplitude $E_{\rm max}/E_0 = \pi a_1 a_2/2$. The total plasma wave amplitude generated by a laser beat wave of length $L = N\lambda_p$ is $E_{\rm max}/E_0 = N\pi a_1 a_2/2$, where N is the number of laser beat periods within the pulse.

The result given by Eq. (33) was based on linear plasma theory, $|\phi| \ll 1$. Various nonlinear effects were neglected. In particular, as discussed in Sec. II.C, as the plasma wave amplitude increases the plasma wave period increases. Since the period of the beat wave is fixed, whereas the period of the plasma wave is increasing, the plasma wave will eventually become out of phase with the laser beat wave. This resonant detuning of the plasma wave from the beat wave will limit the amplitude of the plasma wave (Rosenbluth and Liu, 1972).

The nonlinear dynamics of the beat wave generation in 1D with $\omega_p^2/\omega^2 \ll 1$ can be examined using the nonlinear Poisson equation Eq. (17). Analysis of Eq. (17) indicates that the nonlinear plasma wavelength is given by $\lambda_{Np} = (4/k_p)(1+\phi_s)^{1/2}E_2(\varrho)$, where ϕ_s is the maximum amplitude of the plasma wave, $\varrho = 1-(1+\phi_s)^{-2}$, and E_2 is the complete elliptic integral of the second kind. In the limit $\phi_s^2 \ll 1$, $\lambda_{Np} \simeq \lambda_p(1+3\phi_s^2/16)$, which indicates that the nonlinear plasma wavelength increases as the plasma wave amplitude increases. Hence, in the limit $\phi_s^2 \ll 1$, the nonlinear plasma wave number is given by

$$k_{Np} \simeq k_p(1 - 3\phi_s^2/16). \tag{34}$$

The detuning and saturation of the plasma wave can be estimated as follows. The growth of the plasma wave will stop when the phase difference between the laser beat wave and the plasma wave is $\pi/2$, i.e., $\int d\zeta(k_p - k_{Np}) \simeq \pi/2$. Using the linear result for the plasma wave amplitude, $\phi_s = a_1 a_2 k_p|\zeta|/4$, yields a detuning distance $L_t = (2\pi/a_1^2 a_2^2)^{1/3}4/k_p$. Hence, the plasma wave amplitude will saturate after a distance L_t behind the front of the laser beam, which gives a plasma wave amplitude of $\phi_{\rm sat} = (2\pi a_1 a_2)^{1/3} = E_{\rm max}/E_0$. A more careful derivation (Rosenbluth and Liu, 1972) of resonant detuning yields a maximum value of the electric field at saturation of

$$E_{\rm max}/E_0 = (16 a_1 a_2/3)^{1/3}, \tag{35}$$

which assumes that the laser beat frequency is exactly equal to the ambient plasma frequency $\Delta\omega = \omega_p$. Saturation occurs because the plasma wave period increases as the wave grows. Hence, to partly compensate for the increasing nonlinear plasma period, the plasma wave can be driven to higher amplitudes by using a laser beat period which is slightly longer (Tang *et al.*, 1985). In other words, the beat frequency is slightly detuned such that $\Delta\omega < \omega_p$. Tang *et al.* (1985) showed that the optimum detuning, which maximizes the plasma wave amplitude at saturation, is given by

$$\Delta\omega_{\rm opt}/\omega_p = 1 - (9 a_1 a_2)^{2/3}/8. \tag{36}$$

This gives a maximum saturation amplitude of

$$E_{\rm max}/E_0 = 4(a_1 a_2/3)^{1/3}. \tag{37}$$

The above results are valid in the limit of weak pump amplitudes $a_1 a_2 \ll 1$ for which the plasma wave is driven to saturation over a large number of beat periods. In the highly nonlinear regime, $a_1 a_2 \gtrsim 1$, however, the same general concepts apply to beat wave generation, i.e., the beat wave amplitude is limited by the increasing nonlinear plasma wavelength and the beat wave amplitude can be optimized by increasing the beat wave period such that $\Delta\omega < \omega_p$. To illustrate this, Eq. (17) is solved numerically (Umstadter *et al.*, 1995) for a laser beat wave consisting of four beat periods, as shown in Fig. 9. The amplitudes of the lasers are $a_1 = a_2 = a_0$, with $a_0 = 1.2$, and linear polarization is assumed, such that $(a_1 a_1)_s = a_0^2/2$, where the subscript s refers to an averaging over the fast laser period. The ambient plasma density is $n_0 = 10^{16}$ cm^{-3} ($\lambda_p = 330$ μm). The case $\Delta\omega = \omega_p$ is shown in Fig. 9(a), and it is clear that the plasma wave amplitude saturates (reaches maximum amplitude) after just the second beat pulse. The effect of the third and fourth beat pulses is to drive the plasma

wave down to a low amplitude. In Fig. 9(b) the beat period has been optimized numerically such that the plasma wave amplitude after the fourth beat pulse is maximized, i.e., the beat period is increased $\Delta\omega < \omega_p$ such that the length of the beat pulse is closer to the final nonlinear plasma wavelength λ_{Np}. This results in a dramatic increase in the final amplitude of the plasma wave electric field, $E_{\max} \simeq 1.4\ E_0 = 13$ GV/m, in comparison to the $\Delta\omega = \omega_p$ case.

The resonant detuning can be overcome by chirping the lasers to compensate for the change in nonlinear plasma wavelength (Deutsch *et al.*, 1991), resulting in a significant increase in the plasma wave amplitude. A modified version of the PBWA based on autoresonant phase locking of the plasma wave to the slowly chirped beat frequency of the driving lasers has also been proposed (Lindberg *et al.*, 2004, 2006). This autoresonant method allows plasma wave amplitudes beyond the detuning limit and is relatively insensitive to variations in plasma and laser parameters.

In addition to resonant detuning, the plasma wave amplitude in the PBWA can be limited by laser-plasma instabilities. Experiments at Ecole Polytechnique observed saturation of the beat-generated plasma wave by a parametric coupling to ion waves (Amiranoff *et al.*, 1992). In general, since the laser pulse lengths in the PBWA are long, $L > \lambda_p$, the beams are subject to various laser-plasma instabilities, which are discussed in Sec. VI.

The observation of plasma wave generation in the PBWA via Thomson scattering was first demonstrated by Clayton *et al.* (1985) and later observed by several groups (Amiranoff *et al.*, 1992; Clayton *et al.*, 1993; Kitagawa *et al.*, 1992). Acceleration of background plasma electrons in the PBWA was first observed by Kitagawa *et al.* (1992) using two lines of a CO_2 laser in a plasma of density 10^{17} cm^{-3}. Plasma electrons were trapped and accelerated to an energy in excess of 10 MeV. A plasma wave amplitude of $\delta n/n_0 = 0.05$ was observed and an acceleration gradient of 1.5 GV/m was estimated. Clayton *et al.* (1993) observed electron acceleration in a series of PBWA experiments preformed at the University of California at Los Angeles (UCLA) using two lines of a CO_2 laser in a plasma of density 9×10^{15} cm^{-3}. A 28 MeV energy gain was observed using a 2 MeV injected electron beam, corresponding to a gradient of 2.8 GV/m and a plasma wave amplitude of $\delta n/n_0 = 0.28$. The UCLA experiments were particularly well diagnosed and various laser-plasma interaction phenomena and instabilities have been observed (Everett *et al.*, 1995a; Leemans *et al.*, 1991, 1992). In experiments at Ecole Polytechnique, Amiranoff *et al.* (1995) observed acceleration in a PBWA experiment using two Nd laser lines in a plasma of density 10^{17} cm^{-3}. The energy of a 3.4 MeV injected electron beam was observed to increase by 1.4 MeV. A plasma wave amplitude of 2% and a gradient of 0.6 GV/m were observed. Plasma wave saturation and parametric coupling to ion waves were also observed in these experiments (Amiranoff *et al.*, 1995). Nonresonant beat wave excitation has also been explored as a method for operating at higher plasma densities (Filip *et al.*, 2004). Extended laser-plasma interaction lengths have been achieved in PBWA experiments through plasma-channel generation (Tochitsky *et al.*, 2005), resulting in enhanced energy gain of injected electrons.

Parametric excitation of plasma waves by counter-propagating lasers has also been explored (Shvets *et al.*, 2002). For example, plasma wave generation via four-wave mixing is possible: two co-propagating laser pulses detuned by ω_p interact with a counter-propagating laser, driving two slow phase velocity waves, and the beating of these slow waves (a super-beat wave) drives a fast plasma wave for acceleration. A variation of scheme is to replace the two detuned co-propagating lasers with a single frequency ultra-short resonant laser pulse (Shvets *et al.*, 1999). The laser intensities required for a given accelerating gradient can be smaller for the counter-propagating geometry compared to the PBWA.

C. Multiple laser pulses

In the previous section discussing the PBWA, it was pointed out that (i) the laser beat wave acted in effect as a series of short laser pulses, (ii) as the plasma wave grew the plasma period increased which led to a loss of resonance with respect to the laser beat pulses, and (iii) the beat period, i.e., the width of the beat pulses, could be adjusted and optimized to maximize the plasma wave amplitude. These general principles can be extended to describe plasma wave generation by a series of short laser pulses (Berezhiani and Murusidze, 1992; Bonnaud *et al.*, 1994; Dalla and Lontano, 1994; Nakajima, 1992; Umstadter *et al.*, 1994). For example, the resonant laser-plasma accelerator (Umstadter *et al.*, 1994) uses an optimized train of short laser pulses to drive a plasma wave, in which the width of each pulse and the spacing between pulses is independently controlled. By optimizing the pulse widths and interpulse spacings, resonance with the plasma wave can be maintained and saturation of the plasma wave by resonant detuning can be eliminated. A sequence of m pulses is optimized when the pulse widths and spacings are chosen to maximize the plasma wave amplitude.

For square pulses in the linear regime ($a^2 \ll 1$ and $E_{\max}/E_0 \ll 1$), the optimum pulse train consists of m identical pulses, each of width $L = \lambda_p/2$ and separated by a distance $(2\ell + 1)\lambda_p/2$, where ℓ is an integer. The plasma wave amplitude will be m times the single pulse value, $E_{\max}/E_0 = ma_0^2$. This result neglects nonlinear effects. In particular, as the nonlinear plasma wavelength increases, resonant detuning will eventually saturate the plasma wave amplitude.

In the nonlinear regime, however, resonance can only be maintained by optimizing both the pulse widths and spacings of each individual pulse. In the 1D limit with $\omega_p^2/\omega^2 \ll 1$, this can be examined by solving Eq. (17).

For square pulse profiles, analytic solutions can be obtained. It can be shown (Bonnaud *et al.*, 1994; Dalla and Lontano, 1994) that the optimal width of the mth pulse L_m, the nonlinear wavelength λ_{Nm} of the wake behind the mth pulse, and the electric field amplitude E_{zm} of the wake behind the mth pulse are given by

$$L_m = (2/k_p)x_m^{1/2}E_2(y_m), \tag{38}$$

$$\lambda_{Nm} = (4/k_p)x_m^{1/2}E_2(\hat{y}_m), \tag{39}$$

$$E_{zm}/E_0 = x_m^{1/2} - x_m^{-1/2}, \tag{40}$$

where $x_m = \gamma_{\perp 1}^2\gamma_{\perp 2}^2\cdots\gamma_{\perp m}^2$, $\gamma_{\perp m}^2 = 1 + a_m^2$, a_m is the amplitude of the mth pulse, E_2 is the complete elliptic integral of the second kind, $y_m^2 = 1 - \gamma_{\perp m}^2 x_m^{-1/2}$ and $\hat{y}_m^2 = 1 - x_m^{-1/2}$. The optimal spacing between the end of the mth pulse and the beginning of the mth+1 pulse is given by $(2\ell+1)\lambda_{Nm}/2$ (ℓ =integer). The maximum normalized electric field of the wake $E_{\max}/E_0$, for an optimized train of m square pulses of equal amplitudes $a_m = a_0$, is plotted in Fig. 10 versus the quantity $a_T^2 = ma_0^2$ (Bonnaud *et al.*, 1994; Dalla and Lontano, 1994). The curves show the results for 1, 3, 4, 10, and 100 pulses. In the linear regime, $E_{zm} = mE_{z1} = ma_0^2E_0$, i.e., these curves are just straight lines. Figure 10, however, shows that in the nonlinear regime, m pulses are more efficient than the linear result, i.e., $E_{zm} > mE_{z1}$. In the highly nonlinear regime, this enhancement can be quite dramatic. Furthermore, Fig. 10 indicates that just a few optimized square pulses are far more efficient than a single pulse.

For square pulse profiles, both the width of the pulse and the spacing between pulses increases for subsequent pulses in the train, since the nonlinear wavelength of the plasma wave is increasing. For more realistic pulse profiles, this is not necessarily the case. Consider the electric field envelope of each pulse modeled by a half period of a sine function, e.g., $a = a_1\sin(\pi\zeta/L_1)$, with $0 < \zeta < L_1$, for the first pulse. The result from a numerical optimization (Bonnaud *et al.*, 1994; Dalla and Lontano, 1994) of Eq. (17) for a train of four sine pulses is shown in Fig. 11. Here, the plasma density is $n_0 = 10^{16}$ cm^{-3} and the pulses are linearly polarized with equal amplitudes $a_m = a_0 = 1.2$. Notice that the pulse width is decreasing, i.e., the width of the first pulse is 940 fs, whereas the width of the fourth laser pulse is 200 fs. From Fig. 11, it can be seen that the pulses are optimized when they reside in the region of the plasma wave for which $\phi < 0$ and $d\phi/d\zeta < 0$, where $\zeta = z - ct$. This is the phase region of the plasma wave for which the laser pulse drives the plasma wave most efficiently. As in the square wave case, λ_{Nm}, and thus the spacing between pulses, increases with each succeeding pulse. For this example, the total laser fluence for the pulse train is $I\tau_{\rm tot} = 2.2$ MJ/cm^2 and the final accelerating field is $E_{\max} \simeq 1.9\ E_0 = 18$ GV/m.

Several techniques may generate a train of short, intense pulses using CPA laser systems (Bonnaud *et al.*, 1994; Dalla and Lontano, 1994). One possible method is to divide the amplified stretched pulse by use of beam splitters, then send the separate pulses to separate compressors with adjustable lengths and delays. Alternatively, Fourier filtering can by used by placing a mask in the pulse stretcher to modify the phase and/or amplitude of the frequency components of the pulse in such a way that, when it is recompressed, a series of pulses with arbitrary spacings and widths will be produced. Preliminary experiments on similar methods have been reported (Liu *et al.*, 1995).

D. Self-modulated laser wakefield accelerator

In the previous section it was described how a train of laser pulses can be used to generate a large amplitude wakefield. Under appropriate conditions, however, it is possible for a single, long laser pulse to break up into a train of short pulses, each of these short pulses having a width on the order of λ_p. Associated with the break up of the long pulse and the formation of the pulse train is a large amplitude plasma wave. This process is referred to as self-modulation (Andreev *et al.*, 1992; Antonsen, Jr. and Mora, 1992; Chen *et al.*, 2004; Coverdale *et al.*, 1995; Esarey *et al.*, 1993a; Gordon *et al.*, 1998; Joshi *et al.*, 1981; Leemans *et al.*, 2002, 2001; Malka *et al.*, 2001; Modena *et al.*, 1995; Moore *et al.*, 1997; Nakajima *et al.*, 1995; Sprangle *et al.*, 1992; Wagner *et al.*, 1997) and was first observed in fluid simulations (Andreev *et al.*, 1992; Antonsen, Jr. and Mora, 1992; Sprangle *et al.*, 1992) of relativistically guided laser pulses. Physically, self-modulation occurs from the plasma wave producing periodic regions of enhanced focusing and diffraction (Esarey *et al.*, 1994). The self-modulation instability resembles a highly 2D version of a forward Raman instability. Forward Raman scattering occurs simultaneously, adding to the modulation, and in the 1D limit, pulse modulation can occur via forward Raman scattering alone (Mori *et al.*, 1994).

The process by which a plasma wave can modulate a laser pulse by producing periodic regions of enhanced focusing and diffraction was first described and analyzed by Esarey and Ting (1990). The self-modulation of relativistically-guided laser pulses was observed in the simulations of Andreev *et al.* (1992), Sprangle *et al.* (1992), and Antonsen, Jr. and Mora (1992, 1993). Krall *et al.* (1993) simulated a self-modulated LWFA, including the acceleration of an injected electron beam, and showed that this configuration can have certain advantages over the standard LWFA. The self-modulation instability was subsequently analyzed by Esarey *et al.* (1994) and Andreev *et al.* (1994, 1995) and, in the 1D limit, RFS was analyzed by Mori *et al.* (1994). Extensive particle-in-cell simulations of short, intense pulses propagating in the high density regime have been carried out by Decker *et al.* (1994) and Bulanov *et al.* (1995).

To operate in the self-modulated regime (Andreev

et al., 1994, 1995; Antonsen, Jr. and Mora, 1992, 1993; Esarey *et al.*, 1994, 1993a; Krall *et al.*, 1993; Sprangle *et al.*, 1992), it is desirable that (i) the pulse length be long compared to the plasma wavelength, $L > \lambda_p$, and (ii) the pulse power to be larger than the power required to guide a long laser beam, $P > P_c(1 - \Delta n/\Delta n_c)$. Here, $P_c = 17(\omega/\omega_p)^2$ GW is the critical power required for relativistic optical guiding, Δn is the depth of a preformed parabolic density channel (if present), $\Delta n_c = 1/\pi r_e r_0^2$ is the critical channel depth, and r_e is the classical electron radius. The optical guiding of laser pulses by relativistic effects and density channels will be discussed more completely in the Sec. V. In the remainder of this section, it will be assumed that the laser pulse is propagating in an initially uniform plasma ($\Delta n = 0$). Since $\lambda_p \propto n_0^{-1/2}$ and $P_c \propto n_0^{-1}$, for fixed laser parameters, the conditions $L > \lambda_p$ and $P > P_c$ can usually be satisfied by operating at a sufficiently high plasma density.

Consider the possibility of generating wakefields with a 300 fs ($L = 90$ μm) laser pulse of wavelength $\lambda = 1$ μm and power $P = 10$ TW. To operate in the standard LWFA configuration, $L \simeq \lambda_p$ implies a density of $n_0 \simeq 1.4 \times 10^{17}$ cm^{-3}. At this density $P \ll P_c \simeq 140$ TW and the effects of relativistic guiding are unimportant. To operate in the self-modulated regime, it is desirable that $L > \lambda_p$ and $P > P_c$. Choosing a plasma density such that $P = 1.5\ P_c$ implies $n_0 \simeq 2.8 \times 10^{18}$ cm^{-3} and $L \simeq 4.5\ \lambda_p$. Hence, for this laser pulse, the self-modulated regime can be reached by increasing the plasma density by a factor of 20 compared to the standard LWFA configuration. Furthermore, the corresponding energy gain can be enhanced by nearly a factor of 10 compared to the standard LWFA configuration, as is indicated by simulations discussed below.

The advantages of the self-modulated LWFA over the standard LWFA are simplicity and enhanced acceleration. Simplicity in that a matching condition of $L \simeq \lambda_p$, a preformed density channel, or special pulse tailoring are not required. Enhanced acceleration is achieved for several reasons: (i) The self-modulated LWFA operates at higher density, hence a larger wakefield will be generated, since $E_z \propto 1/\sqrt{n_0}$, as indicated by Eq. (11). (ii) Since $P > P_c$, the laser pulse will tend to focus to a higher intensity, thus increasing a_0 and E_z. (iii) The wakefield is resonantly excited, i.e., excited by a series of beamlets as opposed to a single pulse as in the standard LWFA. (iv) Relativistic optical guiding allows the modulated pulse structure to propagate for several Rayleigh lengths, thus extending the acceleration distance. The disadvantages of the self-modulated LWFA are (i) at higher densities the laser pulse group velocity ($\simeq$ the plasma wakefield phase velocity) decreases and, hence, electron dephasing from the plasma wakefield can limit the acceleration distance, and (ii) the modulated pulse structure eventually diffracts.

The properties of the self-modulated LWFA are illustrated by the following simulations (Krall *et al.*, 1993). For fixed laser pulse parameters, two cases will be considered: (1) a standard LWFA in which $L \simeq \lambda_p$ and $P < P_c$ and (2) a self-modulated LWFA, in which $L > \lambda_p$ and $P > P_c$. The laser parameters for both these cases are identical: a Gaussian axial intensity profile with a pulse length $L = 90$ μm (300 fs), $\lambda = 1$ μm, $a_0 = 0.7$, $r_0 = 31$ μm (in vacuum, which corresponds to $Z_R = 3$ mm), $P = 10$ TW, and a pulse energy of 1.5 J. The simulation begins at $t = 0$ as the laser pulse enters the plasma, initially converging such that in vacuum it would focus to a minimum spot size of $r_0 = 31$ μm at $ct = 3Z_R$. The plasma density is initially increasing, reaching full density at $ct = 2Z_R$. The simulation continues until $ct = 10Z_R = 3$ cm. In both cases, the acceleration and trapping of a continuous electron beam with initial energy of 3 MeV and normalized emittance $\varepsilon_n = 130$ mm-mrad is considered. The electron beam is initially converging such that in vacuum it would focus to a minimum RMS radius $r_b = 200$ μm at $ct = 3Z_R$. With such a large initial emittance, only a small fraction ($\sim 1\%$) of the particles will be trapped and accelerated.

For the standard LWFA, Case (1), the requirement $L = \lambda_p = 90$ μm implies a density of $n_0 = 1.4 \times 10^{17}$ cm^{-3}. At this density, $P \ll P_c = 140$ TW, such that relativistic guiding effects are unimportant. The presence of the plasma has little effect on the evolution of the laser pulse, which reaches a peak intensity of $|a|^2 = 0.56$ at $ct = 3Z_R$. The evolution of the spot size, Fig. 12, is very close to vacuum diffraction. This is also evident in Fig. 13(a) (dashed line), where the peak accelerating field, plotted versus time, is symmetric about the focus, $ct = 3Z_R$. After $ct = 10Z_R = 3$ cm, a small fraction ($\sim 0.1\%$) of the test electron beam particles have been trapped and accelerated. At $ct = 2$ cm, the peak particle energy is 48 MeV, which implies an average acceleration of 2.4 GeV/m, as shown in Fig. 13(b) (dashed line).

For the self-modulated LWFA, Case (2), the density is increased such that $P = 1.5P_c = 10$ TW, which implies $n_0 = 2.8 \times 10^{18}$ cm^{-3}, which is 20 times higher than in Case (1). At this density $L > \lambda_p = 20$ μm, i.e., the laser pulse now extends over $\simeq 4.5\ \lambda_p$. Figure 14 shows the laser intensity at (a) $ct = 2Z_R$ and (b) $ct = 3.2Z_R$. The axial electric field and the plasma density response on-axis at $ct = 3.2Z_R$ are shown in Figs. 15(a) and 15(b), respectively. The laser pulse has become modulated (three peaks are observable, separated by λ_p) and the plasma wave is highly nonlinear. In addition, relativistic optical guiding effects have focused the laser to a much higher intensity than was observed in Case (1). The evolution of the laser spot size is shown in Fig. 12 indicating that the pulse has focused to a smaller spot size and remains guided over $\simeq 5.5Z_R$. A plot of the peak accelerating field versus time, Fig. 13(a) (solid line), shows that the highly nonlinear fields persist as the laser pulse is optically guided. A maximum accelerating field of $\simeq 130$ GV/m was obtained. Because of the larger fields, a greater fraction (2%) of the test electron beam particles were trapped and accelerated. The peak particle energy of 430 MeV is observed at $ct = 6Z_R = 1.8$ cm.

At $ct = 10Z_R = 3$ cm, however, the peak particle energy has dropped to 290 MeV due to the reduced group velocity of the laser pulse, which causes the electrons to slip out of phase with the wakefield and become decelerated. Figure 13(b) (solid line) shows acceleration to 430 MeV over 1.8 cm which gives an average gradient of 24 GeV/m. This is an order of magnitude increase compared to the standard LWFA of Case (1). In the above fluid simulations, the excited plasma wave was below wavebreaking $E < E_{\rm WB}$, and an externally injected electron beam was used. However, in the experiments discussed below, it is possible to drive the plasma wave in the self-modulated regime to wavebreaking, resulting in copious amounts of self-trapped electrons, albeit with large energy spread.

Evidence for plasma wave generation in the high-density, self-modulated regime was first detected by Coverdale *et al.* (1995). The presence of a plasma wave leads to the generation of Stokes and anti-Stokes lines in the frequency spectrum of the pump laser pulse. The first two anti-Stokes lines were observed by Coverdale *et al.* (1995), the appearance of which were correlated with production of fast electrons, as discussed below. Subsequently, multiple anti-Stokes lines in the forward spectrum of the pump laser have been observed by several other groups (Modena *et al.*, 1995; Ting *et al.*, 1996; Wagner *et al.*, 1997). The plasma wave generation in the self-modulated regime has been measured via coherent Thomson scattering with a frequency-doubled probe pulse (Le Blanc *et al.*, 1996; Ting *et al.*, 1996). The evolution of the plasma wave was observed by varying the time delay between the pump and probe pulses. Evidence for self-channeling and plasma waves excitation over the length of the channel (4 mm, or $\approx 12Z_{\rm R}$) has also been measured via $90^{\rm deg}$ Thomson scattering (Clayton *et al.*, 1998).

Joshi *et al.* (1981) detected fast electrons in an early experiment via forward Raman scattering. A single, long (700 ps), CO_2 laser pulse of modest intensity (10^{15} W/cm^2) interacting with a thin Carbon foil was observed to produce 1.4 MeV electrons. Electron acceleration in the high-density, self-modulated regime has been observed using ultrashort pulses ($\lesssim 1$ ps). Nakajima *et al.* (1995) observed electron acceleration to energies ≥ 18 MeV using a 3 TW, 1 ps, 10^{17} W/cm^2 laser pulse in a plasma of density near 10^{19} cm^{-3}. A laser-solid interaction was used to produce a source of injected electrons with energies near 1 MeV. Particle simulations in 1D suggested acceleration gradients on the order of 30 GV/m. Coverdale *et al.* (1995) observed 2 MeV electrons, which were trapped and accelerated from the background plasma, when a 600 fs, 5 TW, 8×10^{17} W/cm^2 laser pulse propagated in a plasma of density 2×10^{19} cm^{-3}. The generation of electrons was also correlated with the occurrence of anti-stoke lines in the laser pulse spectrum, which indicates the presence of a plasma wave. Modena *et al.* (1995) demonstrated the acceleration of self-trapped electrons to energies ≥ 44 MeV (limit of the detector) using a 1 ps, 20 TW, 5×10^{18} W/cm^2 laser pulse in a plasma of density 1.5×10^{19} cm^{-3}. A large flux of electrons was observed (10^6 electrons/MeV at 44 MeV) and the electron signal was correlated to the broadening of the 5 anti-Stokes lines in the laser spectrum. Estimates based on the electron dephasing length imply an acceleration gradient > 100 GV/m. Acceleration of self-trapped electrons has also been observed by Wagner *et al.* (1997). The electrons were emitted in a well-collimated beam in the forward direction (a divergence angle $\simeq 8^\circ$) and the cross-section of the beam resembled the shape of the cross-section of the laser at focus. By varying the laser pulse energy, a threshold for electron acceleration was observed near $P \simeq P_c$. Subsequently, other research groups have measured energetic electron production in the self-modulated regime (Gordon *et al.*, 1998; Leemans *et al.*, 2001; Malka *et al.*, 2001; Moore *et al.*, 1997). The plasma density dependence on the the electron spectra has been studied, and it was confirmed that the maximum energy increased with decreasing plasma density (Malka *et al.*, 2001), providing further evidence of electron acceleration via plasma waves.

Experiments have shown the importance of pulse shape on self-modulation and electron production (Leemans *et al.*, 2002). These experiments compared electron production for laser pulses with slow and fast rise times. For fast rise times the ponderomotive force is larger, resulting in a larger initial plasma wave, which acts as the seed for the self-modulation instability (Schroeder *et al.*, 2003a). Seeding of self-modulation by ionization-induced wakefields (Fisher and Tajima, 1996; Mori and Katsouleas, 1992) has been studied by Gordon *et al.* (2001), and controlled seeding via ionization-induced wakefields has been demonstrated experimentally (Chen *et al.*, 2004). Experiments and simulations by Malka *et al.* (2002) have discussed an intermediate regime between the standard and self-modulated LWFA, in which the laser pulse is only somewhat longer than the plasma wavelength. In this regime, the pulse undergoes significant self-steepening, resulting in enhanced plasma wave generation.

Another process that can contribute to acceleration in the self-modulated regime ($\lambda_p < L$ and $P > P_c$) is direct laser acceleration (Pukhov *et al.*, 1999). In this mechanism, it is necessary that the accelerated electrons undergo transverse betatron oscillations. When the betatron frequency ω_β is near the laser frequency in the frame of the accelerated electrons, $\omega \sim 2\omega_\beta \gamma^2/\gamma_\perp^2$, energy can efficiently exchange between the electrons and the transverse laser field. This is the inverse process of the electromagnetic instability responsible for the ion channel laser (Whittum *et al.*, 1990). The transverse betatron oscillations are produced by a transverse force that can result from a variety of mechanisms, e.g., the radial structure of the plasma wave ($\phi = \phi_0 \exp(-2r^2/r_0^2)\cos[k_p(z-ct)]$ for a Gaussian laser in the linear regime), forces resulting from induced magnetic fields, or, in the blowout regime, from the formation of an ion channel through the expulsion of background plasma electrons by the radial pon-

deromotive force of the laser. In the blowout regime ($\phi_0 \sim k_p^2 r_0^2/8$), the electrons oscillate with the betatron frequency $\omega_\beta \simeq \omega_p/(2\gamma)^{1/2}$ (Esarey *et al.*, 2002). Gahn *et al.* (1999) have reported multi-MeV electrons accelerated by a 1.2 TW, 200 fs laser pulse channeling in a high-density (10^{20} cm^{-3}) plasma, and have attributed the dominant acceleration process to direct laser acceleration.

E. Blow-out regime

In the mildly relativistic wakefield regime ($a^2 \ll 1$), the wakefield can be described analytically in 3D using cold fluid theory, as is Sec. II.B, which is valid provided that the perturbed fluid quantities remain small (e.g., the perturbed density $|\delta n| \ll n_0$). In the high intensity limit ($a^2 \gtrsim 1$), the wakefield can be described analytically in the 1D limit (broad pulse $k_p r_0 \gg 1$), as in Sec. II.C. However, for a radially bounded pulse in 3D ($k_p r_0 \lesssim 1$) in the high intensity limit, the wakefield must typically be described numerically. For a bounded pulse in 3D, as the intensity increases, the wakefield structure can depart significantly from the sinusoidal form described by linear theory. In addition to wave steepening and period lengthening, which occur in the 1D limit, the radial structure of the wake can exhibit nonlinearities. One such effect is that the wavefront of the plasma wave can be curved, the curvature of which becomes more severe the greater the distance behind the driver, as a result of the nonlinear plasma wavelength being greater on axis (were the wake amplitude is high) than off axis. Another effect is that the laser intensity can be sufficiently high so as to completely expel all of the plasma electrons from the vicinity of the axis (Faure *et al.*, 2004; Geddes *et al.*, 2004; Gordienko and Pukhov, 2005; Mangles *et al.*, 2004; Pukhov and Meyer-ter-Vehn, 2002). This high intensity, 3D regime has been referred to as the blow-out, bubble, or cavitation regime.

This regime of complete expulsion of the plasma electrons from some region about the axis has been studied for both laser (Pukhov and Meyer-ter-Vehn, 2002) and electron beam drivers [referred to as a plasma wakefield accelerator (PWFA)] (Rosenzweig *et al.*, 1991). For electron beam drivers, the blow-out regime was first studied by Rosenzweig *et al.* (1991), and more recently, by the PWFA collaboration using the 30 GeV electron beam at the Stanford Linear Accelerator Center (SLAC) to drive plasma waves (Hogan *et al.*, 2000, 2005). In the blow-out regime of the PWFA ($n_b/n_0 > 1$, $k_p\sigma_z < 1$ and $k_p\sigma_r < 1$, where σ_z and σ_r are the axial and radial bunch lengths, respectively), all the plasma electrons can be expel from the vicinity of and immediately behind the driver. The blow-out region of the wake is characterized by an accelerating field that is constant as a function of radius and varies linearly as a function of distance behind the driver, and a focusing field that is linear as a function of radius. This regime can have beneficial accelerating properties, e.g., because the focusing forces are linear, the emittance of an accelerated electron bunch will be preserved. In the experiments at SLAC, the blow-out wake has led to an energy gain of more than 40 GeV for the electrons in the tail of the drive bunch (Blumenfeld *et al.*, 2007). The majority of electrons in the body of the drive bunch lost energy, which represents the energy needed to generate the plasma wave.

The radial force on a highly relativistic accelerated electron is primarily due to the space charge force of the resulting ion channel. In the blow-out regime, the radial space charge electric field is $E_r = (mc^2/e)k_p^2 r/2 = (k_p r/2)E_0$. At the edge of the of an electron bunch with radius r_b, this can be written in convenient units as $E_r(\mathrm{MV/m}) \simeq 9.06 \times 10^{-15} n(\mathrm{cm}^{-3}) r_b(\mu\mathrm{m})$. For example, this radial force will cause an accelerated electron with $\gamma \gg 1$ to perform betatron oscillations about the axis with a betatron wavelength $\lambda_\beta = (2\gamma)^{1/2}\lambda_p$ (Esarey *et al.*, 2002). Particle-in-cell simulations (Lu *et al.*, 2005) indicate that linear wake result for E_z is fairly accurate in the blow-out region provided $n_b/n_0 \leq 10$, assuming a gaussian drive bunch with $k_p\sigma_z = \sqrt{2}$ and $k_p\sigma_r < 0.3$.

An example of an electron beam driven wake in the blow-out regime is shown in Fig. 17 which shows the spatial plasma density response to an electron beam with energy 0.5 GeV, density $n_b = 10n_0$, rms longitudinal beam size $k_p^2\sigma_z^2 = 2$ (Gaussian longitudinal profile), and rms transverse beam size $k_p^2\sigma_x^2 = 2$ (Gaussian transverse profile), propagating in an initially uniform plasma of density $n_0 = 5 \times 10^{17}$ cm^{-3}. The electron beam is moving toward the right with its center located at $k_p z = 454$. These electron beam parameters are similar to those produced by laser wakefield accelerator experiments at LBNL (Leemans *et al.*, 2006). Figure 17 was obtained using a modified version of the particle-in-cell code PSC (Ruhl, 2000) in 2D using 25 particles per cell and a transverse and longitudinal cell size of 0.33 micron (32 cells per rms beam radius).

For laser drivers, plasma blow-out can occur in many regimes, including the long pulse, self-modulated, and standard LWFA regimes (Kurki-Suonio *et al.*, 1989a; Mora and Antonsen, Jr., 1996; Sprangle *et al.*, 1992; Sun *et al.*, 1987). For example, for a long laser pulse (with a slowly varying axial profile) in a plasma (Sun *et al.*, 1987), the plasma density profile is determined by balancing the radial ponderomotive force with the space charge force. The plasma density in the long pulse, adiabatic limit is then given by

$$n/n_0 = 1 + k_p^{-2}\nabla_\perp^2(1+a^2)^{1/2}, \tag{41}$$

assuming circular polarization. For a Gaussian pulse profile, $a^2 = a_0^2 \exp(-2r^2/r_0^2)$, the on-axis ($r = 0$) density is $n(0)/n_0 = 1 - (4/k_p^2 r_0^2)a_0^2/(1+a_0^2)^{1/2}$. This indicates that complete blowout of the plasma electrons, $n(0) \leq 0$, occurs for a laser intensity satisfying $a_0^2/(1+a_0^2)^{1/2} \geq k_p^2 r_0^2/4$. In the high intensity limit $a_0^2 \gg 1$, blow-out requires $a_0 \geq k_p^2 r_0^2/4$ or, alternatively, a spot size

$r_0 \leq (2/k_p)a_0^{1/2}$. To cavitate the electrons out to a larger radius requires larger intensity. For example, a blow-out region of $r = r_0/\sqrt{2}$ requires $a_0 = 0.82k_p^2r_0^2$, assuming $a_0^2 \gg 5.4$.

For a short ($L \lesssim \lambda_p$), intense ($a^2 \gtrsim 1$) pulse, i.e., a standard LWFA in the highly nonlinear regime, the generation of a large amplitude wake can occur simultaneously with plasma blow-out, in a manner analogous to that of an electron beam driver in the PWFA. Laser blow-out with moderately short pulses was studied by Mora and Antonsen, Jr. (1996) for laser intensities in the range $a_0 = 0.25 - 3$, spot sizes $k_pr_0 = 4 - 16$, and pulses lengths $k_pL \sim 10$ using a quasi-static, time-averaged particle code. Observed was self-steepening, pulse shortening (to $k_pL \sim 2$), self-focused propagation up to $30Z_R$ through an initially uniform plasma, and the complete cavitation (blow-out) of the electrons from the region of the laser pulse with the formation of a highly nonlinear wake. Also observed was the self-trapping of relativistic particles in the wake.

An example of a cavitated wake driven by a short laser pulse in the mildly relativistic regime ($a_0^2 \ll 1$) is shown in Fig. 17, which shows the spatial plasma density response to a laser pulse with $a_0 = 0.35$, rms length 100 μm (half-sine longitudinal profile), spot size $r_0 = 10$ μm (Gaussian transverse profile), and wavelength $\lambda = 0.8$ μm, propagating in an initially uniform plasma of density $n_0 = 8 \times 10^{15}$ cm^{-3} (plasma wavelength $\lambda_p = 300$ μm). The laser is moving toward the right (peak laser field located at $k_pz = 4.9$). Figure 17 was obtained using a modified version of the particle-particle-in-cell code PSC (Ruhl, 2000) in 2D using 4 particles per cell, 24 cells per laser wavelength longitudinally, and 6 cells per laser wavelength transversely.

Laser blow-out with short ($L < \lambda_p$), ultra-intense ($a^2 \gg 1$) pulses has been studied using particle-in-cell simulations and theoretical modelling (Gordienko and Pukhov, 2005; Lu *et al.*, 2006; Pukhov and Meyer-ter-Vehn, 2002; Tsung *et al.*, 2004). For example, Gordienko and Pukhov (2005) present a similarity theory in which the blow-out wake is characterized by the similarity parameter $S = k_p^2/a_0k^2$. They find that optimal wake generation occurs for a laser spot radius of $k_pr_0 \approx a_0^{1/2}$, a pulse length $L = c\tau \leq r_0$, and a power $P > 30(\tau[\mathrm{fs}]/\lambda[\mu\mathrm{m}])^2$ GW. Furthermore, they predict an acceleration length $L_{acc} \approx 0.7(L/\lambda)Z_R$ and the formation of a quasi-monoenergetic electron bunch with energy $E_{mono} \approx 0.65mc^2(L/\lambda)(P[\mathrm{GW}]/8.5)^{1/2}$. Simulation examples are given with $a_0 = 10 - 80$. For the $a_0 = 80$ case (1.5 kJ pulse energy), a quasi-monoenergetic electron peak was observed at 12 GeV after a propagation length of 7200λ.

An analytic theory of wake generation in the blow-out regime has also been carried out by Lu *et al.* (2006). In the high intensity limit ($a_0 \geq 4$), they find that wake generation is optimal when the laser spotsize satisfies $k_pr_0 \simeq 2a_0^{1/2}$. In this case, they predict that the dimensions of the blow-out region, or bubble, is roughly a sphere with a radius $r_B \simeq (2/k_p)a_0^{1/2}$, which is similar to the above result obtained from balancing the radial ponderomotive force with the space charge force. The diameter of the bubble is approximately equal to the nonlinear plasma wavelength $\lambda_{Np} \simeq (2/\pi)(E_m/E_0)\lambda_p \simeq (2a_0^{1/2}/\pi)\lambda_p$, where E_m is the maximum electric field amplitude of the wake. The axial electric field is of the form $E_z = (k_p\zeta/2)E_0$ and is maximum when $\zeta = r_B$, i.e., $E_m = a_0^{1/2}E_0$. The transverse wakefields are electromagnetic with $E_r \simeq (k_pr/4)E_0$ and $B_\theta \simeq -(k_pr/4)E_0$, such that the radial focusing force on a highly relativistic electron moving along the axis is $F_r = E_r - B_\theta = (k_pr/2)E_0$, as noted above. To be in this regime requires a laser power $P \simeq 21.5(a_0r_B/\lambda)^2$ GW, or $P \simeq (a_0^3/8)P_c$ with $a_0 \gtrsim 4$, where P_c is the critical power for relativistic self-focusing. For laser powers in the range $15 \lesssim P \lesssim 100$ TW, reaching the blow-out regime requires plasma densities in the range $2 \times 10^{19} \gtrsim n \gtrsim 2 \times 10^{18}$ cm^{-3}. Particle-in-cell simulations also indicate that electrons can be self-trapped (Faure *et al.*, 2004; Geddes *et al.*, 2004, 2005b; Malka *et al.*, 2005; Mangles *et al.*, 2004; Pukhov and Meyer-ter-Vehn, 2002; Tsung *et al.*, 2004) in the trailing edge of the blow-out region and accelerated up to relativistic energies.

An example of a blow-out wake driven by a short laser pulse in the highly relativistic regime ($a_0^2 \gg 1$) is shown in Figs. 18–20, which shows the spatial plasma density response after propagating $\omega_pt = 127$ [Fig. 18(a)] and $\omega_pt = 633$ [Fig. 18(b)], the spatial profiles of the longitudinal [Fig. 19(a)] and transverse [Fig. 19(a)] electric fields at $\omega_pt = 127$, and line-outs of the longitudinal electric field on axis as a function z [Fig. 19(a)] and the transverse electric field at $k_pz = 113$ as a function of x [Fig. 19(a)] at $\omega_pt = 127$. The initial laser pulse envelope is given by $a = a_0 \exp(-z^2/L^2)\exp(-x^2/r_0^2)$ with $a_0 = 5$, $L = 6$ μm, $r_0 = 9$ μm and $\lambda = 0.8$ μm. The laser enter the plasma of density $n_0 = 7 \times 10^{18}$ cm^{-3} ($\lambda_p = 12$ μm) from the edge of the simulation domain. These result were obtained using a modified version of the particle-in-cell code PSC in 2D with longitudinal cell size $dz = \lambda_0/50$, transverse cell size $dx = \lambda_0/3.2 = r_0/36 = \lambda_p/50$, and 9 particles per cell. The simulation domain uses a moving window that is 80 μm long and 100 μm wide. For these parameters, $k_pr_0 = 4.5 \approx 2\sqrt{a_0}$.

According to the above discussed theories of the blowout regime, the example presented in Figs. 18–20 should produce a spherical bubble with radius $k_pr_B \simeq 2a_0^{1/2}$. For Fig. 18(a), at $\omega_pt = 127$ the peak laser field is $a_0 = 6.3$ (peak at $k_pz = 117$). Hence, theory predicts a bubble diameter of $2k_pr_B \simeq 10$. From Fig. 18(a), however, the bubble is of smaller dimensions and slightly elliptical with a transverse diameter of $2k_pX_B \simeq 7$ (at the position $k_pz = 113$) and a longitudinal diameter of $2k_pZ_B \simeq 8$. For Fig. 18(b), at $\omega_pt = 633$ the peak laser field is similar, $a_0 = 6.2$ (peak at $k_z = 622$), but now the bubble has expanded with transverse diameter of $2k_pX_B \simeq 12$ (a the position $k_pz = 618$) and a longi-

tudinal diameter of $2k_pZ_B \simeq 14$. One reason that the bubble has expanded is that the laser pulse has steepened and shortened, and even thought the peak laser field is approximately the same in Figs. 19(a) and (b), the ponderomotive force is large in Fig. 18(b) due to the larger gradients in the intensity profile due to pulse steepening. Clearly, since the ponderomotive force depends on both the laser intensity amplitude and gradient scale length, so should the properties of the blow-out wake, and this behavior is not captured by the simple scaling law $k_pr_B \simeq 2a_0^{1/2}$, which does not include the effect of the laser intensity gradient scale length or the laser pulse length.

The spatial profiles of the longitudinal and transverse electric fields of the wake are shown in Figs. 19(a) and (b), respectively, at $\omega_p t = 127$. Corresponding lineouts of the longitudinal electric field along the axis as a function of k_pz and the transverse electric field at $k_pz = 113$ as a function of k_px are shown in Figs. 20(a) and (b), respectively. As can be seen in Fig. 20, near the center of the bubble, E_z is approximately a linear function of z and E_x is approximately a linear function of x. Furthermore, the amplitudes of E_z and E_x are comparable, excluding the spike in E_z that occurs near the back of the bubble.

Also evident in Fig. 18(b) is the appearance of a trapped and accelerated electron bunch within the blow-out region. These electrons are self-injected near the back of the bubble. The bunch has a large energy spread with a maximum electron energy of 145 MeV that occurs at the position $k_pz = 610$. The wakefield associated with the trapped bunch can lead to beam loading, which can distort and elongate the blow-out region.

F. Other laser wakefield acceleration regimes

Excitation of large wakefields by laser pulses can be divided roughly in two categories. A "standard" regime in which the laser intensity is sufficiently high ($a_0 \gtrsim 1$) and the laser pulse is sufficiently short (or the gradients in the axial intensity profile sufficient short), $L \lesssim \lambda_p$, such that the initial laser pulse profile immediately drives a large wake. In the standard regime, pulse evolution is not required to excite a large wake. The other general category is the "self-modulated" regime, typically denoted from the standard regime by longer pulses of lower intensities. In the self-modulated regime, the initial laser profile does not immediately drive a sufficiently large wake. In this regime, evolution of the laser pulse is necessary to excite a large wake. Pulse evolution is the result of the initial, low amplitude wake acting back on the laser pulse, such as in the case of the forward Raman or self-modulation instabilities. Although, for some intensity ranges, the standard and self-modulated regimes may correspond to short and long pulse regimes, respectively, there are many intermediate regimes in which self-modulation of the laser pulse by the plasma wave is the dominant mechanism, and some of these regimes have been referred to as "pseudo-resonance" (Kimura *et al.*, 2005) or "forced" laser wakefield regimes (Malka *et al.*, 2002). The precise evolution of both the laser pulse and the wake, however, depends on the precise laser and plasma parameters. Pulse evolution, via the feedback of the wake on the pulse, will eventually play a significant role in the wake evolution in all regimes. Nonlinear effects such as pump depletion and pulse self-steepening will always occur if the laser pulse is allowed to propagate a sufficiently long distance, which effects both the laser profile and the wake amplitude.

G. Acceleration limits and scaling laws

Several mechanisms can limit the energy gain in a laser driven accelerator: laser diffraction, electron dephasing, pump depletion, and laser-plasma instabilities. In vacuum a laser pulse undergoes Rayleigh diffraction, i.e., the laser spot size evolves according to $r_s = r_0(1+z^2/Z_R^2)^{1/2}$, where r_0 is the minimum spot size at the focal point $z = 0$ and $Z_R = kr_0^2/2$ is the Rayleigh length. Without some form of optical guiding, the laser-plasma interaction distance will be limited to a few Z_R. Various methods for optical guiding, such as using a plasma density channel, are discussed in Sec. V. Electron dephasing, i.e., a highly relativistic electron outrunning the plasma wave, can limit the energy gain to a dephasing length L_d, as discussed in Sec. II.E. As the laser driver excites a plasma wave, it loses energy, i.e., it pump depletes (Bulanov *et al.*, 1992; Horton and Tajima, 1986; Teychenné *et al.*, 1994a; Ting *et al.*, 1990). The pump depletion length L_{pd} can be estimated by equating the laser pulse energy to the energy left behind in the wakefield, $E_z^2L_{pd} \simeq E_L^2L$, where E_L is the laser field.

As an illustration, consider a standard LWFA driven by a linearly polarized, square profile laser pulse with $L \simeq \lambda_{Np}/2$ in the 1D limit. The dephasing and pump depletion lengths are given by (Esarey *et al.*, 2004)

$$L_d \simeq \frac{\lambda_p^3}{2\lambda^2} \times \begin{cases} 1, & \text{for } a_0^2 \ll 1, \\ (\sqrt{2}/\pi)a_0/N_p, & \text{for } a_0^2 \gg 1, \end{cases} \tag{42}$$

$$L_{pd} \simeq \frac{\lambda_p^3}{2\lambda^2} \times \begin{cases} 2/a_0^2, & \text{for } a_0^2 \ll 1, \\ (\sqrt{2}/\pi)a_0, & \text{for } a_0^2 \gg 1. \end{cases} \tag{43}$$

where N_p is the number of plasma periods behind the drive laser pulse. In Eq. (42), the factor of $\lambda_p^3/2\lambda^2$ is from requiring a highly relativistic electron (traveling at c) to phase slip by $\lambda_p/4$ (since only 1/4 of a plasma wave period is both accelerating and focusing). In the $a_0^2 \gg 1$ limit of Eq. (42), the factor $1/N_p$ is from the plasma wave period increasing as the laser pulse steepens, which is the dominant effect in determining the plasma wave phase velocity in the nonlinear limit. Furthermore, it can be shown (Esarey *et al.*, 2004) that, initially, the spatial

rate at which the laser pulse energy changes scales as $-1/L_{pd}$ (pump depletion), the rate at which the mean frequency changes scales as $-1/L_{pd}$ (red shifts), and rate at which the mean laser intensity changes scales as $1/L_{pd}$ (pulse steepens).

As an example, consider the linear regime with the parameters $a_0 = 0.3$, $\lambda = 0.8$ μm, and $r_0 = \lambda_p = 33$ μm ($P = 3.3$ TW and $n_0 = 10^{18}$ cm^{-3}). The relevant propagation lengths are $Z_R = 0.43$ cm, $L_d \simeq 2.8$ cm, and $L_{pd} \simeq 62$ cm, i.e., $Z_R \ll L_d \ll L_{pd}$. Furthermore, since $L_d, L_{pd} \propto n_0^{-3/2}$, the dephasing length and pump depletion lengths can be increased by operating at lower densities. Since $L \sim \lambda_p$ in the standard LWFA, lower densities correspond to longer laser pulse durations $L \propto 1/\sqrt{n_0}$. In principle, a static magnetic field can be introduced to reduce dephasing (Katsouleas and Dawson, 1983). Use of an active medium has also been proposed as a method to reduce pump depletion (Fisher *et al.*, 1995).

In the linear regime ($a_0^2 \ll 1$), $L_d \ll L_{pd}$ and the electron energy gain is limited by dephasing, not pump depletion, assuming an axially uniform plasma. However, by appropriately tapering the axial plasma density profile, dephasing limitations can be overcome, resulting in a larger single-stage energy gain (Sprangle *et al.*, 2001). By slowly increasing the plasma density as a function of propagation distance, the phase velocity of the wakefield can be increased, as is described in Sec. IV.D. In principle, an axial density taper can be found for which $v_p = c$ at some point behind the drive laser pulse. In this case, acceleration would be limited by pump depletion, $L_{pd} \sim (\lambda_p^3/\lambda^2)a_0^{-2}$.

In the nonlinear regime ($a_0^2 \gtrsim 1$), $L_d \gtrsim L_{pd}$ and no density tapering is needed, since the electron energy gain is limited by pump depletion, not dephasing. In particular, the regime $a_0^2 \sim 1$, such that $L_d \sim L_{pd}$, has advantages over the linear regime. In addition to not requiring density tapering, a single channel-guided stage with $a_0^2 \sim 1$ results in higher accelerating gradients, shorter channel lengths, efficient depletion of the laser pulse energy, while yielding comparable energy gains.

The the ideal energy gain in a standard LWFA can be estimated by $\Delta W = eE_z L_{acc}$, where L_{acc} is the acceleration length and $E_z = E_0(a_0^2/2)(1 + a_0^2/2)^{-1/2}$ is the maximum electric field amplitude driven by an optimized flat-top, linearly polarized laser pulse in the 1D limit (Esarey *et al.*, 2004). If the acceleration distance is limited by diffraction, $L_{acc} \simeq \pi Z_R < L_d, L_{pd}$, the energy gain in practical units is

$$\Delta W_v[\mathrm{MeV}] \simeq 740(\lambda/\lambda_p)(1 + a_0^2/2)^{-1/2} P[\mathrm{TW}]. \quad (44)$$

If the acceleration distance is limited by dephasing, $L_{acc} \simeq L_{deph}$, the energy gain is

$$\Delta W_d[\mathrm{MeV}] \simeq \frac{630 I[\mathrm{W/cm^2}]}{n[\mathrm{cm^{-3}}]} \times \begin{cases} 1, & a_0^2 \ll 1, \\ (2/\pi)/N_p, & a_0^2 \gg 1. \end{cases} \quad (45)$$

If the acceleration distance is limited by depletion, $L_{acc} \simeq L_{pd}$, the energy gain is

$$\Delta W_{pd}[\mathrm{MeV}] \simeq \begin{cases} 3.4 \times 10^{21}/(\lambda^2[\mu\mathrm{m}] n[\mathrm{cm^{-3}}]), & a_0^2 \ll 1, \\ 400 I[\mathrm{W/cm^2}]/(n[\mathrm{cm^{-3}}]), & a_0^2 \gg 1. \end{cases} \quad (46)$$

These estimates are based on the idealized assumptions stated above and neglect various nonideal effects, such as laser-plasma instabilities. The effects of various instabilities are discussed in Sec. VI.

As an example, consider nonlinear $a_0^2 > 1$ regime, such that the dephasing length is approximately equal to the depletion length. Consider a laser with $P = 100$ TW, $a_0 = 3$, $\lambda = 0.8$ μm, $r_0 = 18$ μm, $I = 1.9 \times 10^{19}$ W/cm^2, 55 fs, and 5.5 J; along with a plasma with $\lambda_p = 33$ μm ($n_0 = 10^{18}$ cm^{-3}) such that $L_L = \lambda_p/2$. For these parameters, the above expressions give a wakefield of $E_z = 190$ GeV/m, an acceleration length of $L_{acc} = 3.8$ cm, and an energy gain of $\Delta W = 7.2$ GeV.

The above scaling laws apply to a LWFA in the standard configuration ($L \sim \lambda_p$) with a broad laser pulse ($k_p^2 r_0^2 \gg 1$) propagating in a density channel that provides guiding. For sufficiently high powers $P \gg P_{cr}$, it may be possible to guide the laser pulse over multiple Z_R without the use of a density channel due to a combination of relativistic self-focusing and ponderomotive self-channeling. This is this case in the so-called blow-out or bubble regime (Pukhov and Meyer-ter-Vehn, 2002). Assuming that the energy gain is limited by dephasing with $a_0 > 1$ again implies $\Delta W_{deph}[\mathrm{MeV}] \simeq 0.9(k_p r_0)^{-2} P[\mathrm{GW}]$, using the above scaling law, only now with the additional constraint $P \gg P_{cr}$. Similar scalings for the energy, i.e., $\Delta W \sim P$, can also be obtained through analytical and numerical studies of the blow-out regime. For example, Gordienko and Pukhov (2005) obtain $\Delta W_{GP}[\mathrm{MeV}] \simeq 0.1(c\tau_L/\lambda)(P[\mathrm{GW}])^{1/2}$. But if $c\tau_L = R_p \lambda_p$, where $R_p \sim 1$ is a constant, and if $P = R_{cr} P_{cr}$, where $R_{cr} \sim 10$ is a constant, then $\Delta W_{GP}[\mathrm{MeV}] \simeq 0.03 R_p R_{cr}^{-1/2} P[\mathrm{GW}]$. Lu *et al.* (2006) find $\Delta W_M[\mathrm{MeV}] \simeq 0.5(\lambda_p/\lambda)^{4/3}(P[\mathrm{GW}])^{1/3}$, which can be written as $\Delta W_M[\mathrm{MeV}] \simeq 0.02 R_{cr}^{-2/3} P[\mathrm{GW}]$ assuming $P = R_{cr} P_{cr}$.

Although ΔW is limited by depletion and dephasing for both a channel-guided LWFA or a self-guided LWFA with $P \gg P_{cr}$, there may be additional advantages to using a channel over relying on self-guiding. One obvious difference is that the additional constraint $P \gg P_{cr}$ need not be satisfied when using a channel. This implies that the channel-guided LWFA may be operated at lower intensities (lower a_0), which may be a more stable regime. The channel may also provide some resistance to instabilities, such as the laser-hose instability. Without a channel, the laser pulse will be subject to some amount of diffractive erosion, since the head of the pulse will not be self-guided, which can limit the propagation distance. For example, if the pulse is self-guided for a distance of $L = R_R Z_R$, where $R_R \gg 1$ is the num-

ber of Rayleigh lengths, then erosion will limit the energy gain and not dephasing when $R_R Z_R < L_{dephase}$, or $R_R(k_p r_0)^3 < 8.5(P[\mathrm{GW}])^{1/2}$. Lastly, it is hoped that by operating a channel-guided LWFA in the "dark-current-free" mode (no self-trapping), a high quality electron bunch can be obtained by injecting a low energy spread, low emittance bunch into the LWFA. If the LWFA is to be operated in the self-guided mode (i.e., the blow-out or bubble regime), it may not be possible to operate in this regime without self-trapping, which may limit the energy spread and emittance of the accelerated bunch.

H. Beam loading

A relativistic, charged particle bunch moving through a plasma can excite a wake in a manner similar to that of an intense laser pulse. For a laser driver, the ponderomotive force expels plasma electrons and initiates a wake. For a relativistic electron bunch, the space charge force of the bunch (with a relativistically large mass) displaces plasma electrons (with a relativistically lighter mass) and initiates a wake. The larger the charge in the bunch, the larger the wake. In a plasma-based accelerator, the wake from the accelerated bunch will be out of phase with, and thus reduce, the wake generated by the drive beam. The process by which the wake produced by the accelerated bunch significantly modifies the fields of the accelerating plasma wave is referred to as beam loading. Beam loading can place severe limitations on the beam current that can be accelerated, the quality of the accelerated particle bunch, and the efficiency of the plasma-based accelerator.

The wakefield generated by a relativistic electron bunch moving through a plasma can be calculated using linear perturbation theory of the cold fluid-Maxwell equations (Katsouleas *et al.*, 1987; Keinings and Jones, 1987; Lu *et al.*, 2005). The normalized density perturbation $\delta n/n_0 < 1$ and normalized axial electric field $E_z/E_0 < 1$ driven in an initially uniform plasma by a short electron bunch (with number density n_b) are given by

$$\left(\frac{\partial^2}{\partial\zeta^2} + k_p^2\right)\frac{\delta n}{n_0} = -k_p^2\frac{n_b}{n_0}, \tag{47}$$

$$\left(\nabla_\perp^2 - k_p^2\right)\frac{E_z}{E_0} = -k_p\frac{\partial}{\partial\zeta}\frac{\delta n}{n_0}, \tag{48}$$

assuming the quasi-static approximation and a highly relativistic beam, $\beta_b \simeq 1$, where $c\beta_b$ is the electron bunch velocity. Solving Eq. (48) for a cylindrically-symmetric beam yields

$$E_z/E_0 = k_p^3\int_\infty^\zeta d\zeta'\int_0^\infty dr' r'\cos[k_p(\zeta-\zeta')] \times I_0\left(k_p r_<\right)K_0\left(k_p r_>\right)n_b(r',\zeta')/n_0, \tag{49}$$

where I_0 and K_0 are the zeroth-order modified Bessel functions of the second kind, and $r_<$ ($r_>$) denote the smaller (larger) of r and r', respectively. An electron bunch will excite a plasma wave provided that the length scale of the axial gradients in the bunch profile (e.g., the bunch length) is comparable to or shorter than the plasma period, e.g., $k_p\sigma_z \lesssim 1$, where σ_z is the bunch length.

For a drive electron bunch with gaussian axial profile of the form $\rho(\zeta) = n_b\exp(-\zeta^2/2\sigma_z^2)$, the axial electric field is given by

$$E_z/E_0 = (2\pi)^{1/2}(n_b/n_0)k_p\sigma_z\exp(-k_p^2\sigma_z^2/2)F_R. \tag{50}$$

Note that the wakefield amplitude is maximum when $k_p\sigma_z = \sqrt{2}$. Here F_R depends on the radial bunch profile. For a flattop radial profile, $\rho(r) = n_b$ for $r \le \sigma_r$ and zero otherwise,

$$F_R(r) = \begin{cases} 1 - k_p\sigma_r K_1(k_p\sigma_r)I_0(k_p r), & \text{for } r < \sigma_r \\ k_p\sigma_r I_1(k_p\sigma_r)K_0(k_p r), & \text{for } r > \sigma_r \end{cases} \tag{51}$$

with I_1 and K_1 the first-order modified Bessel functions. For a wide beam $k_p\sigma_r \gg 1$, $F_R(0) \simeq 1$. For a narrow beam $k_p r_b \ll 1$, $H_R \simeq (k_p^2\sigma_r^2/2)[0.62 - \ln(k_p\sigma_r)]$, assuming $k_p\sigma_r \ll 1$. Note that for a gaussian radial profile, $\rho(r) = n_b\exp(-r^2/2\sigma_r^2)$, $H_R \simeq (k_p^2\sigma_r^2)[0.058 - \ln(k_p\sigma_r)]$, assuming $k_p\sigma_r \ll 1$.

The maximum number of bunch electrons that can be loaded into a small ($\ll \lambda_p$) axial segment of a linear wakefield for acceleration (i.e., the number of electrons required to produce a wakefield that will cancel the accelerating field, which defines the beam loading limit) is (Katsouleas *et al.*, 1987)

$$N_{\max} = \frac{n_0 A_b}{k_p}\frac{E_z}{E_0} \simeq 5\times 10^5\left(\frac{E_z}{E_0}\right)A_b[\mathrm{cm}^2]\sqrt{n_0[\mathrm{cm}^{-3}]}, \tag{52}$$

assuming $E_z/E_0 < 1$, where $A_b \gg \pi/k_p^2$ is the cross-sectional area of the bunch. As the number of bunch electrons N approaches $N_{\max}$, the energy spread scales as $N/N_{\max}$ and the efficiency of converting wake energy to electron energy scales as $(N/N_{\max})(2 - N/N_{\max})$.

IV. ELECTRON TRAPPING AND INJECTION

A. Trapping and Dark Current

The dynamics of an electron in the presence of a plasma wave and a laser pulse is determined by the Hamiltonian in the co-moving frame $H = \left(\gamma_\perp^2 + \tilde{p}^2\right)^{1/2} - \beta_p\tilde{p} - \phi$, as discussed in Sec. II.E. The orbit of an electron with initial normalized momentum $\tilde{p}_t$ will be defined by $H = H_t = (1+\tilde{p}_t^2)^{1/2} - \beta_\varphi\tilde{p}_t$. Trapping of the electron will occur when the orbit defined by H_t coincides with a trapped orbit, defined as lying with the separatrix orbit (defined by H_s), i.e., when $H_t \le H_s$. Solving $H_t = H_s$ yields in the minimum initial electron momentum for trapping in the plasma wave (Schroeder *et al.*,

2006),

$$\tilde{p}_t = \gamma_\varphi \beta_\varphi \left(\gamma_\perp - \gamma_\varphi \phi_{\min}\right) - \gamma_\varphi \left[\left(\gamma_\perp - \gamma_\varphi \phi_{\min}\right)^2 - 1\right]^{1/2}, \quad (53)$$

where $\phi_{\min}$ is the minima of the plasma wave potential. Figure 21 shows the initial momentum $\tilde{p}_t$ required for the electron to be trapped by a plasma wave with amplitude $\hat{E}_m = E_{\rm peak}/E_0$, with $\gamma_\perp = 1$ for a warm plasma [i.e., solving Eq. (21) for the wake potential] with $\beta_{\rm th}^2 = k_{\rm B}T_0/mc^2 = 10^{-4}$. The threshold momentum required for trapping decreases for larger plasma wave amplitude and for lower plasma wave phase velocity.

If the electric field can be well-approximated by the cold result (i.e., $E < E_{\rm WB}$ and $\beta_\varphi \gg \beta_{\rm th}$), then the peak field E_t required for the onset of particle trapping as a function of the initial electron momentum $\tilde{p}_t$ is given by (Schroeder *et al.*, 2006)

$$\left(E_t/E_0\right)^2 \simeq 2\gamma_\perp\left(\gamma_\varphi - 1\right) + 2\gamma_\varphi^2\beta_\varphi\left\{\tilde{p}_t - \left[\left(\beta_\varphi\tilde{p}_t\right)^2 + 2\beta_\varphi\tilde{p}_t\gamma_\perp/\gamma_\varphi\right]^{1/2}\right\}, \quad (54)$$

assuming $\tilde{p}_t \ll 1$ (non-relativistic initial momentum). Note that trapping can always occur, even for plasma waves with ultra-relativistic phase velocities ($\beta_\varphi = 1$), as shown in Fig. 21. For $\gamma_\perp = 1$, $\beta_\varphi = 1$, and $\tilde{p}_t \ll 1$, $\phi_{\min} \simeq -1 + \tilde{p}_t$ and the peak field of an ultra-relativistic plasma wave required for trapping an electron with initial momentum $\tilde{p}_t$ is $E_t/E_0 \simeq \tilde{p}_t^{-1/2}$.

For a thermal plasma electron distribution, electrons on the tail of the distribution may have sufficiently high momentum so as to reside on trapped orbits. For example, assuming an initial Gaussian momentum distribution with initial RMS momentum spread $\beta_{\rm th}^2 = k_{\rm B}T_0/mc^2$, i.e., a momentum distribution $F(\tilde{p}) \propto \exp(-\tilde{p}^2/2\beta_{\rm th}^2)$, the fraction of trapped electrons is (Schroeder *et al.*, 2006)

$$f_{\rm trap} = \frac{1}{2}{\rm erfc}\left(\tilde{p}_t/\sqrt{2}\beta{\rm th}\right), \quad (55)$$

where $\tilde{p}_t$ is given by Eq. (53). Figure 22 shows the fraction of trapped electrons versus the initial temperature of a Gaussian plasma electron momentum distribution for three different nonlinear plasma wave amplitudes driven by a laser in a warm plasma [i.e., $\hat{E}_m$ determined via Eq. (21)] with $k_pL_{\rm RMS} = 1$ and $a_0 = 3.65$ ($\hat{E}_m \simeq 1.75$), $a_0 = 4.15$ ($\hat{E}_m \simeq 2$), and $a_0 = 4.75$ ($\hat{E}_m \simeq 2.25$), with $\gamma_\varphi = 10$. The total number of trapped electrons (i.e., dark current in the plasma accelerator) can be estimated from Eq. (55). For example, for a plasma density of $n_0 = 10^{19}$ cm^{-3}, driver transverse size of $r_\perp = 10$ μm, and accelerator length of 1 mm, a trapping fraction of $f_{\rm trap} = 10^{-3}$ indicates ~ 0.1 nC of trapped charge. This trapping calculation neglects beam loading, which implies the wakefield induced by the trapped electrons is much smaller than the primary plasma wave.

The particle trapping model can be used to estimate the warm hydrodynamic wavebreaking limit. In particular, Eq. (54) obtained from trapping theory provides a good estimate to the hydrodynamic wavebreaking field, Eq. (22), over regimes of interest for laser-plasma accelerators, when $\tilde{p}_t = \sqrt{3}\beta_{\rm th}$. This shows that a significant fraction of the plasma electrons (satisfying $\tilde{p}_t > \sqrt{3}\beta_{rmth}$) can be trapped at the wavebreaking amplitude: $f_{\rm trap} = {\rm erfc}(\sqrt{3/2})/2 \simeq 0.04$ for an initial Gaussian momentum distribution.

As the driver propagates into the plasma, more charge will be trapped until the amplitude of the plasma wave is substantially reduced due to beam loading. The beam loading limit is defined as the number of accelerated electrons required to produce a wakefield that cancels the accelerating field of the plasma wave(Katsouleas *et al.*, 1987). The trapped bunch density is approximately $n_b \simeq f_{\rm trap}n_0z/L_b$, where z is the propagation distance and L_b is the bunch length. Assuming $k_pL_b \lesssim 1$, the wakefield generated by the bunch is given by $E_b/E_0 \simeq k_pL_bn_b/n_0$ in the 1D limit, assuming $E_b/E_0 < 1$. The beam loading limit at which $E_b \simeq E_m$ is then reached after a propagation distance of $z_{\rm BL} \approx k_p^{-1}f_{\rm trap}^{-1}\hat{E}_m$. For $\hat{E}_m \sim 1$ and $f_{\rm trap} \ll 1$, $k_pz_{\rm BL} \gg 1$ and beam loading will only be significant after propagating many plasma periods.

The warm fluid theory of wavebreaking and the trapping calculation assume the quasi-static approximation, i.e., the plasma wave is a traveling wave that is a function of only $\xi = z - v_pt$. This implies that there is sufficiently small trapping and beam loading such that any time dependent damping of the plasma wave is insignificant (i.e., $k_pz_{\rm BL} \gg 1$). At the wavebreaking amplitude, the fraction trapped is $f_{\rm trap} \simeq 4\%$ assuming a Gaussian momentum distribution. For example, if the beam loading estimate discussed above is assumed to approximately apply in the nonlinear limit, then $f_{\rm trap} \simeq 4\%$ and $\hat{E}_{\rm WB} \simeq 3$ imply $z_{\rm BL} \simeq 12\lambda_p$. This simple estimation implies that beam loading can lead to appreciable reduction of the plasma wave after several plasma periods if the field amplitude approaches the hydrodynamic wavebreaking limit.

B. Trapping in the self-modulated LWFA

Perhaps the most basic and simplest form of a laser-plasma injector is the self-modulated LWFA, in which a single laser pulse results in self-trapping and generation of a sub-ps electron bunch, however, with a large energy spread. Typically the self-trapped bunch is of high charge (up to 10 nC), with an energy distribution characterized by a Boltzmann distribution with a few MeV temperature. One possible mechanism for self-trapping is the direct wavebreaking of the plasma wakefield (Gordon *et al.*, 1998; Modena *et al.*, 1995; Tzeng *et al.*, 1997). Since the phase velocity of the wakefield is very near the speed of light, it is difficult to trap the background fluid electrons, which are undergoing the fluid oscillation that sustains the wakefield. The wake will trap the background elec-

trons when the separatrix of the wake overlaps the plasma fluid orbit. Wavebreaking of a cold plasma wave in 1D occurs at $E_{\rm WB} = [2(\gamma_p - 1)]^{1/2} E_0 \gg E_0$. As discussed in Sec. II.D thermal and 2D effects can lower this value, but typically wavebreaking requires nonlinear plasma waves with $E_z > E_0$. The observed wakefield amplitude, however, as measured in several experiments (Ting *et al.*, 1996), appears to be in the range E_z/E_0 ∼10–30%, well below wavebreaking. This suggests that additional laser-plasma instabilities may play a role in lowering the effective wave breaking amplitude.

Alternatively, self-trapping and acceleration can result from the coupling of Raman backscatter (RBS) and Raman sidescatter (RSS) to the wakefield (Esarey *et al.*, 1998). As the pump laser self-modulates, it also undergoes RBS, which is the fastest growing laser-plasma instability (cf. Sec. VI.A). RBS is observed in intense short pulse experiments, with reflectivities as high as 10–30% (Rousseaux *et al.*, 1995; Ting *et al.*, 1996). RBS generates red-shifted backward light of frequency $\omega_0 - \omega_p$ and wavenumber $-k_0$, which beats with the pump laser (ω_0, k_0) to drive a ponderomotive wave $(\omega_p,\ 2k_0)$. As the instability grows, the Raman backscatter beat wave, which has a slow phase velocity $v_p \simeq \omega_p/2k_0 \ll c$, can trap and heat background plasma electrons (Bertrand *et al.*, 1995; Joshi *et al.*, 1981). These electrons can gain sufficient energy and be displaced in phase by the beat wave such that they are trapped and accelerated to high energies in the wakefield. Simulations (Esarey *et al.*, 1998) indicate that coupling to RBS can lead to self-trapping at modest wakefield amplitudes, $E_z/E_0 \simeq 0.25$, much lower than the 1D threshold for wavebreaking.

In 2D, this process can be enhanced by coupling to RSS. As the scattering angle decreases from 180° (backscatter), the Raman growth rate decreases and the phase velocity of the Raman plasma wave increases. The electrons that are initially trapped and heated by RBS can be subsequently trapped by RSS modes propagating at smaller angles, which will accelerate the electrons to higher energies (owing to the higher phase velocity of the RSS modes) (Esarey *et al.*, 1998; Joshi *et al.*, 1981). Eventually, these background electrons can be trapped and accelerated to very high energies by the plasma wave associated with the forward Raman instability or the self-modulation instability, which has $v_p \simeq c$.

When electrons become trapped in the fast wakefield, they become accelerated to high energies as they circulate inside the separatrix of the wake. A large energy spread for the trapped electrons results because (i) some fraction of the background electrons are continually being swept up and trapped in the wakefield as the laser pulse propagates into fresh plasma, and (ii) typically the self-guided propagation distance of the laser pulse is much greater than the dephasing length for trapped electrons, cf. Sec. II.E. In the self-modulated regime the dephasing length can be very short, e.g., $L_d < 50$ μm. This implies that deeply trapped electrons will circulate many revolutions within the separatrix, again resulting in a large energy spread. The maximum energy of the trapped electrons is given by the maximum of the separatrix, which corresponds to an energy $W_{\rm max} \simeq 4\gamma_p^2 \gamma_\perp^{1/2} m_e c^2 E_z/E_0$, for $E_z/E_0 \ll 1$, where γ_p is the phase velocity of the plasma wave.

For many applications, a small energy spread is desired. One method for improving the self-modulated bunch quality is by post-acceleration. For example, the self-modulated bunch could be immediately injected into a second-stage composed of a standard LWFA with $L \sim \lambda_p$ in which the wakefield is produced in a controlled manner at an amplitude below the self-trapping threshold. This could be achieved by using a plasma that transitions from a high plasma density ($\lambda_p \ll L$, self-modulated LWFA) to a low plasma density ($\lambda_p \sim L$, standard LWFA). Simulations (Reitsma *et al.*, 2002) show that in this two-stage acceleration scheme, about 40% of the injected bunch charge can be trapped and accelerated in the LWFA with a reduced energy spread.

C. Optical injection techniques

In principle, if a small energy spread electron bunch of duration small compared to λ_p is injected into the wakefield at the proper phase, then the bunch can be accelerated while maintaining a small energy spread. This becomes problematic in the LWFA, since the wavelength of the accelerating field is small, e.g., $\lambda_p \simeq 30$ μm for $n_0 \simeq 10^{18}$ cm^{-3}. Hence, a low energy spread requires an ultrashort bunch duration $\tau_b < \lambda_p/c$ that is injected at the optimal plasma wave phase with femtosecond timing accuracy. These requirements are very challenging for conventional electron beam injector technology (e.g., RF photo-injectors). On the other hand, the production of ultrashort laser pulses and the femtosecond timing of multiple pulses is routine with compact CPA technology. As discussed below, ultrashort, high intensity laser pulses can be used to inject electrons into a single bucket (plasma wave period) of a standard LWFA (Esarey *et al.*, 1997a; Hemker *et al.*, 1998; Schroeder *et al.*, 1999a; Umstadter *et al.*, 1996b).

1. Ponderomotive injection

Umstadter *et al.* (1996b) first proposed using an additional laser pulse to inject background plasma electrons into the wake for acceleration to high energies. To generate ultrashort electron bunches with low energy spreads, the original laser injection method of (Umstadter *et al.*, 1996b) uses two laser pulses which propagate perpendicular to one another. The first pulse (pump pulse) generates the wakefield via the standard LWFA mechanism, and the second pulse (injection pulse) intersects the wakefield some distance behind the pump pulse. The ponderomotive force $\boldsymbol{F}_p \simeq -(m_e c^2/\tilde{\gamma})\nabla a^2/2$ of the injection pulse can accelerate a fraction of the plasma elec-

trons such that they become trapped in the wakefield. Specifically, the axial (direction of propagation of the pump pulse along the z-axis) ponderomotive force of the injection pulse (propagating along the x-axis) scales as

$$F_z = -(m_e c^2/\tilde{\gamma})(\partial/\partial z)a_1^2/2 \sim (m_e c^2/\tilde{\gamma})a_1^2/r_1, \quad (56)$$

where a_1^2 and r_1 are the normalized intensity and spot size of the injection pulse, respectively. A simple estimate for the change of momentum that an electron will experience owing to the ponderomotive force of the injection pulse is $\Delta p_z \simeq F_z \tau_1 \sim (m_e c^2/\tilde{\gamma})a_1^2\tau_1/r_1$, where τ_1 is the injection pulse duration. It is possible for Δp_z to be sufficiently large that electrons are injected into the separatrix of the wakefield such that they become trapped and accelerated to high energies. To inject into a single plasma wave bucket, it is necessary for both the injection pulse spot size and pulse length to be small compared to the plasma wavelength, i.e., $r_1^2 \ll \lambda_p^2$ and $c^2\tau_1^2 \ll \lambda_p^2$. Simulations (Umstadter *et al.*, 1996b), which were performed for ultrashort pulses at high densities ($\lambda_p/\lambda = 10$ and $E_z/E_0 = 0.7$), indicated the production of a 10 fs, 21 MeV electron bunch with a 6% energy spread. However, high intensities ($I > 10^{18}$ W/cm^2) are required in both the pump and injection pulses ($a_0 \simeq a_1 \simeq 2$). In the work of Umstadter *et al.* (1996b), the pump and injection pulses do not overlap in space and time, and a laser beat wave is not generated, as discussed below.

Simulations by Hemker *et al.* (1998) point out that additional electron injection into one or more wake buckets can result through the influence of the wake associated with the injection pulse, which can be significant because of the high intensity of the injection pulse ($a_1 \gtrsim 1$). Umstadter *et al.* (1996b) also discuss the possibility of injection using an injection pulse that propagates parallel, but some distance behind, the pump pulse. The injection pulse would have a tighter focus (and hence smaller Rayleigh length) than the pump pulse, and would be phased appropriately such that it locally drives the wakefield to an amplitude that exceeds the self-trapping threshold, thus resulting in local trapping and acceleration of electrons. In addition, Umstadter *et al.* (1996b) discusses the possibility of the injection pulse being focused to sufficiently high intensity such that it produces locally additional ionization. The ionized electrons, which are born dephased from the background plasma electron in the wake, could become trapped and accelerated by the wake. Injection by laser-induced ionization and ponderomotive acceleration has also been discussed by Moore *et al.* (1999). Experiments in the high-density regime of laser ionization and ponderomotive acceleration have demonstrated electron injection by this method (Ting *et al.*, 2005).

2. Colliding pulse injection

Beat wave injection using colliding laser pulses (Esarey *et al.*, 1997a, 1999; Fubiani *et al.*, 2004; Kotaki *et al.*, 2004; Schroeder *et al.*, 1999a) differs intrinsically from the method of ponderomotive injection discussed above in that the source and form of the ponderomotive force differs in these two methods. In ponderomotive injection, injection is the result of the ponderomotive force associated with the *envelope* (time-averaged intensity profile) of a single pulse. In beat wave injection, injection is the result of the ponderomotive force associated with the *slow beat wave* of two intersecting pulses. Beat wave injection was first proposed and analyzed by Esarey *et al.* (1997a) in a concept referred to as colliding pulse injection.

Colliding pulse injection (Esarey *et al.*, 1997a, 1999; Schroeder *et al.*, 1999a) uses three short laser pulses: an intense ($a_0^2 \simeq 1$) pump pulse (denoted by subscript 0) for plasma wave generation, a forward going injection pulse (subscript 1), and a backward going injection pulse (subscript 2), as shown in Fig. 23. The frequency, wavenumber, and normalized intensity are denoted by ω_i, k_i, and a_i ($i = 0, 1, 2$). Furthermore, it is assumed that $k_1 \simeq k_0$, $k_2 \simeq -k_0$, and $\omega_1 - \omega_2 = \Delta\omega \gg \omega_p$. The pump pulse generates a plasma wave with phase velocity near the speed of light ($v_{p0} \simeq c$). The forward injection pulse travels at a fixed distance behind the pump pulse, which determines the position (i.e., phase) of the injected electrons. The injection pulses are orthogonally polarized to the pump laser pulse, such that the pump pulse and backward going injection pulse do not beat.

When the injection pulses collide some distance behind the pump, they generate a slow ponderomotive beat wave of the form $a_1 a_2 \cos(\Delta k z - \Delta\omega t)$ (here $\Delta k = k_1 - k_2 \simeq 2k_0$) with a phase velocity $v_{pb} \simeq |\Delta\omega|/2k_0 \ll c$. The axial force associated with this beat wave scales as

$$\begin{aligned} F_z &= -(m_e c^2/\tilde{\gamma})(\partial/\partial z)a_1 a_2 \cos(2k_0 z - \Delta\omega t) \\ &\sim (m_e c^2/\tilde{\gamma})2k_0 a_1 a_2. \end{aligned} \quad (57)$$

During the time in which the two injection pulses overlap, a two-stage acceleration process can occur, i.e., the slow beat wave traps and heats background plasma electrons which, as a result of shifts in their momentum and phase, can be injected into the fast wakefield for acceleration to high energies.

The ratio of the axial force of the beat wave to that of a single pulse in the ponderomotive injection scheme (owing to the gradient in the envelope of the laser intensity) scales as

$$\frac{F_{z,\mathrm{beat}}}{F_{z,\mathrm{env}}} \sim \frac{2k_0 a_1 a_2}{a_p^2/r_p}, \quad (58)$$

where the subscript p refers to the single ponderomotive injection pulse and the contribution of the relativistic Lorentz factor $\tilde{\gamma}$ (which is different for the two cases) is neglected. For comparable injection pulse intensities ($a_1 \simeq a_2 \simeq a_p$), the ratio scales as $4\pi r_p/\lambda_0 \gg 1$, i.e., the axial force of the beat wave is much greater than the ponderomotive force from the intensity envelope of a single pulse. Consequently, colliding pulses can result in electron injection at relatively low intensities

($a_1 \sim a_2 \sim 0.2$), as well as at relatively low densities ($\lambda_p/\lambda \sim 100$), thus allowing for high single-stage energy gains. Furthermore, the colliding pulse concept offers detailed control of the injection process: the injection phase can be controlled via the position of the forward injection pulse, the beat phase velocity via $\Delta\omega$, the injection energy via the pulse amplitudes, and the injection time (number of trapped electrons) via the backward pulse duration.

To help understand the injection mechanism, it is insightful to consider the electron motion in the wakefield and in the colliding laser fields individually. In the absence of the injection pulses, electron motion in a 1D wakefield is described by the Hamiltonian $H_w = \tilde{\gamma} - \beta_p(\tilde{\gamma}^2-1)^{1/2} - \phi(\psi)$, cf. Sec. II.E, where $\phi = \phi_0 \cos\psi$, $v_p = c\beta_p$ is the phase velocity of the plasma wave, $\gamma_p = (1-\beta_p^2)^{-1/2}$, and $\psi = k_p(z - v_p t)$. The electron orbits in phase space $(\tilde{p}_z, \psi)$ are given by $H_w(\tilde{p}_z, \psi) = H_0$, where H_0 is a constant, $\tilde{\gamma}^2 = 1 + \tilde{p}_z^2$, and $\tilde{p}_z$ is the normalized (to $m_e c$) axial momentum of an electron, which is given by

$$\tilde{p}_z = \beta_p \gamma_p^2 \left[H_0 + \phi(\psi)\right] \pm \gamma_p \left\{\gamma_p^2 \left[H_0 + \phi(\psi)\right]^2 - 1\right\}^{1/2}. \quad (59)$$

The 1D separatrix (the boundary between trapped and untrapped orbits) is given by $H_w(\tilde{p}_z, \psi) = H_w(\gamma_p\beta_p, \pi)$, i.e., $H_0 = H_{1D} = 1/\gamma_p - \phi(\pi)$. The maximum and minimum electron momentum on the 1D separatrix occur at $\psi = 0$ and are (in the limits $2\phi_0\gamma_p \gg 1$ and $\gamma_p \gg 1$) $\tilde{p}_{w,\max} \simeq 4\gamma_p^2\phi_0$ and $\tilde{p}_{w,\min} \simeq (4\phi_0)^{-1} - \phi_0$. The 1D theory neglects the effects of transverse focusing. Associated with a 3D wake is a periodic radial field which is $\pi/2$ out of phase with the accelerating field, i.e., there exists a phase region of $\lambda_p/4$ for which the wake is both accelerating and focusing (as opposed to the $\lambda_p/2$ accelerating region in 1D). If an electron is to remain in this phase region, it must lie within the "3D separatrix" defined by $H_w(\tilde{p}_z, \psi) = H_w(\gamma_p\beta_p, \pi/2)$, i.e., Eq. (59) with $H_0 = H_{3D} = 1/\gamma_p - \phi(\pi/2)$. The extremum on the 3D separatrix are given by $\tilde{p}_{w,\max} \simeq 2\gamma_p^2\phi_0$ and $\tilde{p}_{w,\min} \simeq (\phi_0^{-1} - \phi_0)/2$. This value of $\tilde{p}_{w,\max} \simeq 2\gamma_p^2\phi_0$ gives the usual maximum energy gain due to linear dephasing in a 3D wake.

The background plasma electrons lie on an untrapped orbit (below the separatrix) $\tilde{p}_{zf}$ given by $H_w(\tilde{p}_{zf}, \psi) = 1$, i.e., Eq. (59) with $H_0 = 1$. At wavebreaking, the bottom of the separatrix $\tilde{p}_{w,\min}$ coalesces with the plasma fluid orbit, $\tilde{p}_{zf} = \tilde{p}_{w,\min}$. This occurs at the well-known cold wavebreaking field of $E_{WB}/E_0 = [2(\gamma_p - 1)]^{1/2}$.

Consider the motion of electrons in the colliding laser fields in the absence of the wakefield. The beat wave leads to formation of phase space buckets (separatrices) of width $2\pi/\Delta k \simeq \lambda_0/2$, which are much shorter than those of the wakefield (λ_p). In the colliding laser fields, the electron motion is described by the Hamiltonian (Esarey *et al.*, 1997a) $H_b = \tilde{\gamma} - \beta_b \left[\tilde{\gamma}^2 - \gamma_\perp^2(\psi_b)\right]^{1/2}$, where the space charge potential is neglected. Circular polarization is assumed such that $\gamma_\perp^2 = 1 + a_0^2 + a_1^2 + 2a_0a_1\cos\psi_b$, where $\psi_b = (k_1 - k_2)(z - v_b t)$ and $v_b = c\beta_b = \Delta\omega/(k_1 - k_2) \simeq \Delta\omega/2k_0$ is the beat phase velocity, assuming $\omega_p^2/\omega_0^2 \ll 1$. The beat separatrix is given by $H_b(\tilde{p}_z, \psi_b) = H_b(\gamma_b\beta_b, 0)$ with a maximum and minimum axial momenta of

$$\tilde{p}_{b,m} = \gamma_b\beta_b \left[1 + (a_0 + a_1)^2\right]^{1/2} \pm 2\gamma_b(a_0a_1)^{1/2}. \quad (60)$$

An estimate for the threshold for injection into the wakefield can be obtained by a simple phase-space island overlap criteria. This is done by considering the effects of the wakefield and the beat wave individually, as done above, and by requiring that the beat wave separatrix overlaps both the wakefield separatrix and the plasma fluid oscillation (illustrated in Fig. 24): (i) the maximum momentum of the beat wave separatrix $\tilde{p}_{b,\max}$ exceeds the minimum momentum of the wakefield separatrix $\tilde{p}_{w,\min}$, i.e., $\tilde{p}_{b,\max} \geq \tilde{p}_{w,\min}$, and (ii) the minimum momentum of the beat wave separatrix $\tilde{p}_{b,\min}$ be less than the plasma electron fluid momentum $\tilde{p}_{zf}$, i.e., $\tilde{p}_{b,\min} \leq \tilde{p}_{zf}$. Conditions (i) and (ii) imply a beat wave threshold (Esarey *et al.*, 1997a; Schroeder *et al.*, 1999a)

$$(a_1a_2)_{\rm th}^{1/2} = \frac{(1 - H_0)}{4\gamma_b(\beta_p - \beta_b)}, \quad (61)$$

and an optimal wake phase for injection (location of the forward injection pulse)

$$\cos\psi_{\rm opt} = \phi_0^{-1}\left[(1 - \beta_b\beta_p)\gamma_b\gamma_\perp(0) - (1 + H_0)/2\right], \quad (62)$$

where $H_0 = H_{1D} = 1/\gamma_p + \phi_0$ for the 1D wake separatrix and $H_0 = H_{3D} = 1/\gamma_p$ for the 3D wake separatrix (trapped and focused). In the limits $\gamma_p^2 \gg 1$, $\beta_b^2 \ll 1$, and $a_i^2 \ll 1$, Eqs. (61) and (62) become $4(a_1a_2)_{\rm th}^{1/2} \simeq (1 - H_0)(1 + \beta_b)$ and $2\phi_0\cos\psi_{\rm opt} \simeq 1 - H_0 - 2\beta_b$ with $H_{1D} \simeq \phi_0$ and $H_{3D} \simeq 0$. As an example, $\phi_0 = 0.7$, $\beta_b = -0.02$, and $\gamma_p = 50$ imply a threshold of $(a_1a_2)_{\rm th}^{1/2} \simeq 0.25$ and an optimal injection phase of $\psi_{\rm opt} \simeq 0$ for injection onto a trapped and focused orbit.

To further evaluate the colliding laser injection method, the motion of test particles in the combined wake and laser fields was simulated in 3D (Schroeder *et al.*, 1999a). In the numerical studies, the laser pulse axial profiles were half-period sine waves (linearly polarized with Gaussian radial profiles) with peak amplitude a_i and length L_i. The wakefield is assumed to be nonzero for $\psi \leq 3\pi/4$ (see Fig. 23) and the test particles are loaded uniformly with $\psi > 3\pi/4$ (initially at rest).

An example of the injection process is given in Fig. 25, which shows the evolution in longitudinal phase space of the test electron distribution (a) before the collision of the injection laser pulses (in the untrapped fluid orbit of the wake) at $\omega_p t = 36$, (b) during the collision (crossing the wake separatrix) at $\omega_p t = 39$, (c) after the collision at $\omega_p t = 50$, and (d) the resulting energetic electron bunch at $\omega_p t = 150$. Fig. 25 also shows the 1D wake separatrix. The parameters are $a_1 = a_2 = 0.32$, $L_0 = 4L_1 = 4L_2 = \lambda_p = 40$ μm, $\phi_0 = 0.7$, $\lambda_0 = \lambda_2 = 0.8$ μm, $\lambda_1 = 0.83$ μm,

and $r_0 = r_1 = r_2 = 15$ μm, with the position of the forward injection pulse centered at $\psi_{\rm inj} = -12.6$. After $z \simeq 0.7$ mm of propagation following the collision, Fig. 25(d), the bunch length is 1 fs with a mean energy of 38 MeV, a fractional energy spread of 0.2%, and a normalized transverse emittance of 0.9 mm-mrad. The trapping fraction $f_{\rm trap}$ is 3%, corresponding to 2.6×10^6 bunch electrons. Here, $f_{\rm trap}$ is defined as the fraction of electrons trapped that were initially loaded in a region of length $\lambda_p/4$ with $r \leq 2$ μm (simulations indicate that electrons loaded outside this region are not trapped). Note that the bunch number can be increased by increasing the laser spot sizes (i.e., laser powers). For example, when the laser spot sizes are doubled, $r_i = 30$ μm in the simulation of Fig. 25 (all other parameters as in Fig. 25), the number of trapped electrons increases to 1.5×10^7 and the normalized transverse emittance increases to 3.9 mm-mrad. Estimates indicate that space charge effects can be neglected while the bunch remains inside the plasma (Schroeder *et al.*, 1999a).

Colliding pulse injection can also be envisioned using two laser pulses, with the same polarization, such that the tail of the pump laser pulse beats with the counterpropagating pulse, trapping electrons in the plasma wave (Fubiani *et al.*, 2004; Kotaki *et al.*, 2004). The initial set of optical trapping experiments use this simpler two-pulse geometry (Faure *et al.*, 2006; Kotaki, 2007; Leemans, 2004; Nakamura *et al.*, 2004) are discussed in Sec. VII.C.

D. Density transitions

Bulanov *et al.* (1998) describe how a downward transition in the plasma density with a scale length L_{tr} long compared to λ_p could be used to induce local self-trapping in the plasma wave. Consider the position of a phase peak on a plasma wave of the form $\phi = \phi_0 \cos k_p \zeta$ (where $-\zeta = ct - z$ is the distance behind the drive beam) located N periods behind the drive beam. Before the density transition, the phase peak is located at $|\zeta_1| = N\lambda_{p1}$, and after the transition, the phase peak is located at $|\zeta_2| = N\lambda_{p2}$, where λ_{p1} (n_1) and λ_{p2} (n_2) are the plasma wavelengths (densities) before and after the transition with $\lambda_{p1} < \lambda_{p2}$ ($n_1 > n_2$). The density transition changes the location of the phase peak by the relative amount $\Delta|\zeta_p| = N(\lambda_{p1} - \lambda_{p2})$. If this transition occurs over a length L_{tr}, then the change in the phase velocity is $\Delta v_p/c \simeq N(\lambda_{p1} - \lambda_{p2})/L_{tr}$. This effect increases proportional to the distance behind the driver (increasing N), as well as the magnitude of the density gradient, $(\lambda_{p1} - \lambda_{p2})/L_{tr} \simeq d\lambda_p/dz = -(\lambda_p/2n)dn/dz$.

More rigorously, the phase velocity of the wake during a density transition can be calculated by considering the local phase of the wake, which is given to leading order by $\psi = k_p(z)(z - ct)$, where $v_g \simeq c$ has been assumed since changes to the group velocity due to a slow variation in density are small in an underdense plasma $\omega_p^2/\omega^2 \ll 1$. Using the definitions of the effective frequency $\omega_{p,\rm eff} = -\partial\psi/\partial t$ and wavenumber $k_{p,\rm eff} = \partial\psi/\partial z$ of the plasma wave, the local phase velocity of the wake is given by $v_p = \omega_{p,\rm eff}/k_{p,\rm eff}$, i.e.,

$$v_p/c = [1 + (\zeta/k_p)dk_p/dz]^{-1}. \tag{63}$$

For a small variation, $v_p/c - 1 \simeq -(\zeta/k_p)dk_p/dz = -(\zeta/2n)dn/dz$. Since $\zeta < 0$ behind the drive pulse, the wake phase velocity will decrease for decreasing density $dn/dz < 0$.

Local wave breaking of the wake will occur at the point at which the local phase velocity equals the fluid velocity of the plasma electrons. To leading order, the size of the fluid oscillation depends on the intensity of the drive pulse, the pulse length, and the local plasma density. Since the "resonance" for exciting a large amplitude wake is rather broad, $L \sim \lambda_p$ (weakly dependent on density), a large wake can be excited on the density ramp with a fluid velocity given approximately by $v_e/c \simeq E_z/E_0$, where $E_z/E_0 \ll 1$ is the normalized electric field amplitude of the wake. According to fluid theory, wavebreaking of a wake will always occur on a density down ramp at a sufficiently large distance behind the drive pulse (assuming the wake is not damped by some other mechanism), since Eq. (63) indicates that the wake phase velocity will continue to decrease as a function of time for a fixed point on the density down ramp. Using Eq. (63), wavebreaking ($v_p = v_e$) will occur at a distance behind the drive pulse given by $\zeta = 2(c/v_e - 1)n/(dn/dz)$. For example, if $v_e/c = 1/3$ and $L_{tr} = n|dn/dz|^{-1} = 3\lambda_p$, then wavebreaking occurs at $|\zeta| = 12\lambda_p$.

Bulanov *et al.* (1998) performed 1D particle-in-cell simulations of a laser pulse with $a_0 = 2$ and $L = 12\lambda$ propagating in a plasma with $\lambda_{p1} = 23.4\lambda$, $\lambda_{p2} = 25\lambda$, and $L_{tr} = 24\lambda$. These simulations found that the plasma wave breaks on the ramp and injects a significant number of electrons into the wake, in apparently the second bucket behind the laser pulse, which are accelerated to high energy but with a large energy spread. Tomassini *et al.* (2003) preformed 2D particle-in-cell simulations showing generation of well-collimated, short electron beams via a decreasing plasma density gradient.

Suk *et al.* (2001) consider the limit of a step function downward plasma density transition ($n_1 = 5 \times 10^{13}$ cm^{-3} and $n_2 = 3.5 \times 10^{13}$ cm^{-3}) and a wake generated by an electron beam driver of energy 16 MeV, bunch length $0.16\lambda_{p2}$, bunch radius $0.089\lambda_{p2}$, and peak density $n_b = 2.4n_1 = 3.4n_2$. Using 2D particle-in-cell simulations, the trapped electron bunch, after propagating a few plasma wavelengths past the transition, had a total charge near 0.5 nC, a bunch length near $0.09\lambda_{p2}$, and electron energies in the range 5–15 MeV. Trapping across a parabolic density profile, which has the advantage of ease of experimental production and control, has also been considered (Kim *et al.*, 2004). Electron injection via a sharp laser-induced plasma density ramp (scale length of ramp less than the plasma wavelength) has been demonstrated in the self-modulated LWFA regime (Chien *et al.*, 2005).

V. PULSE PROPAGATION AND GUIDING

To describe laser pulse propagation in a fully-ionized plasma, it is convenient to represent the electric $\boldsymbol{E}$ and magnetic fields $\boldsymbol{B}$ by the scaler Φ and vector $\boldsymbol{A}$ potentials, $\boldsymbol{E} = -\nabla\Phi - \partial\boldsymbol{A}/\partial ct$ and $\boldsymbol{B} = \nabla \times \boldsymbol{A}$, and to use Coulomb gauge, $\nabla \cdot \boldsymbol{A} = 0$. In terms of the normalized potentials $\phi = e\Phi/m_e c^2$ and $\boldsymbol{a} = e\boldsymbol{A}/m_e c^2$, the wave equation and the Poisson equation are given by, respectively,

$$\left(\nabla^2 - \frac{1}{c^2}\frac{\partial^2}{\partial t^2}\right)\boldsymbol{a} = k_p^2 \frac{n}{n_0}\frac{\boldsymbol{u}}{\gamma} + \frac{1}{c}\frac{\partial}{\partial t}\nabla\phi, \qquad (64)$$

$$\nabla^2\phi = k_p^2\left(n - n_i\right)/n_0, \qquad (65)$$

where $\boldsymbol{u} = \gamma\boldsymbol{v}/c = \boldsymbol{p}/m_e c$ is the normalized electron fluid momentum, $\gamma = (1-\beta^2)^{1/2} = (1+u^2)^{1/2}$ is the relativistic Lorentz factor, n is the plasma electron density, n_i is the initial density profile (prior to the passage of the laser pulse), $n_0 = n_i(r=0)$ with $r=0$ corresponding to the direction of propagation (the z-axis), and $\omega_{p0} = ck_p = (4\pi n_0 e^2/m_e)^{1/2}$. Here and in the following, it is assumed that the ions remain stationary, which is typical for short pulse lasers ($\lesssim 1$ ps) propagating in underdense plasma ($\omega_{p0}^2/\omega^2 \ll 1$). Furthermore, collisions and thermal effects are neglected, since the collision time is typically much greater than the laser pulse length and the thermal velocity is typically much less than the quiver velocity of an electron in the laser field.

The first term on the right-hand side of Eq. (64) is the contribution due to the plasma current $\boldsymbol{J}$. In the cold fluid limit, $\boldsymbol{J} = -en\boldsymbol{u}/\gamma$, where the plasma density n and momentum $\boldsymbol{u}$ satisfy the continuity and momentum equations, which are given by, respectively,

$$\partial n/\partial ct + \nabla\cdot(n\boldsymbol{u}/\gamma) = 0, \qquad (66)$$

$$\left[\partial/\partial ct + (\boldsymbol{u}/\gamma)\cdot\nabla\right]\boldsymbol{u} = \nabla\phi + \partial\boldsymbol{a}/\partial ct - (\boldsymbol{u}/\gamma)\times(\nabla\times\boldsymbol{a}). \qquad (67)$$

It is also convenient to introduce the independent variables $\zeta = z - ct$ and $\tau = t$, where ζ is an approximate measure of the distance back from the head of the pulse (which is moving with a group velocity $v_g \simeq c$). Initially, the front of the laser pulse is assumed to be at $\zeta = 0$ and the pulse body extends into the region $\zeta \le 0$ (the plasma is unperturbed in the region $\zeta > 0$). In terms of the ζ, τ coordinates, the wave equation is given by (Esarey *et al.*, 1993a)

$$\left(\nabla_\perp^2 + \frac{2}{c}\frac{\partial^2}{\partial\zeta\partial\tau} - \frac{1}{c^2}\frac{\partial^2}{\partial\tau^2}\right)\boldsymbol{a} \simeq k_p^2\frac{n}{n_0\gamma}\boldsymbol{u}. \qquad (68)$$

On the right-hand side of Eq. (68), the term $\nabla\partial\phi/\partial ct$ has been neglected, since the fast part of the electrostatic potential, $\phi \sim \exp(ik\zeta)$, is typically small compared to relevant terms contributing to the fast part of the plasma current. Typically, the third term on the left-hand side of Eq. (68) can be neglected. As discussed in Sec. II, the leading order transverse motion is the quiver motion. Hence, for a wide variety of phenomena, it is sufficient to approximate $\boldsymbol{u} = \boldsymbol{a}$ on the right-hand side of Eq. (68).

The wave equation can be further simplified by the slowly varying envelope approximation. Assuming a linearly polarized laser field with a transverse component of the form $\boldsymbol{a}_f = \hat{\boldsymbol{a}}_s(r,\zeta,\tau)\exp(ik\zeta)/2 + \text{c.c.}$, the wave equation describing the evolution of the slowly varying amplitude $\hat{\boldsymbol{a}}_s$ is given by

$$\left(\nabla_\perp^2 + 2i\omega\frac{\partial}{\partial\tau} + \frac{2}{c}\frac{\partial^2}{\partial\zeta\partial\tau}\right)\hat{\boldsymbol{a}}_s = k_p^2\rho_s\hat{\boldsymbol{a}}_s, \qquad (69)$$

where $\rho_s = (n/n_0)/\gamma$, $\boldsymbol{u}_{\perp f} \simeq \boldsymbol{a}_f$, $\omega = ck$ is the laser frequency, and the subscripts f and s denote the fast and slow components, respectively. The small term $\partial^2/\partial\tau^2$ has been neglected in the wave operator, however, the $\partial^2/\partial\zeta\partial\tau$ term is retained so as to correctly describe variations in the laser pulse group velocity. The paraxial approximation is the result of neglecting the term $\partial^2/\partial\zeta\partial\tau$. Throughout the following, the subscripts s and f will be dropped for convenience.

A useful approximation in the study of short pulse interactions with plasmas is the quasi-static approximation (QSA), which was first applied to nonlinear laser-plasma interactions by Sprangle *et al.* (1990a,b). In the QSA, the plasma fluid equations are written in terms of the independent variables ζ and τ, as above. The QSA assumes that in the time it takes the laser pulse to transit a plasma electron (i.e., the slippage time for an electron through the laser pulse), the laser pulse does not significantly evolve. In other words, $\tau_L \ll \tau_E$, where $\tau_L = L/c$ is the laser pulse duration and τ_E is the laser pulse evolution time, which is typically one the order of a Rayleigh (diffraction) length. Thus the plasma electrons experience a static (independent of τ) laser field. In the QSA, the $\partial/\partial\tau$ derivatives are neglected in the plasma fluid equations which determine the plasma response to the laser pulse. The $\partial/\partial\tau$ derivatives, however, are retained in the wave equation which describes the evolution of the laser pulse. The QSA allows the laser-plasma interaction to be calculated in an iterative fashion. For a fixed τ, the plasma response to the laser field is determined as a function of ζ by solving the QSA fluid equations [e.g., Eq. (16) in the 1D limit]. Using this fluid response, the wave equation is then solved to update the laser pulse in τ.

The fluid quantity $\rho = n/\gamma n_0$ in Eq. (69) can determined from the quasi-static fluid equations. For example, in the 1D limit, it can be shown (Esarey *et al.*, 1993b) that $\rho \simeq (1+\phi)^{-1}$, where ϕ satisfies Eq. (16). In 2D and assuming $v_g \simeq c$, it can be shown (Krall *et al.*, 1994) that

$$\rho \simeq (1+\Psi)^{-1}(\rho_0 + k_p^{-2}\nabla_\perp^2\Psi), \qquad (70)$$

where ρ_0 is the initial value of ρ (prior to the laser pulse) and the quantity $\Psi = \phi - a_z$ satisfies

$$\frac{\partial^2\Psi}{\partial\zeta^2} = \left(k_p^2\rho - \nabla_\perp^2\right)u_z + \frac{\partial}{\partial\zeta}\nabla_\perp\cdot\boldsymbol{u}_\perp, \qquad (71)$$

with $\boldsymbol{u}_\perp = (k_p^2\rho)^{-1}\partial_\zeta(\nabla_\perp\Psi)$ and $u_z = [u_\perp^2 + a^2 - \Psi(2+\Psi)]/[2(1+\Psi)]$. The wake potential Ψ is related to the axial electric field E_z induced in the plasma by $k_p\hat{E}_z = -\partial\Psi/\partial\zeta$, where $\hat{E}_z = E_z/E_0$ and $E_0 = m_e c\omega_{p0}/e$ is the cold, nonrelativistic wavebreaking field.

A useful quantity in discussing phenomena such as optical guiding is the index of refraction η_r. The effective index of refraction η_r is defined by setting the right-hand side of Eq. (69) equal to $k^2(1-\eta_r^2)\boldsymbol{a}$, which yields $\eta_r \simeq 1 - k_p^2\rho/2k^2$.

A. Optical guiding in plasmas

The optical guiding mechanisms (Esarey *et al.*, 1997b) discussed below are based on the principle of refractive guiding. Refractive guiding becomes possible when the radial profile of the index of refraction, $\eta_r(r)$, exhibits a maximum on-axis, i.e., $\partial\eta_r/\partial r < 0$. Since $\eta_r \simeq ck_z/\omega$, $\partial\eta_r/\partial r < 0$ implies that the phase velocity along the propagation axis is less than it is off-axis. This causes the laser phase fronts to curve such that the beam focuses towards the axis.

The index of refraction for a small amplitude electromagnetic wave propagating in a plasma of uniform density $n = n_0$, in the 1D limit, is given by $\eta_r = (1-\omega_p^2/\omega^2)^{1/2}$. For large amplitude waves, however, variations in the electron density and mass will occur, i.e., $\omega_p^2 \to (\omega_{p0}^2/\gamma)n/n_0$. Hence, the general expression for the index of refraction for a large amplitude electromagnetic wave in a plasma is given by (Sprangle *et al.*, 1992, 1990b)

$$\eta_r(r) \simeq 1 - \frac{\omega_{p0}^2}{2\omega^2}\frac{n(r)}{n_0\gamma(r)}, \tag{72}$$

assuming $\omega_{p0}^2/\omega^2 \ll 1$. The index of refraction profile $\eta_r(r)$ can be modified by the relativistic factor $\gamma(r)$ or the radial density profile $n(r)$. The leading order motion of the electrons in the laser field is the quiver motion $\boldsymbol{p}_\perp = m_e c\boldsymbol{a}$ and, hence, $\gamma \simeq \gamma_\perp = (1+a^2)^{1/2}$. A laser intensity profile peaked on-axis $\partial a^2/\partial r < 0$ leads to $\partial\eta_r/\partial r < 0$ and the possibility of guiding (i.e., relativistic self-focusing). The density profile can have contributions from a preformed density channel $\Delta n_p \sim \Delta n r^2/r_0^2$ or a plasma wave $\delta n \sim \delta\hat{n}(r)\cos k_p\zeta$, where $n = n_0 + \Delta n_p + \delta n$. A radial density profile which has a minimum on-axis (i.e., a channel) implies $\partial\eta_r/\partial r < 0$ and the possibility of guiding. In the limits $a^2 \ll 1$, $|\Delta n_p/n_0| \ll 1$ and $|\delta n/n_0| \ll 1$, the refractive index is (Esarey *et al.*, 1996)

$$\eta_r \simeq 1 - \frac{\omega_{p0}^2}{2\omega^2}\left(1 - \frac{a^2}{2} + \frac{\Delta n_p}{n_0} + \frac{\delta n}{n_0}\right). \tag{73}$$

In the above expression, the $a^2/2$ term is responsible for relativistic optical guiding (Litvak, 1969; Max *et al.*, 1974; Sprangle *et al.*, 1987a; Sun *et al.*, 1987), the $\Delta n_p/n_0$ term is responsible for preformed density channel guiding (Durfee III *et al.*, 1995; Durfee III and Milchberg, 1993; Gaul *et al.*, 2000; Geddes *et al.*, 2004, 2005a; Johnson and Chu, 1974; Sprangle and Esarey, 1992; Sprangle *et al.*, 1992; Steinhauer and Ahlstrom, 1971; Volfbeyn *et al.*, 1999), and the $\delta n/n_0$ term is responsible for self-channeling (Esarey *et al.*, 1993a; Kurki-Suonio *et al.*, 1989b; Sprangle *et al.*, 1992; Sun *et al.*, 1987), plasma wave guiding (Esarey and Ting, 1990; Sprangle *et al.*, 1990a; Ting *et al.*, 1990), and self-modulation of long laser pulses (Andreev *et al.*, 1992; Antonsen, Jr. and Mora, 1992; Esarey *et al.*, 1994; Sprangle *et al.*, 1992).

B. Relativistic optical guiding

The self-focusing of laser beams by relativistic effects was first considered by Litvak (1969) and Max *et al.* (1974). In the standard theory of relativistic optical guiding (Sprangle *et al.*, 1987a), only the effects of the transverse quiver motion of the electrons are included in the expression for η_r, i.e., $n = n_0$ and $\gamma = \gamma_\perp(r)$, where $\gamma_\perp^2 = 1 + a^2(r)$ and circular polarization is assumed. Inclusion of the self-consistent density response, however, indicates that relativistic self-focusing is ineffective in preventing the diffraction of short ($L \lesssim \lambda_p$) laser pulses (Sprangle *et al.*, 1992, 1990a).

In the weakly-relativistic limit ($a^2 \ll 1$), the refractive index is given by

$$\eta_r \simeq 1 - (\omega_{p0}^2/2\omega^2)(1 - a^2/2), \tag{74}$$

where the density response has been neglected ($n = n_0$). Refractive guiding requires $\partial\eta_r/\partial r < 0$, which is satisfied for a laser intensity profile peaked on-axis, $\partial a^2/\partial r < 0$. The paraxial wave equation with a refractive index given by Eq. (74) has the form of a Schrödinger equation with a third order nonlinearity, as in nonlinear optics where $\eta_r = \eta_0 + \eta_2 I$. Hence, self-focusing will occur when the laser power P exceeds a critical power P_c (Sprangle *et al.*, 1987a).

An equation for the laser spot size $r_s(\zeta, z)$ can be derived by applying a method such as the source dependent expansion (SDE) method (Sprangle *et al.*, 1987b) to the paraxial wave equation [Eq. (69) neglecting the term $\partial^2/\partial\zeta\partial\tau$]. In effect, the SDE method assumes that the radial intensity profile is approximately Gaussian, $|a|^2 = (a_0 r_0/r_s)^2\exp(-2r^2/r_s^2)$, and finds a best fit for the spot size $r_s(\zeta, z)$ locally in space and time. Using the index of refraction given by Eq. (74), the laser spot size evolves according to (Sprangle *et al.*, 1987a)

$$\frac{d^2R}{dz^2} = \frac{1}{Z_R^2 R^3}\left(1 - \frac{P}{P_c}\right), \tag{75}$$

where $R = r_s/r_0$ is the normalized spot size, r_0 is the minimum spot size in vacuum, and $Z_R = kr_0^2/2$ is the vacuum Rayleigh length. The first term on the

right-hand side of Eq. (75) represents vacuum diffraction, whereas the second term term represents relativistic self-focusing. Here, $P/P_c = k_p^2 a_0^2 r_0^2/16$ for circular polarization (for linear polarization, $a_0^2 \to a_0^2/2$). The critical power for relativistic self-focusing is $P_c = 2c(e/r_e)^2(\omega/\omega_{p0})^2$, where $r_e = e^2/m_e c^2$, or in practical units,

$$P_c(\mathrm{GW}) \simeq 17.4\ (\omega/\omega_{p0})^2. \tag{76}$$

The solution to Eq. (75) with $dr_s/dz = 0$ at $z = 0$ is

$$r_s^2/r_0^2 = 1 + (1 - P/P_c)z^2/Z_R^2, \tag{77}$$

which indicates that the spot size diffracts for $P < P_c$, remains guided or "matched" ($r_s = r_0$) for $P = P_c$, and focuses for $P > P_c$. Equation (75) predicts "catastrophic" focusing for $P > P_c$. This results from the approximation $(1+a^2)^{-1/2} \simeq 1 - a^2/2$ in the $a^2 \ll 1$ limit. Higher-order nonlinearities will prevent the laser from focusing indefinitely (Sprangle *et al.*, 1987a).

The above discussion of relativistic guiding neglected the electron density response δn in the expression for the index of refraction. The effectiveness of relativistic guiding can be strongly influenced by the plasma response. In particular, relativistic optical guiding is ineffective in preventing the diffraction of sufficiently short pulses, $L \lesssim \lambda_p/\gamma_\perp$ (Sprangle *et al.*, 1992, 1990a), because the index of refraction becomes modified by the laser pulse on the plasma frequency time scale, not the laser frequency time scale. Typically, relativistic guiding only affects the body of long pulses, $L > \lambda_p$.

In the 1D ($r_s^2 k_p^2 \gg 1$) and weakly-relativistic ($a^2 \ll 1$) limits, nonlinear quasi-static theory (Sprangle *et al.*, 1990a) indicates that the self-consistent electron density response satisfies $\delta n/n_0 - a^2/2 \simeq -\delta\phi$, hence,

$$\eta_r \simeq 1 - (\omega_{p0}^2/2\omega^2)(1 - \delta\phi), \tag{78}$$

where $\delta\phi$ is the normalized electrostatic potential which satisfies

$$\left(\partial^2/\partial\zeta^2 + k_p^2\right)\delta\phi = k_p^2 a^2/2. \tag{79}$$

For long laser pulses with sufficiently smooth envelopes, $|\partial a^2/\partial\zeta| \ll |k_p a^2|$, $\partial^2\phi/\partial\zeta^2$ can be neglected in Eq. (79) (which neglects the generation of plasma waves) and $\delta\phi \simeq a^2/2$. Hence, in the long pulse limit $L \gg \lambda_p$, the index of refraction has the form given by Eq. (73) and the standard theory of relativistic focusing discussed above can be applied to the body of long pulses. Although long pulses can be guided by relativistic effects, they can also be unstable to self-modulation (Andreev *et al.*, 1992; Antonsen, Jr. and Mora, 1992; Sprangle *et al.*, 1992) and laser-hose instabilities (Shvets and Wurtele, 1994; Sprangle *et al.*, 1994), which are discussed in more detail in the Sec. VI.B.

Short pulse $L \lesssim \lambda_p$ diffraction, even in the regime $P \gtrsim P_c$, can be most easily shown as follows. For very short pulses $L < \lambda_p$, the k_p^2 term can be neglected on the left-hand side of Eq. (79). For example, a short pulse with a constant intensity profile ($a^2 = a_0^2$) induces a space charge potential given by $\phi \simeq k_p^2 a_0^2 \zeta^2/4$, and the refractive index becomes

$$\eta_r \simeq 1 - (\omega_{p0}^2/2\omega^2)(1 - k_p^2 a_0^2 \zeta^2/4), \tag{80}$$

as opposed to Eq. (74). This indicates that the effective critical power for a short pulse (Sprangle *et al.*, 1990a) is $P_{c,sp} \simeq 2P_c/(k_p^2\zeta^2) \gg P_c$, since $k_p^2\zeta^2/2 \ll 1$ for a short pulse. In particular, $P_{c,sp}$ becomes infinite at the leading edge of the pulse $\zeta \to 0$. Hence, the leading portion $L < \lambda_p$ of a laser pulse will diffractively erode even when $P \simeq P_c$.

Simulations (Sprangle *et al.*, 1992), based on a 2D-axisymmetric quasi-static fluid model, confirm the inability of relativistic guiding to prevent the diffraction of short laser pulses. The results are shown in Fig. 26 for the parameters $\lambda_p = 0.03$ cm ($n_0 = 1.2\times10^{16}$ cm^{-3}), $r_0 = \lambda_p$ (Gaussian radial profile), $\lambda = 1$ μm ($Z_R = 28$ cm), and $P = P_c$. The initial axial laser profile is given by $|\hat{a}_(\zeta)| = a_0 \sin(-\pi\zeta/L)$ for $0 < -\zeta < L = c\tau_L$, where $a_0 = 0.9$ for the above parameters. Simulations are performed for two laser pulse lengths, $L = \lambda_p$ ($\tau_L = 1$ ps) and $L = \lambda_p/4$ ($\tau_L = 0.25$ ps). The spot size at the pulse center versus normalized propagation distance $c\tau/Z_R$ is shown in Fig. 26 for (a) the vacuum diffraction case, (b) the $L = \lambda_p/4$ pulse, and (c) the $L = \lambda_p$ pulse. The $L = \lambda_p/4$ pulse diffracts almost as if in vacuum. The $L = \lambda_p$ pulse experiences a small amount of initial guiding before diffracting. A preformed parabolic plasma density channel, however, is effective in guiding the $L = \lambda_p$ pulse, as shown in Fig. 26(d), where the channel depth is given by $\Delta n = 1/\pi r_e r_0^2 = 1.3\times10^{15}$ cm^{-3} and the density on-axis is $n_0 = 1.2\times10^{16}$ cm^{-3}.

Experiments on relativistic self-guiding have been performed for laser pulses propagating in gas-filled chambers, pulsed gas jets, or plasmas generated by exploding foils (Borghesia *et al.*, 1997; Borisov *et al.*, 1992; Chiron *et al.*, 1996; Clayton *et al.*, 1998; Krushelnick *et al.*, 1997; Leemans *et al.*, 2002; Monot *et al.*, 1995; Wagner *et al.*, 1997; Young *et al.*, 1995). For example, in experiments using gas jets (Clayton *et al.*, 1998; Krushelnick *et al.*, 1997; Leemans *et al.*, 2002; Santala *et al.*, 2001a; Wagner *et al.*, 1997), the laser pulse was typically observed to propagate through the entire width of the jet ($\sim$ few mm, which corresponds to a few tens of Z_R, depending on the focusing optics used) when $P > P_c$. Many of these occurred in the self-modulated LWFA regime, and accelerated electrons were also observed (Clayton *et al.*, 1998; Krushelnick *et al.*, 1997; Leemans *et al.*, 2002; Santala *et al.*, 2001a; Wagner *et al.*, 1997). In most of these experiments, ponderomotive self-channeling also occurs simultaneously with relativistic self-focusing, as discussed in Sec. V.D.

C. Preformed plasma density channels

The concept of using a plasma density channel to guide a laser beam dates back to early studies of laser fusion (Johnson and Chu, 1974; Steinhauer and Ahlstrom, 1971). Density channels in plasmas have been created by a number of methods. An intense laser pulse propagating in a plasma can create a channel through a combination of ponderomotive and thermal effects. The creation of a density channel through the hydrodynamic expansion of the radial plasma profile was observed in the early 1970's in long-pulse (150 ns) CO_2 laser experiments (Johnson and Chu, 1974). The length of such a channel, however, is limited to the propagation distance of the laser pulse which creates the channel, and the utility of using such a channel to guide a laser pulse many Rayleigh lengths is limited. High power, short laser pulses can be guided in plasma channels created by a variety of methods, including laser-induced hydrodynamic expansion (Durfee III and Milchberg, 1993; Gaul *et al.*, 2000; Geddes *et al.*, 2004, 2005a; Milchberg *et al.*, 1996; Volfbeyn *et al.*, 1999) and capillary discharges (Butler *et al.*, 2002; Ehrlich *et al.*, 1998; Hooker *et al.*, 2000; Hosokai *et al.*, 2000; Luther *et al.*, 2004; Zigler *et al.*, 1996).

To understand the basic principles of channel guiding, consider a parabolic density channel of the form $n = n_0 + \Delta n r^2/r_0^2$, where $\Delta n = n(r_0) - n(0)$ is the channel depth. For a low power $P \ll P_c$, low intensity $a^2 \ll 1$ laser pulse, the index of refraction is given approximately by

$$\eta_r = 1 - \frac{\omega_{p0}^2}{2\omega^2}\left(1 + \frac{\Delta n}{n_0}\frac{r^2}{r_0^2}\right). \tag{81}$$

Analysis of the paraxial wave equation with an index of refraction of this form indicates that the spot size r_s of a Gaussian laser beam with $a^2 = (a_0 r_0/r_s)^2 \exp(-2r^2/r_s^2)$ evolves according to (Esarey *et al.*, 1994)

$$\frac{d^2R}{dz^2} = \frac{1}{Z_R^2 R^3}\left(1 - \frac{\Delta n}{\Delta n_c}R^4\right). \tag{82}$$

The first term on the right-hand side represents the effects of vacuum diffraction and the second term represents the focusing effects of the channel. Equation (82) indicates that a Gaussian beam will be guided at the matched beam spot size $r_s = r_0$ provided that the channel depth Δn is equal to the critical channel depth given by (Sprangle and Esarey, 1992; Sprangle *et al.*, 1992)

$$\Delta n_c = (\pi r_e r_0^2)^{-1}, \tag{83}$$

or $\Delta n_c(\mathrm{cm}^{-3}) = 1.13 \times 10^{20}/r_0^2(\mu\mathrm{m})$, where $r_e = e^2/(m_e c^2)$ is the classical electron radius.

The general solution to Eq. (82) for the initial ($z = 0$) conditions $dr_s/dz = 0$ and $r_s = r_i$ is (Esarey *et al.*, 1994)

$$2\frac{r_s^2}{r_i^2} = 1 + \frac{\Delta n_c r_0^4}{\Delta n r_i^4} + \left(1 - \frac{\Delta n_c r_0^4}{\Delta n r_i^4}\right)\cos\left(k_{\mathrm{os}} z\right), \tag{84}$$

where $k_{\mathrm{os}} = (2/Z_R)(\Delta n/\Delta n_c)^{1/2}$ and r_i is the injected spot size. A matched beam requires $\Delta n r_i^4 = \Delta n_c r_0^4$, e.g., $r_i = r_0$ and $\Delta n = \Delta n_c$. If the beam is not matched within the channel, the spot size oscillates between $r_s^2 = r_i^2$ and $r_s^2 = \Delta n_c r_0^4/\Delta n r_i^2$ with an average value $\langle r_s^2 \rangle = (r_i^2/2)(1 + \Delta n_c r_0^4/\Delta n r_i^4)$. The oscillation period within the channel is $\lambda_{\mathrm{os}} = 2\pi/k_{\mathrm{os}} = \pi Z_R(\Delta n_c/\Delta n)^{1/2}$. The laser beam will remain confined within the channel provided that the maximum radius of the channel r_{ch} is sufficiently large, i.e., $r_{\mathrm{ch}} > r_s$.

To illustrate the effectiveness of optical guiding using preformed density channels, the results of two simulations are presented, both based on the 2D-axisymmetric fluid model discussed in Sec. V. The first simulation (Esarey *et al.*, 1993a) is of a channel-guided LWFA with an ultrashort ($L \simeq \lambda_p$), high-intensity ($a_0 \sim 1$) laser pulse, the results of which are shown in Figs. 27, 28, and 29. In this example, the initial axial laser profile is given by $|\hat{a}(\zeta)| = a_0 \sin(-\pi\zeta/L)$ for $0 < -\zeta < L$, with $a_0 = 0.72$ and $L = 120$ μm (400 fs). Also, $\lambda = 1$ μm and $r_0 = 60$ μm (Gaussian radial profile), which implies $Z_R = 1.1$ cm and $P = 40$ TW. The density on-axis is chosen such that $L = \lambda_p$ ($n_0 = 7.8 \times 10^{16}$ cm^{-3}) and a parabolic profile is assumed with $\Delta n = (\pi r_e r_0^2)^{-1} = 3.2 \times 10^{16}$ cm^{-3}.

Figure 27(a) shows the evolution of the laser spot size versus normalized propagation distance $c\tau/Z_R$. The laser pulse remains guided by the density channel, the laser spot size exhibiting small oscillations about its initial value over the full $20Z_R = 23$ cm simulation length. After $c\tau = 20Z_R$, the pulse profile shows very little distortion from its initial profile. A surface plot of the electron density profile at $c\tau = 20Z_R$ is shown in Fig. 28. The initial, unperturbed parabolic profile can be seen at $\zeta = 0$, and the distortion of the channel by the laser pulse, including the excitation of a large amplitude wakefield along the axis, is evident in the region $\zeta < 0$. In this example nearly all the electrons have been expelled from the vicinity of the laser pulse. The radial variation in the channel density causes a radial variation in the plasma wavelength and curvature of the plasma wavefronts. A slight axial damping of the plasma wave also occurs, as evident in Fig. 29, where the axial electric field E_z is plotted versus ζ along the axis at $c\tau = 20Z_R$. The effects of the wakefields on a continuous 2 MeV electron beam with an initial normalized transverse emittance $\varepsilon_n = 1.0$ mm-mrad and RMS radius $r_b = 10$ μm was also simulated. After $c\tau = 20$ cm, approximately 70% of the beam electrons were trapped and accelerated. The peak electron energy increases nearly linearly with propagation distance with an average acceleration gradient of 5.25 GeV/m (1 GeV in 20 cm).

The second simulation is an example of mismatched laser propagation in a channel, which extends from 0.5 cm $< z <$ 1.5 cm with $n_0 = 5 \times 10^{18}$ cm^{-3}, $\Delta n_p(r_{\mathrm{ch}}) = 4n_0/5$, and $r_{\mathrm{ch}} = 150$ μm (parameters near those of the experiment in (Ehrlich *et al.*, 1996)). Here, a $\lambda = 0.8$ μm, 100 fs, 30 GW (3 mJ), 1.6 times-diffraction-

limited laser pulse is focused on the channel entrance with spot size $r_s = 15$ μm. Owing to the low laser power, the pulse does not become self-modulated. Figure 30 shows that the laser spot size oscillates about its matched value of $r_0 = 28$ μm, emerging from the 1 cm long channel with a radius of 45 μm and a divergence angle of 14 mrad, in approximate agreement with the experiment of (Ehrlich *et al.*, 1996).

The above discussion concerned parabolic channel profiles. Other channel profiles, however, may offer different advantages. Durfee III *et al.* (1995) discuss the formation of "leaky" channels, in which the channel is approximately parabolic out to some radius, after which the density falls off to zero. Such a profile occurs naturally in the creation of plasma channels by hydrodynamic expansion of a hot plasma core in a gas. Higher order transverse modes may not be guided by such a channel, and Antonsen, Jr. and Mora (1995) have described how leaky channels can stabilize certain instabilities, such as small angle forward Raman scattering (Antonsen, Jr. and Mora, 1993; Mori *et al.*, 1994), self-modulation (Andreev *et al.*, 1992; Esarey *et al.*, 1994; Sprangle *et al.*, 1992), and laser-hosing (Shvets and Wurtele, 1994; Sprangle *et al.*, 1994). Hollow channels (e.g., a square channel with density zero on-axis out to the channel radius) may have beneficial properties with regard to particle acceleration (Chiou *et al.*, 1995; Schroeder *et al.*, 1999b). Within the hollow channel, where the plasma density is essentially zero, the transverse profile of the axial wakefield is uniform, thus providing uniform acceleration of an injected beam. The wakefield in such a channel, however, may be damped through resonant absorption in the channel walls (Shvets *et al.*, 1996).

The ability to guide intense laser pulses over many Z_R is an essential element of a high energy LWFA. Plasma channel guiding of short laser pulses was first demonstrated in hydrodynamically formed plasma channels produced by focusing a relatively intense laser beam with an axicon lens (Durfee III and Milchberg, 1993; Milchberg *et al.*, 1996). In these pioneering experiments, high Z-gases were used to facilitate the ionization process. High Z-gases, however, are susceptible to further ionization when used with ultra-high intensity lasers, and, therefore, a method was needed to allow the use of low Z-gases. By separating out the ionization and heating phase of the channel formation, channels were produced in hydrogen gas with the ignitor-heater method (Volfbeyn *et al.*, 1999).

Another laser-induced channel guiding technique utilizes a pump-probe method (Krushelnick *et al.*, 1997; Wagner *et al.*, 1997). In these experiments, an intense pump pulse with $P > P_c$ was guided through a gas jet through a combination of relativistic self-focusing and ponderomotive self-channeling. The ponderomotive force of the pump pulse created a plasma channel after its passage. This channel was then used to guided a low power probe pulse propagating along the axis.

In addition to laser-induced channels, guiding has also been demonstrated in plasma channels produced by capillary discharges (Butler *et al.*, 2002; Ehrlich *et al.*, 1998; Hooker *et al.*, 2000; Hosokai *et al.*, 2000; Luther *et al.*, 2004; Zigler *et al.*, 1996). One present advantage of capillary discharges over that of laser-induced plasma channels is length. Laser-induced channels have typically been limited to a few mm, whereas capillary discharges can be on the order a few cm. Possible disadvantages of capillary discharges include a limited lifetime and the introduction of higher Z impurities due to wall ablation.

Other channel techniques have also been considered, such as evacuated and gas-filled capillaries (Dorchies *et al.*, 1999), laser-ablated capillaries (Kitagawa *et al.*, 2004), discharge-initiated laser-induced channels (Gaul *et al.*, 2000), as well as laser-induced channels using a cluster jet (Kumarappan *et al.*, 2005), which has the possible advantage of producing lower density channels. Prior to 2004, however, all demonstrations of guiding in preformed plasma density channels were limited to the mildly relativistic regime, i.e., $a_0^2 \ll 1$.

Channeling at relativistic intensities (Geddes *et al.*, 2004, 2005a) was realized with preformed guiding channels created using a variation of the ignitor-heater method. In these experiments, a plasma was formed in a 2.5 mm long supersonic H_2 gas jet with an atomic density of 3–4$\times 10^{19}$ cm^{-3} by an ignitor pulse (15 mJ, 60 fs) that is co-axial with the drive pulse, then heated by a heater pulse (150 mJ, 250 ps). Figure 31 shows the basic experimental setup. Hydrodynamic expansion of the plasma formed a channel that guided a relativistically intense drive pulse that was focused at the entrance to the channel. The drive pulse (500 mJ, 55 fs) was focused with an off-axis parabola to a spot of 7–8.5 μm FWHM resulting in a laser intensity of 1.1×10^{19} W/cm^2).

The ignitor-heater method provides the ability to tailor the channel properties. By varying the time delay between the heater and drive pulses, energy of the heater pulse, and spatial overlap, channels can be created with different radial density profiles. Figure 32 shows an example of mode images of laser spots at 4 TW (7 μm input spot, 7×10^{18} W/cm^2). With the channel on, the output spot (b) matches the input (a). The mode imager resolution is restricted by f# constraints in the target chamber, and measures a 12 μm FWHM spot size for both input and output. Hence, the guided intensity is between 10^{18} and 2.5×10^{18} W/cm^2, with the lower limit set by the 12 μm mode imager observation and the upper limit set by the input spot size. In the absence of any plasma, a large mode size consistent with vacuum diffraction is observed (c), and with the gas jet on but the channel off (d) diffraction is increased by ionization effects (Leemans *et al.*, 1992; Rankin *et al.*, 1991), showing that self guiding alone is insufficient to efficiently guide the laser pulse.

D. Ponderomotive self-channeling

The radial ponderomotive force of a long laser pulse ($L > \lambda_p$) propagating in an initially uniform plasma can expel electrons from the axis thus creating a density channel (i.e., self-channeling or electron cavitation) (Esarey *et al.*, 1993a; Kurki-Suonio *et al.*, 1989b; Sprangle and Esarey, 1992; Sprangle *et al.*, 1992; Sun *et al.*, 1987). This can enhance the effects of relativistic self-focusing. Consider a long ($L \gg \lambda_p$) axially uniform laser pulse propagating in an initially uniform plasma. The steady-state radial force balance indicates that the space charge force is equal to the ponderomotive force, i.e., $\nabla_\perp \phi = \nabla_\perp \gamma_\perp$, where $\gamma_\perp = (1+a^2)^{1/2}$ (with circular polarization). This implies a density perturbation via the Poisson equation $\nabla_\perp^2 \phi = k_p^2 \delta n/n_0$ given by (Kurki-Suonio *et al.*, 1989b; Sprangle *et al.*, 1992; Sun *et al.*, 1987)

$$\delta n/n_0 = k_p^{-2} \nabla_\perp^2 (1+a^2)^{1/2}, \tag{85}$$

assuming $|\delta n/n_0| \leq 1$. The corresponding index of refraction is given by

$$\eta_r \simeq 1 - \frac{\omega_{p0}^2}{2\omega^2} \left[\frac{1 + k_p^{-2} \nabla_\perp^2 (1+a^2)^{1/2}}{(1+a^2)^{1/2}} \right]. \tag{86}$$

This can also be derived from 2D nonlinear plasma theory via Eq. (70). In the long pulse limit $L \gg \lambda_p$, $|\partial \Psi/\partial \zeta| \ll |k_p \Psi|$ and $(1+\Psi) \simeq (1+a^2)^{1/2}$, which yields Eq. (86). Neglected in Eq. (86) is the generation of plasma waves, which can lead to the self-modulation of long pulses.

In the limit $a^2 \ll 1$, a Gaussian laser profile $a^2 = a_0^2 \exp(-2r^2/r_0^2)$ creates a density profile $\delta n = -\delta n(0)(1 - 2r^2/r_0^2)\exp(-2r^2/r_0^2)$. Along the axis, the depth of the ponderomotive channel is given by $\delta n(0) = a_0^2 \Delta n_c$, where Δn_c is given by Eq. (83). Analysis of the paraxial wave equation with a density perturbation given by $\delta n/n_0 = k_p^{-2} \nabla_\perp^2 a^2/2$ indicates that the normalized spot size of a Gaussian laser pulse evolves according to (Sprangle *et al.*, 1991)

$$\frac{d^2 R}{dz^2} = \frac{1}{Z_R^2 R^3} \left(1 - \frac{P}{P_c} - \frac{\delta n(0)}{2\Delta n_c} R^{-2} \right). \tag{87}$$

where $\delta n(0) = a_0^2 \Delta n_c$ and $a^2 \ll 1$ is assumed. Hence, in the limit $P/P_c \ll 1$, the ponderomotive channel depth required to guide a laser pulse is $\delta n(0) \geq 2\Delta n_c$. Clearly, when $a_0 < 1$, the ponderomotive self-channel alone will not guide the laser pulse. Furthermore, $|\delta n/n_0| < 1$ implies $a_0^2 < 2(P/P_c)^{1/2}$ and $\delta n(0) < 2(P/P_c)^{1/2} \Delta n_c$. Hence, $P/P_c \leq 1$ implies $\delta n(0) < 2\Delta n_c$, which again indicates that the ponderomotive channel alone will not guide the laser pulse. For laser powers approaching the critical power $P \to P_c$, guiding is achieved predominantly by relativistic self-focusing. Ponderomotive self-channeling can enhance this effect, but does not dramatically alter the power threshold for guiding. More detailed studies (Sun *et al.*, 1987), which include the effects of relativistic self-focusing and ponderomotive self-channeling, conclude that the threshold power for guiding is $P(\mathrm{GW}) \geq 16.2(\omega^2/\omega_{p0}^2)$.

E. Plasma wave guiding

An ultrashort ($L < \lambda_p$) laser pulse can be guided by a plasma wave, provided that the laser pulse is properly phased within the wakefield and the wakefield amplitude is sufficiently large (Esarey and Ting, 1990; Sprangle *et al.*, 1990a; Ting *et al.*, 1990). The effective index of refraction for a low power ($P/P_c \ll 1$), low intensity ($a^2 \ll 1$) laser pulse propagating in a plasma wave is given by

$$\eta_r \simeq 1 - (\omega_{p0}^2/2\omega^2)(1 + \delta n/n_0), \tag{88}$$

where δn is the density oscillation of the plasma wave, which is assumed to be unaffected by the low intensity laser pulse. Consider a plasma wave of the form $\delta n = \delta \hat{n}(r) \sin(k_p \zeta)$, where $\delta \hat{n} > 0$ and $d\delta \hat{n}/dr < 0$. In regions where $\sin(k_p \zeta) < 0$, the plasma wave acts as a local density channel and enhances focusing, and in regions where $\sin(k_p \zeta) > 0$, the plasma wave enhances diffraction. Notice that a test laser pulse experiences maximum focusing at the minimum of δn (i.e., $\zeta = -\pi/2$). As discussed in Sec. II.G, it can be shown that a short laser pulse can be frequency upshifted by a plasma wave wakefield provided that it resides in the phase region where $\partial \delta n/\partial \zeta < 0$. In particular, maximum frequency upshifting occurs at the maximum of $-\partial \delta n/\partial \zeta$ (i.e., $\zeta = -\pi$ for the above example). In general, for a sinusoidal plasma wave, a test laser pulse will experience both enhanced focusing and frequency upshifting over a $|k_p \Delta \zeta| = \pi/4$ phase region of the plasma wave. Furthermore, Eq. (88) describes how a plasma wave can lead to the modulation of a long ($L > \lambda_p$) laser pulse (Esarey and Ting, 1990), as illustrated schematically in Fig. 33.

In addition to a plasma wave acting as a local density channel and providing periodic regions of enhanced focusing and diffraction as described above, a plasma wave can enhance the self-focusing of long ($L \gg \lambda_p$) laser pulses by several other methods. For example, the electric field profile E_{pw} of the plasma wave can provide an additional radial ponderomotive force via ∇E_{pw}^2 (Joshi *et al.*, 1982). In addition, the oscillatory motion of the plasma electrons in the plasma wave can contribute to the relativistic Lorentz factor (Mori *et al.*, 1988). Furthermore, the plasma wave can lead to the generation of higher-order Stokes and anti-Stokes light waves (i.e., energy cascading) which can affect self-focusing (Gibbon and Bell, 1988). These effects have been observed in experiments (Joshi *et al.*, 1982) and simulations (Gibbon and Bell, 1988; Mori *et al.*, 1988) of two-frequency laser-plasma interactions, in which the plasma wave is resonantly driven by the laser beat wave.

VI. LASER-PLASMA INSTABILITIES

Laser plasma instabilities can limit the laser propagation distance and degrade the performance of a laser-driven accelerator. This section will provide a brief

overview of a few instabilities that are relevant to short-pulse laser-driven accelerators: stimulated forward and backward Raman scattering (Esarey and Sprangle, 1992; Kruer, 1988; McKinstrie and Bingham, 1992; Sakharov and Kirsanov, 1994), self-modulation (Andreev *et al.*, 1992; Antonsen, Jr. and Mora, 1992, 1993; Esarey *et al.*, 1994; Sprangle *et al.*, 1992), and laser-hose instabilities (Shvets and Wurtele, 1994; Sprangle *et al.*, 1994). In particular, this section will consider instabilities relevant to laser pulses short compared to the ion response time. Other instabilities present in long-pulse laser-plasma interactions, such as parametric coupling to ion modes, which have been observed in PBWA experiments (Amiranoff *et al.*, 1992), will not be discussed.

A. Stimulated Raman Scattering

Stimulated Raman scattering involves the interaction of a light wave with an electron plasma wave (Kruer, 1988). In its most basic form, it consists of the decay of the pump laser field, of frequency and wavenumber $(\omega_0, \boldsymbol{k}_0)$, into an electron plasma wave $(\omega, \boldsymbol{k})$ and two daughter light waves, namely, a Stokes wave $(\omega_0 - \omega, \boldsymbol{k}_0 - \boldsymbol{k})$ and an anti-Stokes wave $(\omega_0 + \omega, \boldsymbol{k}_0 + \boldsymbol{k})$. Typically, $\omega \simeq \omega_p + i\Gamma$ where the growth rate Γ is obtained through a standard linear instability analysis. In such an analysis, the pump laser field is assumed to be a 1D plane wave of the form $a \sim a_0 \exp(i\boldsymbol{k}_0 \cdot \boldsymbol{r} - i\omega_0 t)$. Perturbations are introduced $\delta a \sim \exp[i(\boldsymbol{k}_0 \pm \boldsymbol{k}) \cdot \boldsymbol{r} - i(\omega_0 \pm \omega)t]$ and the linearized equations are then solved to determine the behavior of the instability. Since the pump laser is assumed to be a 1D plane wave, the 3D evolution of the pump laser is not taken into consideration. In particular, the effects of diffraction and self-focusing are neglected. Strictly speaking, the resulting analysis is only valid for times short compared to the characteristic evolution time τ_E of the pump laser, e.g., $t < \tau_E \sim Z_R/c$. In practice, however, the growth rates obtained from such an analysis can be adequate estimates provided that the mode frequency and growth rate are large compared to τ_E^{-1}.

For an infinite, 1D plane wave pump field, the purely temporal Raman growth rates, i.e., $\delta a \sim \exp(\Gamma t)$ with growth rate Γ independent of t, can be obtained in a straightforward manner. The basic treatment of forward and backward Raman scattering is presented in the monograph by Kruer (1988). Temporal growth rates for the various Raman modes in various regimes has been summarized by Antonsen, Jr. and Mora (1993). For short laser pulses, however, the growth and propagation of the instability with respect to the laser pulse front must be correctly taken into consideration. Antonsen, Jr. and Mora (1992, 1993) first applied convective instability analysis, or a spatiotemporal analysis, to Raman instabilities in order to account for the short-pulse character of the instability.

1. Backward Raman scattering

In Raman backscattering (RBS), the pump wave (ω_0, k_0) decays into a plasma wave (ω, k) and a backward going scattered wave $(\omega_0 - \omega, k_0 - k)$, where $\omega \simeq \omega_p$ and $k \simeq 2k_0$. The standard temporal growth rate (Kruer, 1988), in the limits $a_0^2 \ll 1$ and $\omega_p \ll \omega_0$, i.e., the weakly-coupled regime, is $\Gamma = (a_0/2)(\omega_p \omega_0)^{1/2}$. In general, the scattered mode can propagate at some angle θ with respect to the pump wave, i.e., sidescatter, and the growth rate is given by $\sin(\theta/2)$ times the RBS result. The spatiotemporal analysis indicates that the number of e-folds N_e of the instability, $\delta a \sim \exp(N_e)$, is given by (Antonsen, Jr. and Mora, 1993)

$$N_e \simeq (a_0^2 k_p k_0/8)^{1/2} |\zeta|. \tag{89}$$

In effect, since the scattered wave is moving opposite to the pump, the temporal growth is modified by $ct \to |\zeta|/2$, where $\zeta = z - ct$ is a measure of the distance back from the front of the laser pulse.

Typically, RBS is the fastest growing of the Raman scattering instabilities. In laser-plasma accelerators, RBS is significant for a number of reasons. At low pump laser intensities, the spectrum of the backscattered radiation can be used to determine $\omega - \omega_p$, and hence the plasma density can be determined experimentally. For high pump intensities, however, it has been observed that the backscattered spectrum broadens (Darrow *et al.*, 1992; Krushelnick *et al.*, 1998) and, in some cases, becomes extremely broad, such that the $\omega - \omega_p$ peak can no longer be distinguished. Raman sidescatter and backscatter can erode the back of a long pulse, $L > \lambda_p$, since energy is being transported out of the pulse. This erosion has been observed in fluid (Andreev *et al.*, 1995; Antonsen, Jr. and Mora, 1993) and particle simulations (Bulanov *et al.*, 1995; Decker *et al.*, 1996b).

As the RBS mode grows to large amplitude, it can trap the background plasma electrons, thus heating the plasma and creating a fast tail on the electron distribution. The phase velocity of the RBS plasma wave is $v_p = \omega/k = \omega_p/2k_0 \ll c$. Since $v_p/c \ll 1$, the plasma wave can trap the background thermal electrons. The resulting fast electrons can be subsequently trapped by Raman scattered modes propagating at smaller angles θ, which will accelerate the electrons to higher energies (Bertrand *et al.*, 1995; Esarey *et al.*, 1998; Joshi *et al.*, 1981). Eventually, these background electrons can be trapped and accelerated to very high energies by the plasma wave associated with the forward Raman instability or the self-modulation instability, which has $v_p \simeq c$. This mechanism may explain how background plasma electrons can be trapped and accelerated to high energies, as is observed in experiments (Coverdale *et al.*, 1995; Gahn *et al.*, 1999; Gordon *et al.*, 1998; Leemans *et al.*, 2001; Malka *et al.*, 2001; Nakajima *et al.*, 1995; Ting *et al.*, 1997; Wagner *et al.*, 1997) and simulations (Bulanov *et al.*, 1995; Decker *et al.*, 1996b) in the self-modulated or forward Raman scattering regimes.

For sufficiently large relativistic plasma wave amplitudes, self-trapping of background plasma electrons can also result in electron bunch generation and acceleration (Modena *et al.*, 1995).

For high pump intensities, theory predicts that stimulated backscattering occurs in the strongly coupled or Compton regime (Antonsen, Jr. and Mora, 1993; Everett *et al.*, 1995b; Leemans *et al.*, 1991; Schroeder *et al.*, 2003b; Shvets *et al.*, 1997), for which $\omega \sim \Gamma \gg \omega_p$ and the number of e-folds is $N_e = (\sqrt{3}/2)(\omega_p^2\omega_0 a_0^2/4)^{1/3}|\zeta|/\gamma_\perp$. In addition, 1D nonlinear theory predicts that for a linearly polarized pump laser field, stimulated backscattered harmonic radiation can be generated (Esarey and Sprangle, 1992) at frequencies given approximately by $(2\ell+1)\omega_0$ (ℓ = integer), i.e., odd harmonics. Although the growth rate for the higher harmonics can be significant when $a_0^2 \gg 1$, thermal effects, i.e., trapping of the background plasma electrons, can severely limit the generation of higher harmonics (Esarey and Sprangle, 1992).

2. Forward Raman scattering

In Raman forward scattering (RFS) (Kruer, 1988), the scattered waves propagate parallel (or nearly parallel) to the pump wave, and the associated plasma wave has a phase velocity $v_p \simeq c$. Hence, the plasma wave can be used to accelerate electrons to high energies. The RFS instability can serve as the basis for a LWFA (Esarey *et al.*, 1996; Joshi *et al.*, 1981; Mori *et al.*, 1994; Tajima and Dawson, 1979), in which a single long ($L > \lambda_p$) laser pulse becomes modulated via RFS and drives a large amplitude plasma wave. A LWFA based on RFS can be viewed as the 1D analogue to the self-modulated LWFA.

The physical mechanism of RFS can be understood by the following 1D description (Mori, 1997). Consider a long uniform laser pulse propagating in the presence of an initially small amplitude plasma wave of the form $\delta n = \delta n_0 \sin k_p\zeta$ with $\delta n_0 > 0$. Since the local group velocity v_g is given by $v_g/c \simeq 1 - \omega_p^2(\zeta)/2\omega_0^2$, the local group velocity decreases in regions where $\delta n > 0$ and increases in regions where $\delta n < 0$. This tends to modulate the laser pulse such that the intensity modulations are $\pi/2$ out of phase with the density wave, i.e., $a \simeq a_0 + \delta a$, where $\delta a = \delta a_0 \cos k_p\zeta$ and $\delta a_0 > 0$. This intensity modulation feeds back via $(\partial^2/\partial\zeta^2 + k_p^2)\delta n/n_0 = (\partial^2/\partial\zeta^2)a^2/2$ and drives the plasma wave to larger amplitudes, resulting in the RFS instability.

Several regimes of the RFS can be identified (Antonsen, Jr. and Mora, 1993; Decker *et al.*, 1996a; McKinstrie and Bingham, 1992; Schroeder *et al.*, 2003b), such as a 4-wave regime, in which both $\omega_0 \pm \omega_p$ modes are resonant, and a 3-wave regime, in which only $\omega_0 - \omega_p$ is resonant with the pump laser and the plasma wave. The temporal growth rate in the 4-wave resonant regime is $\Gamma_4 = \omega_p^2 a_0/2\sqrt{2}\omega_0$, the temporal growth rate in the 4-wave nonresonant regime is $\Gamma_{4nr} = \sqrt{3}\omega_p(a_0\omega_p^2/4\omega_0^2)^{2/3}/2$, and the temporal growth rate in the 3-wave regime is $\Gamma_3 = \omega_p a_0(\omega_p/\omega_0)^{1/2}/4$. The spatiotemporal analysis (Antonsen, Jr. and Mora, 1993; Decker *et al.*, 1996a; Schroeder *et al.*, 2003b) indicates, however, that as the RFS instability grows, it passes through these various regimes, depending on the relative value of $|\zeta|/c\tau$, where $\zeta = z - ct$ and $\tau = t$ are the independent coordinates. The number of e-foldings for these three RFS modes and the corresponding spatiotemporal regimes are roughly given by (Antonsen, Jr. and Mora, 1993; Decker *et al.*, 1996a; Schroeder *et al.*, 2003b)

$$N_e \simeq 2\Gamma_4(|\zeta|\tau/c)^{1/2}\ , \quad \text{for } a_0^2\frac{|\zeta|}{c\tau} \gg 2\frac{\omega_p^2}{\omega_0^2}, \tag{90}$$

$$N_e \simeq \frac{3}{2}\Gamma_{4nr}(2|\zeta|\tau^2/c)^{1/3}\ , \quad \text{for } 8\frac{\omega_p^5}{\omega_0^5} \ll \frac{a_0^2}{2}\frac{|\zeta|}{c\tau} \ll \frac{\omega_p^2}{\omega_0^2}, \tag{91}$$

$$N_e \simeq 2\Gamma_3(|\zeta|\tau/c)^{1/2}, \quad \text{for } a_0^2\frac{|\zeta|}{c\tau} \ll 16\frac{\omega_p^5}{\omega_0^5}\ , \tag{92}$$

where $a_0^2 \ll 1$ and $\omega_p^2/\omega_0^2 \ll 1$ are assumed. Decker *et al.* (1996a) describe that for a fixed ζ within the pulse, the RFS instability transitions through the various regimes as a function of time. A similar analysis has been applied by Antonsen, Jr. and Mora (1993) to describe small angle RFS, the resulting growth rate is proportional to Γ_3, similar to Eq. (92). As a side note, the paraxial approximation to the wave operator $(\nabla_\perp^2 + 2ik_0\partial/\partial c\tau)$ is not sufficient to describe direct ($\theta = 0$) RFS; retention of the term $2\partial^2/\partial\zeta\partial c\tau$ is necessary to describe on-axis RFS. This was done in the fluid simulation of the self-modulated LWFA presented in Sec. III.D, i.e., the effects of both the RFS and self-modulation instabilities are included. A nonparaxial theory (Esarey *et al.*, 2000), describing the nonlinear coupling of RFS and self-modulation instabilities, has found that the self-modulation instability often dominates in regimes of interest to the self-modulated LWFA.

In addition, it is also possible for a RFS mode to undergo multiple scattering, sometimes referred to as cascading (Gibbon and Bell, 1988; Joshi *et al.*, 1981), resulting in multiple waves with frequencies $\omega_0 \pm \ell\omega_p$ (ℓ = integer). It is possible to interpret this as photon acceleration, or phase-modulation by the plasma wave, of the scattered light wave (Mori *et al.*, 1994). Numerous high-order Stokes and anti-Stokes lines have been observed in simulations of RFS (Decker *et al.*, 1994). Multiple (Coverdale *et al.*, 1995; Moore *et al.*, 1997; Wagner *et al.*, 1997) (up to the fifth (Modena *et al.*, 1995)) anti-Stokes lines have been observed in RFS or self-modulated LWFA experiments.

B. Self-modulation and laser-hose instabilities

A formalism has been developed (Esarey *et al.*, 1994, 2000; Sprangle *et al.*, 1994) to describe the 3D evolution of laser pulses in plasmas, including the effects of diffraction, relativistic and channel guiding, finite pulse

duration, and coupling to the self-consistent plasma wave generated by the pulse structure. This formalism has been used to describe a class of "whole-beam" instabilities, which includes self-modulation (Esarey *et al.*, 1994; Sprangle *et al.*, 1994) and laser-hose (Sprangle *et al.*, 1994) instabilities. In this formalism, equations are derived to describe the evolution of the local laser pulse spot size $x_s(\zeta,t)$ and the local laser pulse centroid $x_c(\zeta,t)$, where the transverse profile of the laser field is assumed to be a Gaussian of the form $a \sim \exp\left[-(x-x_c)^2/x_s^2\right]$ (the y profile can be similarly defined). The self-modulation instability consists of a periodic "sausaging" of the laser spot size x_s and the laser-hose consists of a periodic "kinking" of the laser centroid x_c, as show schematically in Fig. 34. In their most basic forms, the self-modulation and laser-hose instabilities are described by spot size and centroid perturbations of the forms $\delta x_{s,c} \sim \exp(\Gamma_{s,c}t + ik_p\zeta)$, i.e., having a period equal to the plasma wavelength $\lambda_p = 2\pi/k_p$ and a spatiotemporal growth rate $\Gamma_{s,c} = \Gamma_{s,c}(\zeta,t)$. Intrinsically, these instabilities involve a coupling to a plasma wave, and the dynamics of the instabilities are determined by the enhanced diffraction and focusing of the laser pulse owing to the presence of the plasma wave.

The physical mechanism underlying self-modulation has been described previously in Sec. III.D. The physical mechanism for laser hosing (Shvets and Wurtele, 1994; Sprangle *et al.*, 1994) is somewhat similar. Consider a long, $L > \lambda_p$, guided laser pulse $P/P_c = 1 - \Delta n/\Delta n_c$, with a centroid which is initially perturbed at the plasma wavelength $x_c \simeq x_{c0}\sin(k_p\zeta)$. This periodic centroid displacement will drive an asymmetric plasma wave. Notice that for $x_c^2/x_s^2 \ll 1$, the intensity profile is approximately $a^2 \simeq a_0^2(1 + 4xx_c/x_s^2)\exp(-2x^2/x_s^2)$. At a fixed x position above the axis, $x = x_0$, the laser intensity modulation has the form $a^2(x_0)/a_0^2 \sim 1 + 4(x_0x_{c0}/x_s^2)\sin(k_p\zeta)$, which drives a plasma wave. At a fixed x position below the axis, $x = -x_0$, the laser intensity is similarly modulated, but π out of phase with respect to the $x = x_0$ modulation. Hence, the plasma wave driven below the axis is π out of phase with respect to the plasma wave driven above the axis, i.e., an asymmetric (with respect to x) plasma wave. Roughly speaking, the plasma wave has the form $\delta n \sim -(x/x_s)\cos(k_p\zeta)$. The laser pulse will tend to focus into the regions of reduced plasma density. For the asymmetric plasma wave, the laser pulse evolves in such a way as to enhance the initial centroid perturbation and the process proceeds in an unstable manner.

Equations describing the behavior of the spot size $x_s(\zeta,\tau)$ and centroid $x_c(\zeta,\tau)$ can be derived by analyzing the paraxial wave equation including the effects of a performed parabolic density channel and the self-consistent plasma response given by

$$\frac{\delta n}{n_0} = \int_0^\zeta d\zeta' \cos[k_p(\zeta-\zeta')]\frac{\partial}{\partial\zeta'}\frac{a^2(\zeta')}{2}. \qquad (93)$$

In the limits $a^2 \ll 1$ and $k_p^2 r_0^2 \gg 1$, x_s and x_c obey equations of the form (Sprangle *et al.*, 1994)

$$\left(\frac{\partial^2}{\partial\hat{\tau}^2} + \frac{\Delta n}{\Delta n_c}\right)\hat{x}_c = -4k_p\int_0^\zeta d\zeta' \sin[k_p(\zeta'-\zeta)]\,[x_c(\zeta') - x_c(\zeta)]\,F_c(\zeta',\zeta)\frac{P(\zeta')}{P_c}, \qquad (94)$$

and

$$\frac{\partial^2\hat{x}_s}{\partial\hat{\tau}^2} - \left(1 - \frac{\hat{x}_s P}{\hat{y}_s P_c} - \frac{\Delta n}{\Delta n_c}\hat{x}_s^4\right)\hat{x}_s^{-3} = 4\hat{x}_s\int_0^\zeta d\zeta' \cos[k_p(\zeta'-\zeta)]\frac{\partial}{\partial\zeta'}\left[F_s(\zeta',\zeta)\frac{P(\zeta')}{P_c}\right]. \qquad (95)$$

Also, $\hat{y}_c$ and $\hat{y}_s$ obey equations similar to Eqs. (94) and (95), respectively. In the above, $\hat{x}_c = x_c/r_0$, $\hat{y}_c = y_c/r_0$, $\hat{x}_s = x_s/r_0$, $\hat{y}_s = y_s/r_0$, $\hat{\tau} = c\tau/Z_R$, $Z_R = kr_0^2/2$ is the Rayleigh length, $\Delta n_c = (\pi r_e r_0^2)^{-1}$ is the critical channel depth, $P(\zeta)/P_c = a^2 x_s y_s k_p^2/16$ is the laser power normalized to the critical power, and $F_{s,c}(\zeta',\zeta)$ are functions which depend on x_s, y_s, x_c, and y_c and couple the spot size dynamics to the centroid dynamics (Sprangle *et al.*, 1994).

The right-hand side of Eq. (94) indicates that if $x_c(\zeta) = x_c(\zeta')$ initially (i.e., a uniform centroid), $x_c(\zeta)$ will not increase. Hence, the laser-hose instability requires a non-uniform head-to-tail centroid displacement (Sprangle *et al.*, 1994) $\partial x_c/\partial\zeta \neq 0$. The right-hand side of Eq. (95) indicates that axial gradients in the laser power $\partial P/\partial\zeta \neq 0$ will lead to modulations in the laser envelopes (x_s, y_s), which can grow in an unstable manner as discussed in Sec. III.D. Both the self-modulation and laser-hose instabilities can occur in either a uniform plasma ($\Delta n = 0$) or in a preformed density channel.

In the absence of a centroid perturbation, i.e., $x_c = 0$ (no hosing), self-modulation is described by Eq. (95). For an axisymmetric pulse ($x_s = y_s = r_s$), $F_{s,c} = [R^2(\zeta) + R^2(\zeta')]^{-2}$ with $R = r_s/r_0$ (Esarey *et al.*, 1994). The second, third, and fourth terms on the left-hand side of Eq. (95) represent the effects of vacuum diffraction, relativistic focusing, and channel focusing, respectively, whereas the term on the right-hand side represents the nonlinear coupling of the laser envelope to the plasma wave. Equation (95) describes well-known laser pulse

evolution, such as the inability of relativistic guiding to prevent the diffraction of short pulses $L < \lambda_p$ (Sprangle *et al.*, 1992, 1990a,b; Ting *et al.*, 1990).

The evolution of a long, axially uniform laser beam can be examined in the limit where the effect of the plasma wave is neglected, i.e., the nonlinear coupling term on the right-hand side of Eq. (95) is set equal to zero. Neglecting the coupling term, the solution to Eq. (95) for the initial ($z = 0$) conditions $dr_s/dz = 0$ and $r_s = r_i$ is (Esarey *et al.*, 1994)

$$\frac{r_s^2}{r_i^2} = \frac{\Delta n_c r_0^4}{2\Delta n r_i^4}\left[1 - \frac{P}{P_c} + \frac{\Delta n r_i^4}{\Delta n_c r_0^4} - \left(1 - \frac{P}{P_c} - \frac{\Delta n r_i^4}{\Delta n_c r_0^4}\right)\cos\left(k_{\rm os} z\right)\right], \quad (96)$$

where $k_{\rm os} = (2/Z_R)(\Delta n/\Delta n_c)^{1/2}$ and r_i is the injected spot size. For $P \le P_c$, the spot size oscillates between $r_s^2 = r_i^2$ and $r_s^2 = (1 - P/P_c)\Delta n_c r_0^4/(\Delta n r_i^2)$ with an oscillation period $\lambda_{\rm os} = 2\pi/k_{\rm os} = \pi Z_R(\Delta n_c/\Delta n)^{1/2}$. A matched beam with $r_s = r_i = r_0$ requires $P = P_M$, where (Esarey *et al.*, 1994)

$$P_M = P_c(1 - \Delta n/\Delta n_c), \quad (97)$$

i.e., the effective critical power P_M for guiding is reduced by a finite density channel (assuming $\Delta n \le \Delta n_c$). Notice that for $r_i = r_0$ and $(k_{\rm os} z)^2 \ll 1$, Eq. (96) reduces to $r_s^2/r_0^2 = 1 + (1 - P/P_c - \Delta n/\Delta n_c)(z/Z_R)^2$. This indicates that beam will initially focus for $P > P_M$ or diffract for $P < P_M$ with an effective Rayleigh length of $Z_R(1 - P/P_c - \Delta n/\Delta n_c)^{-1/2}$.

The effect of the plasma wave on the spot size evolution is described by the right-hand side of Eq. (95). The initial effect of the plasma wave can be estimated by approximating $R(\zeta') = R(\zeta)$ within the integral in Eq. (95), i.e., initially the spot size is uniform throughout the pulse. In this limit the right-hand side of Eq. (95) can be written as $(-\delta n/\Delta n_c)/(2R^3)$, where δn is the initial density perturbation given by Eq. (93). The rise associated with the front of the pulse gives a nonzero value of $\partial a^2/\partial\zeta$ that generates a finite amplitude density wake. Throughout the body of a long, flat-top pulse, this density wake has the form $\delta n = \delta\hat{n}\cos(k_p\zeta)$. In particular, for a flat-top pulse with a fast rise, $k_p^2 L_{\rm rise}^2 \ll 1$, Eq. (93) yields $\delta n/n_0 = -(a_0^2/2)\cos(k_p\zeta)$ and the right-hand side of Eq. (95) can be written as $(-\delta n/2\Delta n_c)R^{-3} = R^{-3}(P/P_c)\cos(k_p\zeta)$. Hence, at the phase regions where $\cos(k_p\zeta) = -1$, focusing requires $P \ge P_M/2$ (for $k_p^2 L_{\rm rise}^2 \gg 1$, the initial wake δn vanishes and focusing requires $P \ge P_M$). Clearly, the effect of the initial density wake $\delta n(\zeta)$ is to produce ζ-periodic regions of enhanced focusing and diffraction. This causes the laser intensity to become modulated at λ_p, which subsequently enhances the density wake at later times. This is the basis of the self-modulation instability.

For sufficiently small perturbations, $x_s/r_0 \ll 1$ and $x_c/r_0 \ll 1$, Eqs. (94) and (95) decouple and self-modulation and the laser-hose instability can be analyzed independently. The growth of the instabilities for a long ($L \gg \lambda_p$), optically-guided ($P = P_M$) laser pulse can be analyzed by perturbing Eq. (95) about the matched-beam equilibrium. Asymptotic growth rates can be obtained in various regimes using standard methods. The number of e-folds $N_e = \Gamma_{c,s}\tau$ in the various regimes are given by (Esarey *et al.*, 1994; Sprangle *et al.*, 1994):
Long pulse regime: $k_p|\zeta|Z_R/z \gg 4\alpha_1 P_c/P$

$$N_e = \frac{3\sqrt{3}}{4}\left(\alpha_2\frac{P}{P_c}k_p|\zeta|\frac{z^2}{Z_R^2}\right)^{1/3}, \quad (98)$$

Intermediate regime: $(\alpha_3/4)(P/P_c) \ll k_p|\zeta|Z_R/z \ll 4\alpha_1 P_c/P$

$$N_e = \left(\alpha_3\frac{P}{P_c}k_p|\zeta|\frac{z}{Z_R}\right)^{1/2}, \quad (99)$$

Short pulse regime: $k_p|\zeta|Z_R/z \ll (\alpha_3/4)(P/P_c)$

$$N_e = \frac{3\sqrt{3}}{4}\left(\alpha_3\frac{P}{P_c}k_p^2|\zeta|^2\frac{z}{Z_R}\right)^{1/3}. \quad (100)$$

For the laser-hose instability, $\alpha_1 = \alpha_2 = \alpha_3 = 1$. For self-modulation, $\alpha_1 = \sqrt{2}(2 - P/P_c)^{3/2}$ ($\sqrt{2} \le \alpha_1 \le 4$), $\alpha_2 = 2$, and $\alpha_3 = \sqrt{2}(2 - P/P_c)^{-1/2}$ ($1 \le \alpha_3 \le \sqrt{2}$). Hence, the number of e-folds is a function of the dimensionless parameters P/P_c, $k_p|\zeta|$, and z/Z_R.

Some insight can be gained by comparing N_e for self-modulation in the long-pulse regime to that of RFS in the 4-wave nonresonant regime (discussed in Sec. VI.A). Equations (91) and (98) indicate the self-modulation is dominant provided $k_p^2 r_0^2 \ll k_0^2/k_p^2$. This supports the assertion that self-modulation dominates in the 2D limit, whereas RFS dominates in the 1D limit, roughly speaking, when $k_p r_0 \gg k_0/k_p$. These two growth rates, however, occur in different spatiotemporal regimes, hence, comparison of the growth of self-modulation and RFS is more complicated (Esarey *et al.*, 2000).

To illustrate the behavior of the coupled self-modulation and laser-hose instabilities, Eqs. (94) and (95) are solved numerically (Sprangle *et al.*, 1994). Consider an initially uniform plasma with a 16 TW, 1 ps laser pulse with wavelength $\lambda = 1$ μm and initial spot size $r_0 = 60$ μm ($Z_R = 1.1$ cm) in a plasma of density $n_0 = 1.2 \times 10^{18}$ cm^{-3} ($\lambda_p = 30$ μm). For these parameters, $P(\zeta) = P_c$ at the center of the pulse. Initially, $\hat{x}_s = \hat{y}_s = 1$ and the centroid has a 1% random perturbation such that $|\partial \ln x_c/\partial\zeta| \ll 1/\lambda_0$.

As the laser propagates, the high intensity center of the pulse remains guided ($\hat{x}_s \simeq 1$). However, the front and back portions of the pulse, with $P < P_c$, diffract, and the coupled hose and modulation instabilities grow within the guided portion of the pulse as illustrated in Figs. 35 and 36. Figure 35 shows the normalized laser intensity on-axis $|\hat{a}|^2 = 16P(\zeta)/(P_c\hat{x}_s\hat{y}_s k_p^2 r_0^2)$ at $\hat{\tau} = 0$ and at $\hat{\tau} = 3.2$. Figure 36 plots $\hat{x}_s(\zeta)$ and $\hat{x}_c(\zeta)$ at $\hat{\tau} = 3.2$ and shows a significant level of hosing, with $|\hat{x}_c|$ as large

as 0.5. In addition to the modulation of the envelope at λ_p, the second harmonic at $\lambda_p/2$ is present, indicating the coupling between the hose and self-modulation instabilities. The spatial modulation of the laser envelope at $\lambda_p/2$ is due to the dependence of the driving terms on the centroid motion. The second harmonic is not observed when the initial centroid perturbation is sufficiently small, 0.1% for the present parameters.

The presence of the laser-hose instability can strongly modify the structure of the wakefield generated by the laser pulse. To illustrate this point, consider an initial centroid perturbation of 10% (Sprangle *et al.*, 1994). Here, the centroid motion dominates both the development of the wakefield and the evolution of the envelope. The spot size modulations are dominated by the second harmonic component. Figure 37 shows the transverse profiles of both the longitudinal and transverse wakefields, at $\hat{\tau} = 1.8$, near the back of the pulse. The transverse field E_x is nearly symmetric and peaked on-axis while the longitudinal field E_z is nearly antisymmetric and vanishes on-axis. This wakefield symmetry is opposite to that which occurs without hosing, i.e., in the absence of the hose instability, E_x is antisymmetric and vanishes on-axis, while E_z is symmetric and peaked on-axis.

Although the modulation instability can enhance the wakefield amplitude and acceleration in the LWFA, the laser-hose instability should generally be avoided. To avoid significant levels of hosing, the initial laser centroid must be sufficiently smooth. Equations (98)–(100) indicate that the growth of the hose instability can be reduced by decreasing the pulse length ($k_p|\zeta|$), the laser power (P/P_c), or the interaction distance ($c\tau/Z_R$). Further simulations (Sprangle *et al.*, 1994) indicate that by appropriately varying (i.e., detuning) either the plasma density and/or the depth of the preformed plasma channel as a function of ζ in the laboratory frame, the laser-hose and self-modulation instability can be substantially reduced.

VII. HIGH QUALITY BUNCH PRODUCTION

As described in the previous sections, a decade worth (1994-2004) of experiments by many groups demonstrated that, by focusing intense laser pulses onto a neutral gas, relativistic electron bunches can be produced. Typically, prior to 2004, the accelerated electron energy spectrum was characterized by an exponential or Boltzmann-like distribution, with the majority of electrons at modest energies (a few MeV). The total accelerated charge was large (up to several nC), but the number of electrons at high energy (tens of MeV) was an exponentially small fraction of the total charge. Figure 38 shows an example of a typical exponential energy spectrum (Leemans, 2004). Over the years, the properties of these bunches improved. For example, higher laser pulse energies led to more charge and higher observed maximum electron energies (up to a few hundred MeV) (Mangles *et al.*, 2005). Conversely, electron bunches were produced with "smaller" lasers, capable of operating at higher repetition rate (Malka *et al.*, 2002). Laser pulse shape effects were studied (Leemans *et al.*, 2002; Schroeder *et al.*, 2003a), and applications were explored such as radio-isotope production (Ledingham *et al.*, 2003; Leemans *et al.*, 2001; Santala *et al.*, 2001b), THz radiation generation (Leemans *et al.*, 2003; Schroeder *et al.*, 2004), x-ray generation (Catravas *et al.*, 2001; Esarey *et al.*, 2002; Leemans *et al.*, 2000; Rousse *et al.*, 2004), and ultrafast chemistry (employing the ultrafast nature of the electron bunches) (Brozek-Pluskab *et al.*, 2005). Although steady progress was made, the 100 percent electron beam energy spread remained a major limitation.

A. High quality bunches at the 100 MeV level

In 2004 a major milestone was achieved with the production and measurement of high quality electron bunches. Three different groups [located at the Rutherford Appleton Laboratory (RAL) in the United Kingdom, Lawrence Berkeley National Laboratory (LBNL) in the United States, and the Laboratoire d'Optique Appliquée (LOA) in France] announced measurement of electron bunches with narrow energy spread containing a significant amount of charge in a bunch with a small divergence (Faure *et al.*, 2004; Geddes *et al.*, 2004; Mangles *et al.*, 2004). In the case of the LBNL experiments (Geddes *et al.*, 2004), this was accompanied by the achievement of another major milestone: the guiding of relativistically intense ($> 10^{18}$ W/cm^2) laser pulses within preformed plasma channels (Geddes *et al.*, 2005b) and the self-trapping and acceleration of electrons within these channels (Geddes *et al.*, 2005b). Guiding of high intensity laser pulses in plasma channels is necessary in order to extend the acceleration length and the energy gain up to the multi-GeV range with reasonable size laser systems that can operate at high repetition rates.

To obtain the mono-energetic bunches, the RAL and LOA groups used relatively large laser spot sizes. This effectively increases the diffraction (or Rayleigh range, Z_R) of the laser pulse, thereby permitting propagation over distances on the order of the gas jet length. The RAL collaboration used a 16 TW, 40 fs laser pulse focused (25 μm spot size, 10^{18} W/cm^2) on a plume of a gas jet with a plasma density of 2×10^{18} cm^{-3}. A narrow energy spread bunch was observed at 78 ± 2 MeV with 20 pC of charge (Mangles *et al.*, 2004). The LOA experiments used a 30 TW, 33 fs laser pulse focused (18 μm spot size, 3×10^{18} W/cm^2) on a plume of a gas jet with a plasma density of 6×10^{18} cm^{-3}. A narrow energy spread bunch was observed at 170 ± 15 MeV with 500 pC of charge (Faure *et al.*, 2004). Plasma density scans indicated that there was an optimal laser-plasma coupling parameters for production of high-charge mono-energetic electron beams, as predicted in the bubble regime, and in

agreement with 3D PIC simulations (Faure *et al.*, 2004; Malka *et al.*, 2005).

The LBNL experiments used a 9 TW, 55 fs laser pulse focused to a relatively tight spot size (8.5 μm FWHM, 10^{19} W/cm^2). To mitigate the short Z_R of the laser pulse, a preformed plasma channel (with an on-axis density of 2×10^{19} cm^{-3}) was used to guide the laser pulse through the gas jet. A narrow energy spread bunch was observed at 86 ± 2 MeV with 300 pC of charge within the narrow peak. Electrons with energies as high as 150 MeV were observed. With the preformed channels and laser input powers at the 8–10 TW level, electron bunches with narrow energy spread were observed (Geddes *et al.*, 2004). Using the 55° fine resolution magnetic spectrometer, bunches containing 2×10^9 electrons with two percent energy spread around 86 MeV were observed with a divergence on the order of 3 mrad. Bunches containing 10^9 electrons at energies between 135–170 MeV were observed using the 5° port of the magnetic spectrometer. An example of a narrow energy spread spectrum is shown in Fig. 39. The normalized geometric emittance, obtained from assuming that the bunch comes from a source approximately the size of the laser spot, is 1–2 π mm-mrad, competitive with state of the art radio-frequency facilities.

Based on experiment, simulation, and theory, the production of monoenergetic bunches in a laser-plasma accelerator requires the following four steps: Step 1 consists of exciting a wakefield. For a self-modulated LWFA, this typically occurs after the laser has propagated a sufficiently long distance within the plasma, such that the self-modulation instability (i.e., the feedback of the wake on the pulse and the self-consistent evolution of both the wake and the pulse) excites a large amplitude wakefield. Step 2 consists of a method for trapping and the initial injection of the electrons into the wake. For a self-modulated LWFA, this can be the result of wake wave-breaking (i.e., sufficiently large plasma wave amplitude for self-trapping of background electrons). Step 3 consists of termination of the self-trapping or injection process. If trapping is not terminated, low energy electrons would continuously be injected into the wake over the entire length of acceleration, resulting in a large energy spread. One mechanism to accomplish this is by beam loading, i.e., the injected electron bunch is of sufficient charge so as to reduce the amplitude of the wake below the self-trapping threshold. Step 4 is acceleration of the electron bunch over a distance equal to the dephasing length. If acceleration occurs over distances longer than the dephasing length, the trapped bunch will continue to circulate around the separatrix, losing energy and increasing its energy spread. Optimum acceleration would occur over a distance equal to the dephasing length, such that the trapped bunch exits the plasma near the top of the separatrix (i.e., the accelerating phase-space bucket), with maximum energy and minimum energy spread.

Particle-in-cell simulations (using the code VORPAL (Nieter and Cary, 2004)) were performed in parameter regimes relevant to the LBNL experiments (Geddes *et al.*, 2004). The simulated laser envelope and particle phase space as a function of propagation distance are shown in Fig. 40, and the wake density is shown in Fig. 41. In these simulations (Geddes *et al.*, 2005b), it is observed that in the first few hundred microns of propagation of the laser pulse in the channel, the wake amplitudes (and hence the amount of trapped particles) are small. As the laser pulse envelope starts distorting through the self-modulation instability, developing features that have rise times on the order of or shorter than the plasma period, a plasma wake is excited that is large enough to trap and accelerate particles. Once enough charge is accumulated in the accelerating bucket, the injection process can be terminated due to beam loading, i.e., the field of the accelerated bunch modifies the wakefield and reduces its amplitude to below the trapping threshold. Pump depletion of the laser pulse energy (lost to wake excitation) can also reduce the wake amplitude below the trapping threshold. If the trapped electrons propagate beyond a dephasing distance, the electrons lose energy, which leads to a broad energy distribution.

B. High quality bunches at the 1 GeV level

In 2006, high quality electron bunches at the 1 GeV level were demonstrated in channel-guided LWFA experiments at LBNL [Ref]. In these experiments, the energy gain was extended the the GeV range by using higher laser powers (e.g., 40 TW), using longer plasma channels (e.g., 3.3 cm), and using lower plasma densities (e.g., 10^{18} cm^{-3}) so as to extend the dephasing length. Previous LBNL experiments at the 100 MeV level created plasma channels in a gas jet with a laser ionization and heating technique (Geddes *et al.*, 2004, 2005b; Volfbeyn *et al.*, 1999). Due to laser heating being inefficient at low densities, suitable plasma channels could only be produced in gas jets at densities $> 10^{19}$ cm^{-3}, limiting the dephasing length and restricting electron energies to about 100 MeV.

To overcome the limitations of gas jets, a gas-filled capillary discharge waveguide (Butler *et al.*, 2002; Spence and Hooker, 2001) was used to produce cm-scale, lower density plasma channels. The experiments used a 10 Hz repetition rate Ti:sapphire laser system ($\lambda = 810$ nm) delivering down to 40 fs full width half maximum (FWHM) pulses with up to 40 TW peak power. These pulses were focused by a 2 m focal length off-axis parabola (f/25) to $r_s = 25$ μm at the capillary entrance (an input intensity $\sim 10^{18}$ W/cm^2). The capillaries (Spence and Hooker, 2001) were laser machined into 33 mm long sapphire blocks with diameters ranging from 190 μm to 310 μm. Hydrogen gas, introduced through two holes near the capillary ends, was ionized by striking a discharge between electrodes at the capillary ends, producing an approximately parabolic plasma channel. Accelerator performance was optimized by adjusting the initial gas den-

sity and the delay between onset of the discharge current and arrival of the laser pulse (from 1.0 to 4.0×10^{18} cm^{-3} in a ∼100 ns timing window). Electron bunch energy was measured by a 1.2 T single-shot magnetic spectrometer that deflected the electrons onto a 1.2 m long phosphor screen, covering energies from 0.03 GeV up to 1.1 GeV.

Figure 42 shows energy spectra of electron bunches produced at (a) 0.5 GeV with ∼50 pC charge, and at (b) 1.0 GeV with ∼30 pC charge, obtained using 12 TW (70 fs input) and 38 TW (40 fs input) laser pulses, respectively. In both cases the electron bunches had percent-level energy spread and a divergence of 1.2–2.0 mrad (rms).

Bunches at ∼0.5 GeV were obtained using a 225 μm diameter capillary for a density of 3.4 to 4.3×10^{18} cm^{-3} and for laser power ranging from 12 TW (70 fs) to 18 TW (40 fs). The performance for the 225 μm diameter capillary-guided accelerator was found to be reproducible for delays of 70–120 ns and 12 TW laser peak power, with every laser shot resulting in an electron bunch at 0.5 GeV ±10% and an rms spread <5%. Fluctuations in electron bunch energy were directly correlated with those in laser power. For lower power (<12 TW), no electron bunches were observed suggesting that the wake amplitude was below the self-trapping threshold.

The GeV electron bunch was obtained in a 310 μm diameter channel capillary for $P = 38$ TW and a density of 4.9×10^{18} cm^{-3}. In this larger diameter channel, transverse wakefields are reduced but the guiding properties are less ideal as it requires a larger matched spot size than was injected. For lower laser power (<38 TW), no electron bunches were observed. For higher laser powers, the spectrum always showed structure with significant shot-to-shot fluctuations due in part to the self-trapping mechanism being sensitive to small variations in the laser and plasma parameters (Geddes *et al.*, 2005b).

Particle-in-cell simulations in 2D and 3D confirm that the injection and acceleration mechanism is similar to that which occurs in the gas jet experiments at the 100 MeV level. The initial profile of the laser pulse injected into the channel produces a wake with an amplitude that is too low to produce self-trapping. Over the first few mm of propagation, the wake feeds back on the laser pulse, leading to self-modulation and self-steepening, which further increases the wake amplitude. A blow-out or cavitated wake is eventually produced of sufficient amplitude so as to allow self-trapping. Trapping continues until there is sufficient trapped charge so as to beam load the wake, reducing its amplitude, and terminating the self-trapping process. Over the next ∼ 1 cm of propagation, the bunch accelerates as the laser energy depletes. Laser depletion occurs after roughly a dephasing length, resulting in the production of narrow energy spread electron bunch with an energy near 1 GeV.

C. High quality bunches from colliding pulse injection

In addition to stable electron bunches generated at the 0.5 GeV level via self-trapping in the channel-guided LWFA experiments described in the previous section, stable electron bunches at the 100 MeV level were also generated in 2006 by colliding pulse injection within a gas jet in experiments at LOA (Faure *et al.*, 2006). These experiments used a two pulse, collinear, counterpropagating geometry, in which injection results from the beat wave produced when the backward pulse overlaps the forward drive pulse that generates the wakefield (Fubiani *et al.*, 2004). Specifically, two 30 fs laser pulses with linear polarization were focussed at the edge of a 2 mm supersonic helium gas jet. The pump pulse was focused to an intensity of $I_0 = 3.4 \times 10^{18}$ W/cm^2 ($a_0 = 1.3$) and the injection pulse intensity was $I_1 = 4.3 \times 10^{17}$ W/cm^2 ($a_1 = 0.4$). The electron bunch was passed through an electron spectrometer, which measured the electron bunch angular distribution, energy distribution and charge.

For densities at or below $n_e = 7.5 \times 10^{18}$ cm^{-3}, the nonlinear evolution of the pump laser pulse through self-focusing and self-steepening was not strong enough to cause significant injection of electrons into the wakefield. However, at $n_e = 7.5 \times 10^{18}$ cm^{-3}, the addition of the injection pulse produced a monoenergetic electron bunch. The electron bunches obtained in this manner were very stable. A series of 20 consecutive shots was carried out to estimate the statistical fluctuations of the bunch, giving a peak energy of 117 ± 7 MeV, an energy spread of 11 ± 2%, a charge of 19 ± 6.8 pC, a divergence of 5.8 ± 2 mrad, and a pointing stability of 0 ± 1.8 mrad (here the ± signifies the standard deviation about the mean). By varying the delay between the two pulses, the collision point, and hence the acceleration length, within the gas jet was varied. This allowed the electron bunch energy to be tuned from 50 MeV (with 25% energy spread) to 250 MeV (with 5% energy spread). Furthermore, when the polarizations of the two laser pulses were orthogonal, no electron bunch was produced, which suggests that the injection mechanism depends on parallel polarization and the production of a beat wave.

D. High quality bunches from down ramp injection

Stable electron bunches at the 1 MeV level have been demonstrated experimentally at LBNL by focusing a 10 TW, 50 fs laser (2×10^{19} W/cm^2) on the downstream edge of a 750 μm wide gas jet of density 2×10^{19} cm^{-3} (Geddes *et al.*, 2007). The mechanism for self-trapping of electrons from the background plasma is due to down ramp injection, as discussed in Sec. IV.D. At the downstream edge of the gas jet, a decreasing plasma density causes λ_p to increase with propagation. Wake fronts then fall further behind the laser as it propagates, decreasing the wake phase velocity to the point where background plasma electrons become trapped.

Using this method, stable (over hundreds of shots) electron bunches were produced with low absolute momentum spread. Electron bunches were generated with order nC charge (15% charge stability), mean momenta 0.76 MeV/c, 170 keV/c FWHM momentum spread, 20 keV/c momentum stability, 20 keV/c transverse momentum, and 2 mrad (2 keV/c) RMS pointing stability. Examples of the momentum distribution of the bunch as obtained from a magnetic spectrometer are shown in Fig. 43. Furthermore, measurements of coherent THz emission imply a bunch duration on the order of 100 fs.

One possible application of such a source would be as an electron injector into a second stage (dark current free) of a LWFA for acceleration to high energy. Simulations predict that post acceleration of a highly quality bunch can nearly preserve the absolute momentum spread and emittance. Hence, post acceleration of bunches produced by down ramp injection could potentially lead to the generation of electron bunches at GeV (or greater) energies with 100 keV/c level momentum spread.

VIII. SUMMARY AND PROSPECTS

Perhaps the three most fundamental physics issues concerning laser-plasma accelerators are (i) can an ultrahigh accelerating field be generated, (ii) can this accelerating field be sustained over a sufficiently long propagation distance so as to provide a substantial single-stage electron energy gain, and (iii) can an ultrashort electron bunch be injected and accelerated while maintaining high bunch quality? Theory and simulation indicate that these requirements can be met. Experimental progress is proceeding at a rapid pace, and the generation of ultrahigh accelerating fields, the guiding of high intensity laser pulses over many diffraction (Rayleigh) lengths, and the production of high quality relativistic electron bunches have been demonstrated. Much of the experimental success can be attributed to the development of chirped-pulse amplification (Maine *et al.*, 1988; Mourou and Umstadter, 1992; Perry and Mourou, 1994; Strickland and Mourou, 1985), which has revolutionized laser technology by providing compact sources of multi-TW, sub-ps laser pulses. In the future, numerous accelerator applications will benefit from high-average power sources of intense laser pulses, which requires further technological advances.

The problem of generating a large amplitude plasma wave by an intense laser pulse, for the most part, is well-understood. Theoretically, wakefield generation can be examined by assuming a non-evolving drive laser pulse and by calculating the plasma response to the ponderomotive force. This ponderomotive force can be associated with the envelope of a single laser pulse (e.g., a standard LWFA in the linear regime or a bubble wake in the highly nonlinear regime), a laser pulse train, envelope variations on an unstable laser pulse (e.g., self-modulated LWFA), or the beat wave produced by two co-propagating laser pulses of different frequencies (e.g., PBWA). Wakefield generation is optimized when the laser envelope spatial gradients are on the order of the plasma wavelength λ_p. Analytical solutions or simple numerical models exist in the 3D linear regime ($a_0^2 \ll 1$) and in the 1D nonlinear ($a^2 \gtrsim 1$) regime. In the 2D and 3D nonlinear regime, wakefield generation can be examined with a variety of quasi-static fluid and particle-in-cell codes. Unresolved theoretical issues pertaining to wakefield generation include the detailed study of wavebreaking, especially in 2D and 3D, dynamics of the highly nonlinear blowout regime, wakefield decay in nonuniform plasmas, thermal effects, and self-trapping.

Laser pulse propagation in underdense plasma is affected by a variety of phenomena, including relativistic self-focusing, ponderomotive self-channeling, preformed density channels, plasma wave generation, pump depletion, and instabilities, as discussed in Sects. V and VI. In terms of fundamental limits to the energy gain in single-stage LWFA, the most severe is typically diffraction, i.e., the Rayleigh length is usually much shorter than the dephasing length and pump depletion length. Hence, some form of optical guiding is required. Relativistic self-guiding, which occurs when $P \geq P_c \simeq 17\lambda_p^2/\lambda^2$ GW, strongly affects the body of a long ($L > \lambda_p$) laser pulse. The leading portion of the pulse ($\lesssim \lambda_p$), however, will diffractively erode due to the self-consistent response of the plasma density to the laser field. The self-focusing of a long pulse can be enhanced by the ponderomotive blowout of the plasma electrons from the axis, i.e., electron cavitation. In addition, the body of long, relativistically-guided pulse is subject to instabilities (Raman scattering, self-modulation, and laser hosing). Preformed plasma density channels are effective in the guiding of short ($L < \lambda_p$) laser pulses when $\Delta n \geq \Delta n_c = 1/(\pi r_e r_0^2)$. For long pulses ($L > \lambda_p$), relativistic effects can reduce this criterion, i.e., $\Delta n/\Delta n_c \geq 1 - P/P_c$. In addition, if the pulse is sufficiently short ($L \lesssim \lambda_p$), the detrimental effects of various instabilities may be reduced, owing to the reduced growth of the unstable mode within the pulse.

Once diffraction is overcome and the laser pulse is guided by, for example, a plasma density channel, the propagation distance will be limited by a variety of nonlinear phenomena. For example, a laser pulse on the order of or longer than a plasma wavelength will undergo self-modulation, generally defined as the pulse evolution resulting from the feed back of the plasma wave (wakefield) on the laser pulse. For a long laser pulses, $L \gg \lambda_p$, self-modulation can lead to an unstable axial modulation of the pulse profile at λ_p, with the associated excitation of a large wakefield that can grow to the point of wavebreaking, resulting in electron self-trapping and acceleration. For shorter pulses, $L \sim \lambda_p$, self-modulation can still play a dramatic role via pulse shortening and self-steepening. For example, as a pulse with $L \sim \lambda_p$ enters a plasma, the initial intensity profile may only drive a

mildly nonlinear wake, but as this wake feeds back on the laser pulse, the intensity profile shortens and steepens, which can result in a highly nonlinear wake and the self-trapping of electrons. Hence, self-shortening and self-steeping can play an important role in the transition of a mildly nonlinear wake to a highly nonlinear blowout regime. Furthermore, the physics of self-modulation is intrinsically coupled to that of pump depletion, since as the laser pulse excites the plasma wave, it loses energy. Analytic studies of laser pulse evolution, for the most part, are limited to the linear regime in which, for example, analytic expressions for instability growth rates are readily obtained. The self-consistent problem of plasma wave generation by an evolving drive laser pulse is typically of sufficient complexity as to require numerical simulation. Self-consistent simulations of laser-plasma accelerators have been performed in the 2D and 3D nonlinear regime using both fluid and particle-in-cell codes.

To generate a high-quality electron bunch, it is highly desirable that a bunch be injected with a length short compared to λ_p. Due to the shortness of λ_p ($\lesssim$ 100 μm), this is not yet achievable using conventional photo-injectors, in which the production of femtosecond bunches is problematic. Alternatively, several novel laser-based methods for injecting electrons into a plasma wave have been proposed and studied. This is includes self-trapping of background plasma electrons, which can occur as the plasma wave amplitude approaches the wavebreaking amplitude for both long laser pulses, such as in the self-modulated regime, or for short laser pulses, as in the blowout regime. In a plasma channel, curvature of the plasma wavefronts becomes more severe with distance behind the laser pulse and can lead to wavebreaking. A density downramp causes the phase velocity of the plasma wave to decrease, which can lead to wavebreaking at a sufficiently far distance behind the pump laser pulse. Instead of relying on wavebreaking and self-trapping, one or more additional ultrashort (short compared to λ_p) laser pulses can be used to injection electrons directly into the wakefield. This can be done by either using the ponderomotive force of the injection pulse, or the slow beat wave generated by two counterpropagating laser pulses. These laser injection methods show great promise, since the injection process can be controlled in detail by adjusting the timing of the injection pulses with respect to the plasma wave phase, as well as by adjusting the injection pulse amplitude and duration. Once injected, it is important that the electron bunch be accelerated while maintaining high quality, e.g., maintaining a small energy spread and emittance. This may require controlling the transverse focusing forces of the wakefield by, for example, tailoring the transverse plasma density profile and/or the transverse laser intensity profile.

Experimentally, many groups have measured ultrahigh accelerating fields and accelerated electrons. Large accelerating fields (>200 GV/m) have been measured directly from optical probing techniques or inferred from the measurement of accelerated electrons. Large amounts of self-trapped electrons (up to several nC) have been accelerated in the self-modulated LWFA regime, with maximum electron energies up to a few hundred MeV. Prior to 2004, however, the electron energy spectrum in the self-modulated regime was typically characterized by an exponential distribution with the majority of the electrons at low energy ($\sim$ MeV) and a long tail extending out to high energies, e.g., $>$ 300 MeV when using PW-level Nd:glass laser system and a 2 mm diameter gas jet (Mangles *et al.*, 2005). Such an exponential energy distribution of the accelerated electrons is typical of this first-generation of "brute force" experiments, in which a single high power ($>$ few TW) laser pulse interacts with a gas jet plume of a couple of mm diameter and of relatively high density ($\sim 10^{19}$ cm^{-3}).

Two important experimental milestones towards the development of a laser-plasma accelerator were achieved in 2004: channel guiding of relativistically intense ($a_0^2 \gtrsim 1$) laser pulses over many diffraction lengths (Geddes *et al.*, 2004), and the production of high quality electron bunches at relativistic energies ($\sim$ 100 MeV), with high charge (up to $\sim$ nC), low energy spread ($\sim$ few percent) and low normalized emittance ($\sim \pi$ mm-mrad) (Faure *et al.*, 2004; Geddes *et al.*, 2004; Mangles *et al.*, 2004). These results were obtained by a careful choice of laser and plasma parameters and/or a tailoring of the plasma density profile. In these experiments the electrons were self-trapped by the 10-100 TW laser pulse from the background plasma using mm-scale gas jet sources. High quality bunches were obtained by controlling the acceleration length so that it was equal to the dephasing length, such that the trapped bunch exits the plasma near the top of the separatrix (i.e., the accelerating phase-space bucket), with maximum energy and minimum energy spread. Matching of the acceleration length and the dephasing length was accomplished by either using a preformed plasma channel (Geddes *et al.*, 2004), or by using higher power laser pulses with larger laser spot sizes (which increases the propagation length) (Faure *et al.*, 2004; Mangles *et al.*, 2004), along with lower plasma densities (which increases the dephasing length). In 2006 high quality electron bunches were produced at the 1 GeV using 100 TW level laser pulses in a cm-scale plasma channel. Again, the electrons were self-trapped from the background plasma (a capillary discharge), and high quality bunches were obtained by acceleration over a dephasing length (Leemans *et al.*, 2006).

Another important experimental milestone was achieved in 2006: controlled injection and acceleration of electrons using the colliding pulse method (Faure *et al.*, 2006). High quality electron bunches at the 100 MeV level were generated with multi-10 TW laser pulses in a mm-scale gas jet using a two pulse, collinear, counterpropagating geometry. When the polarizations of the two laser pulses were orthogonal, no electron bunch was produced, which suggests that the injection mechanism depends on parallel polarization and the production of a laser beat wave.

Although not the focus of this review article, an important experimental milestone in the field of electron beam-driven plasma-based accelerators was achieved in 2007 (Blumenfeld *et al.*, 2007): the energy doubling of a significant fraction of electrons in a multi-10 GeV electron bunch using a meter-scale plasma. These experiments used the 50 fs, 42 GeV electron bunches from the 3 km long linear accelerator at the Stanford Linear Accelerator Center, propagating through a 85 cm plasma. The front portion of the electron bunch generated a large amplitude plasma wakefield, which subsequently accelerated electrons in the tail of the bunch to energies as high as 85 GeV.

Although much progress has been made, in many respects laser-plasma accelerator experiments are still in their infancy. One important challenge is to stabilize the performance of the accelerator. Since the electron energy depends linearly on laser intensity in the linear wakefield regime [see, e.g., Eq. (45)], stable electron bunch energies to the few percent level requires control of the laser pulse energy, pulse length, and spot size is needed at the few percent level. Novel methods for controlling laser pulse properties and pointing stability are being developed in industry for short pulse systems that may meet these requirements. Similarly, plasma densities must be controlled at the percent level to ensure that the wake amplitude ($\propto n^{1/2}$), dephasing length ($\propto n^{-3/2}$), and energy gain ($\propto 1/n$) remain constant. Novel time-resolved diagnostics need to be developed and implemented to allow, for example, measurement of the slice emittance and energy spread of fs-duration electron bunches.

Perhaps the most severe fundamental limit to the single-stage energy gain in a laser-plasma accelerator is pump depletion, i.e., energy is transferred out of the laser pulse and into the plasma wakefield as the laser propagates. In the nonlinear regime, theory and simulation indicate that the pump depletion length is on the order of the dephasing length. To extend the electron energy beyond the limits of pump depletion will require multiple stages. This requires additional challenges such as the synchronization of laser pulses with fs accuracy, the alignment of plasma structures with micron accuracy, and the development of novel methods of laser coupling into subsequent stages.

One possible approach to the realization of an all-optical accelerator at the 10 GeV level is to use two stages. The first could be an injector at the 100 MeV level that utilized either self-trapping or a laser triggered injection method such as colliding pulse. This electron bunch could then be injected into a second stage that would accelerate the bunch through a plasma channel in a mildly nonlinear wakefield regime without additional self-trapping (dark current free). Estimates based on linear wakefield theory predict a maximum single-stage energy gain on the order of $\Delta W(\mathrm{GeV}) \simeq I_0(\mathrm{W/cm^2})/n_0(\mathrm{cm^{-3}})$. Hence, a second stage that used a few hundred fs laser pulse with an intensity of 10^{18} W/cm^2 in a plasma of density 10^{17} cm^{-3} may provide a single-stage energy gain as high as 10 GeV. As can be seen from the basic scaling laws, reducing the density and lengthening the distance over which the plasma channel extends is essential to reach multi-GeV energies.

The performance of laser-plasma accelerators, as well as essentially all applications of these accelerators, would benefit greatly from improvements in laser technology: higher peak powers, higher pulse energies, higher repetition rates, and the development of higher average power laser systems. Currently, 100 TW laser systems are limited to the 10 Hz regime (average powers on the order of 10 W). As a simple estimate of the type of laser pulses needed to drive a high charge, single-stage accelerator, consider producing a 10 GeV electron bunch containing 1 nC of charge (6×10^9 electrons). This represents 10 J worth of electron kinetic energy and, assuming a laser to particle beam efficiency between 1–10%, requires therefore 100–1000 J of laser energy per pulse. It is hence essential that plasma accelerator technology and laser technology be developed in parallel, if the goal of all-optical linear accelerators is to be realized. Such an accelerator holds the promise of offering unique electron bunches, having femtosecond duration and containing 100's of pC of charge, with an emittance that equals or surpasses conventional linacs. If the development continues to be successful, it will serve as a compact multi-GeV module for high energy physics applications, as well as the basis for novel radiation sources, including the next generation of femtosecond light sources.

ACKNOWLEDGMENTS

The authors acknowledge the many contributions from the members of the LOASIS Program at Lawrence Berkeley National Laboratory (C. Geddes, E. Cormier-Michel, K. Nakamura, B. Shadwick, J. van Tilborg, and Cs. Tóth) and the many insightful conversations with the researchers in the plasma-based accelerator community.

This work was supported by the Director, Office of Science, Office of High Energy Physics, of the U.S. Department of Energy under Contract No. DE-AC02-05CH11231.

REFERENCES

Akhiezer, A. I., and R. V. Polovin, 1956, Zh. Eksp. Teor. Fiz. **30**, 915, [JEPT **3**, 696 (1956)].

Amiranoff, F., S. Baton, D. Bernard, B. Cros, D. Descamps, L. F. Dorchies, F. Jacquet, V. Malka, J. Marquès, G. Matthieussent, P. Mine, A. Modena, *et al.*, 1998, Phys. Rev. Lett. **81**(5), 995.

Amiranoff, F., D. Bernard, B. Cros, F. Jacquet, G. Matthieussent, P. Miné, P. Mora, J. Morillo, F. Moulin, A. E. Specka, and C. Stenz, 1995, Phys. Rev. Lett. **74**(26), 5220.

Amiranoff, F., M. Laberge, J. R. Marquès, F. Moulin, E. Fabre, B. Cros, G. Matthieussent, P. Benkheiri,

F. Jacquet, J. Meyer, P. Miné, C. Stenz, *et al.*, 1992, Phys. Rev. Lett. **68**(25), 3710.
Andreev, N. E., L. M. Gorbunov, V. I. Kirsanov, K. Nakajima, and A. Ogata, 1997, Phys. Plasmas **4**(4), 1145.
Andreev, N. E., L. M. Gorbunov, V. I. Kirsanov, A. A. Pogosova, and R. R. Ramazashvili, 1992, Pis'ma Zh. Eksp. Teor. Fiz. **55**, 551.
Andreev, N. E., L. M. Gorbunov, V. I. Kirsanov, A. A. Pogosova, and R. R. Ramazashvili, 1994, Physica Scripta **49**, 101.
Andreev, N. E., V. I. Kirsanov, and L. M. Gorbunov, 1995, Phys. Plasmas **2**(6), 2573.
Antonsen, Jr., T. M., and P. Mora, 1992, Phys. Rev. Lett. **69**(15), 2204.
Antonsen, Jr., T. M., and P. Mora, 1993, Phys. Fluids B **5**(5), 1440.
Antonsen, Jr., T. M., and P. Mora, 1995, Phys. Rev. Lett. **74**(22), 4440.
Banerjee, S., S. Sepke, R. Shah, A. Valenzuela, A. Maksimchuk, and D. Umstadter, 2005, Phys. Rev. Lett. **95**(3), 035004.
Berezhiani, V. I., and I. G. Murusidze, 1990, Phys. Lett. A **148**, 338.
Berezhiani, V. I., and I. G. Murusidze, 1992, Physica Scripta **45**, 87.
Bernard, D., F. Amiranoff, W. P. Leemans, E. Esarey, and C. Joshi, 1999, Nucl. Instrum. Methods Phys. Res. A **432**(2–3), 227.
Bertrand, P., A. Ghizzo, S. J. Karttunen, T. J. H. Pattikangas, R. R. E. Salomaa, and M. Shoucri, 1995, Phys. Plasmas **2**(8), 3115.
Birdsall, C. K., A. B. Langdon, V. Vehedi, and J. P. Verboncoeur, 1991, *Plasma Physics via Computer Simulations* (Adam Hilger, Bristol, Eng.).
Blumenfeld, I., C. E. Clayton, F.-J. Decker, M. J. Hogan, C. Huang, R. Ischebeck, R. Iverson, C. Joshi, T. Katsouleas, N. Kirby, W. Lu, K. A. Marsh, *et al.*, 2007, Nature **445**(7129), 741.
Bonnaud, G., D. Teychenné, and J. Bobin, 1994, Phys. Rev. E **50**(1), R36.
Borghesia, M., A. J. MacKinnon, L. Barringer, R. Gaillard, L. A. Gizzi, C. Meyer, O. Willi, A. Pukhov, and J. Meyer-ter-Vehn, 1997, Phys. Rev. Lett. **78**(5), 879.
Borisov, A. B., A. V. Borovskiy, V. V. Korobkin, A. M. Prokhorov, O. B. Shiryaev, X. M. Shi, T. S. Luk, A. McPherson, J. C. Solem, K. Boyer, and C. K. Rhodes, 1992, Phys. Rev. Lett. **68**(15), 2309.
Brozek-Pluskab, B., D. Gliger, A. Halloua, V. Malka, and Y. A. Gauduel, 2005, Radiat. Phys. Chem. **72**(2), 149.
Bulanov, S., N. Naumova, F. Pegoraro, and J. Sakai, 1998, Phys. Rev. E **58**(5), R5257.
Bulanov, S. V., I. N. Inovenkov, V. I. Kirsanov, N. M. Naumova, and A. S. Sakharov, 1992, Phys. Fluids B **4**(7), 1935.
Bulanov, S. V., V. I. Kirsanov, and A. S. Sakharov, 1989, JETP Lett. **50**, 198.
Bulanov, S. V., F. Pegoraro, and A. M. Pukhov, 1995, Phys. Rev. Lett. **74**(5), 710.
Bulanov, S. V., F. Pegoraro, A. M. Pukhov, and A. S. Sakharov, 1997, Phys. Rev. Lett. **78**(22), 4205.
Butler, A., D. J. Spence, and S. M. Hooker, 2002, Phys. Rev. Lett. **89**(18), 185003.
Catravas, P., E.Esarey, and W. P. Leemans, 2001, Meas. Sci. Technol. **12**, 1828.
Chen, W., T. Chien, C. Lee, J. Lin, J. Wang, and S. Chen, 2004, Phys. Rev. Lett. **92**(7), 075003.
Chen, X. L., and R. N. Sudan, 1993, Phys. Fluids B **5**(4), 1336.
Chien, T., C. Chang, C. Lee, J. Lin, J. Wang, and S. Chen, 2005, Phys. Rev. Lett. **94**(11), 115003.
Chiou, T. C., T. Katsouleas, C. Decker, W. B. Mori, G. Shvets, and J. S. Wurtele, 1995, Phys. Plasmas **2**, 310.
Chiron, A., G. Bonnaud, A. Dulieu, J. L. Miquel, G. Malka, M. Louis-Jacquet, and G. Mainfray, 1996, Phys. Plasmas **3**(4), 1373.
Clayton, C. E., M. J. Everett, A. Lal, D. Gordon, K. A. Marsh, and C. Joshi, 1994, Phys. Plasmas **1**(5), 1753.
Clayton, C. E., C. Joshi, C. Darrow, and D. Umstadter, 1985, Phys. Rev. Lett. **54**(21), 2343.
Clayton, C. E., K. A. Marsh, A. Dyson, M. Everett, A. Lal, W. P. Leemans, R. Williams, and C. Joshi, 1993, Phys. Rev. Lett. **70**(1), 37.
Clayton, C. E., K. Tzeng, D. Gordon, P. Muggli, W. B. Mori, C. Joshi, V. Malka, Z. Najmudin, A. Modena, D. Neely, and A. E. Dangor, 1998, Phys. Rev. Lett. **81**(1), 100.
Coffey, T. P., 1971, Phys. Fluids **14**(7), 1402.
Conde, M., and C. Eyberger (eds.), 2006, *Advanced Accelerator Concepts*, volume 877 (AIP, New York).
Coverdale, C. A., C. B. Darrow, C. D. Decker, W. B. Mori, K. Tzeng, K. A. Marsh, C. E. Clayton, and C. Joshi, 1995, Phys. Rev. Lett. **74**(23), 4659.
Dalla, S., and M. Lontano, 1994, Phys. Rev. E **49**(3), R1819.
Darrow, C., C. Coverdale, M. Perry, W. Mori, C. Clayton, K. Marsh, and C. Joshi, 1992, Phys. Rev. Lett. **69**(3), 442.
Dawson, J. M., 1959, Phys. Rev. **113**(2), 383.
Dawson, J. M., 1983, Rev. Mod. Phys, **55**, 403.
Decker, C. D., and W. B. Mori, 1994, Phys. Rev. Lett. **72**(4), 490.
Decker, C. D., W. B. Mori, and T. Katsouleas, 1994, Phys. Rev. E **50**(5), R3338.
Decker, C. D., W. B. Mori, T. Katsouleas, and D. E. Hinkel, 1996a, Phys. Plasmas **3**(4), 1360.
Decker, C. D., W. B. Mori, K. Tzeng, and T. Katsouleas, 1996b, Phys. Plasmas **3**(5), 2047.
Deutsch, M., B. Meerson, and J. E. Golub, 1991, Physics of Fluids B: Plasma Physics **3**(7), 1773, URL `http://link.aip.org/link/?PFB/3/1773/1`.
Dewa, H., H. Ahn, , H. Harano, M. Kando, K. Kinoshita, S. Kondoh, H. Kotaki, K. Nakajima, H. Nakanishi, A. Ogata, H. Sakai, *et al.*, 1998, Nucl. Instrum. Methods Phys. Res. A **410**, 357.
Dorchies, F., J. R. Marquès, B. Cros, G. Matthieussent, C. Courtois, T. Vélikoroussov, P. Audebert, J. P. Geindre, S. Rebibo, G. Hamoniaux, and F. Amiranoff, 1999, Phys. Rev. Lett. **82**(23), 4655.
Durfee III, C. G., J. Lynch, and H. M. Milchberg, 1995, Phys. Rev. E **51**(3), 2368.
Durfee III, C. G., and H. M. Milchberg, 1993, Phys. Rev. Lett. **71**, 2409.
Ebrahim, N. A., 1994, J. Appl. Phys. **76**(11), 7645.
Ehrlich, Y., C. Cohen, D. Kaganovich, A. Zigler, R. F. Hubbard, P. Sprangle, and E. Esarey, 1998, J. Opt. Soc. Am. B **15**, 2416.
Ehrlich, Y., C. Cohen, A. Zigler, J. Krall, P. Sprangle, and E. Esarey, 1996, Phys. Rev. Lett. **77**, 4186.
Esarey, E., B. Hafizi, R. Hubbard, and A. Ting, 1998, Phys. Rev. Lett. **80**(25), 5552.
Esarey, E., R. F. Hubbard, W. P. Leemans, A. Ting, and P. Sprangle, 1997a, Phys. Rev. Lett. **79**(14), 2682.

Esarey, E., J. Krall, and P. Sprangle, 1994, Phys. Rev. Lett. **72**, 2887.
Esarey, E., and W. P. Leemans, 1999, Phys. Rev. E **59**, 1082.
Esarey, E., and M. Pilloff, 1995, Phys. Plasmas **2**(5), 1432.
Esarey, E., C. B. Schroeder, E. Cormier-Michel, B. A. Shadwick, C. G. R. Geddes, and W. P. Leemans, 2007, Phys. Plasmas **14**, 056708.
Esarey, E., C. B. Schroeder, W. P. Leemans, and B. Hafizi, 1999, Phys. Plasmas **6**(5), 2262.
Esarey, E., C. B. Schroeder, B. A. Shadwick, J. S. Wurtele, and W. P. Leemans, 2000, Phys. Rev. Lett. **84**(14), 3081.
Esarey, E., B. A. Shadwick, P. Catravas, and W. P. Leemans, 2002, Phys. Rev. E **65**, 056505.
Esarey, E., B. A. Shadwick, C. B. Schroeder, and W. P. Leemans, 2004, in *Advanced Accelerator Concepts*, edited by V. Yakimenko (AIP, New York), pp. 578–584.
Esarey, E., and P. Sprangle, 1992, Phys. Rev. A **45**(8), 5872.
Esarey, E., P. Sprangle, and J. Krall, 1995, Phys. Rev. E **52**, 5443.
Esarey, E., P. Sprangle, J. Krall, and A. Ting, 1996, IEEE Trans. Plasma Sci. **24**(2), 252.
Esarey, E., P. Sprangle, J. Krall, and A. Ting, 1997b, IEEE J. Quantum Electron. **33**(11), 1879.
Esarey, E., P. Sprangle, J. Krall, A. Ting, and G. Joyce, 1993a, Phys. Fluids B **5**(7), 2690.
Esarey, E., and A. Ting, 1990, Phys. Rev. Lett. **65**, 1961.
Esarey, E., A. Ting, and P. Sprangle, 1988, Appl. Phys. Lett. **53**, 1266.
Esarey, E., A. Ting, and P. Sprangle, 1990, Phys. Rev. A **42**, 3526.
Esarey, E., A. Ting, P. Sprangle, and G. Joyce, 1989, Comments Plasma Phys. Controlled Fusion **12**, 191.
Esarey, E., A. Ting, P. Sprangle, D. Umstadter, and X. Liu, 1993b, IEEE Trans. Plasma Sci. **21**, 95.
Everett, M., A. Lal, D. Gordon, C. E. Clayton, K. A. Marsh, and C. Joshi, 1994, Nature **368**, 527.
Everett, M. J., A. Lal, C. E. Clayton, W. B. Mori, T. W. Johnston, and C. Joshi, 1995a, Phys. Rev. Lett. **74**(12), 2236.
Everett, M. J., A. Lal, D. Gordon, K. Wharton, C. E. Clayton, W. B. Mori, and C. Joshi, 1995b, Phys. Rev. Lett. **74**(8), 1355.
Faure, J., Y. Glinec, A. Pukhov, S. Kiselev, S. Gordienko, E. Lefebvre, J.-P. Rousseau, F. Burgy, and V. Malka, 2004, Nature **431**(7008), 541.
Faure, J., C. Rechatin, A. Norlin, A. Lifschitz, Y. Glinec, and V. Malka, 2006, Nature **444**(7120), 737.
Filip, C. V., R. Narang, S. Tochitsky, C. E. Clayton, P. Musumeci, R. B. Yoder, K. A. Marsh, J. B. Rosenzweig, C. Pellegrini, and C. Joshi, 2004, Phys. Rev. E **69**(2), 026404.
Fisher, D. L., and T. Tajima, 1996, Phys. Rev. E **53**(2), 1844.
Fisher, D. L., T. Tajima, M. C. Downer, and C. W. Siders, 1995, Phys. Rev. E **51**(5), 4860.
Fritzler, S., E. Lefebvre, V. Malka, F. Burgy, A. E. Dangor, K. Krushelnick, S. P. D. Mangles, Z. Najmudin, J.-P. Rousseau, and B. Walton, 2004, Physical Review Letters **92**(16), 165006 (pages 4), URL `http://link.aps.org/abstract/PRL/v92/e165006`.
Fubiani, G., E. Esarey, C. B. Schroeder, and W. P. Leemans, 2004, Phys. Rev. E **70**(1), 016402.
Gahn, C., G. D. Tsakiris, A. Pukhov, J. Meyer-ter-Vehn, G. Pretzler, P. Thirolf, D. Habs, and K. J. Witte, 1999, Phys. Rev. Lett. **83**(23), 4772.
Gaul, E. W., S. P. Le Blanc, A. R. Rundquist, R. Zgadzaj, H. Langhoff, and M. C. Downer, 2000, Appl. Phys. Lett. **77**(25), 4112.
Geddes, C. G. R., K. Nakamura, G. R. Plateau, C. Toth, E. Cormier-Michel, E. Esarey, C. B. Schroeder, J. Cary, and W. P. Leemans, 2007, Stable ultrafast electron bunches with low absolute momentum spread from plasma down ramp injection.
Geddes, C. G. R., C. Toth, J. van Tilborg, E. Esarey, C. B. Schroeder, D. Bruhwiler, C. Nieter, J. Cary, and W. P. Leemans, 2004, Nature **431**(7008), 538.
Geddes, C. G. R., C. Toth, J. van Tilborg, E. Esarey, C. B. Schroeder, J. Cary, and W. P. Leemans, 2005a, Phys. Rev. Lett. **95**(14), 145002.
Geddes, C. G. R., C. Tóth, J. van Tilborg, E. Esarey, C. B. Schroeder, D. Bruhwiler, C. Nieter, J. Cary, and W. P. Leemans, 2005b, Phys. Plasmas **12**, 056709.
Gibbon, P., and A. R. Bell, 1988, Phys. Rev. Lett. **61**(14), 1599.
Gorbunov, L., P. Mora, and T. M. Antonsen, Jr., 1996, Phys. Rev. Lett. **76**(14), 2495.
Gorbunov, L. M., and V. I. Kirsanov, 1987, Sov. Phys. JETP **66**, 290.
Gorbunov, L. M., P. Mora, and T. M. Antonsen, Jr., 1997, Phys. Plasmas **4**(12), 4358.
Gordienko, S., and A. Pukhov, 2005, Phys. Plasmas **12**, 043109.
Gordon, D., K.-C. Tzeng, C. E. Clayton, A. E. Dangor, V. Malka, K. A. Marsh, A. Modena, W. B. Mori, P. Muggli, Z. Najmudin, D. Neely, C. Danson, *et al.*, 1998, Phys. Rev. Lett. **80**(10), 2133.
Gordon, D. F., B. Hafizi, P. Sprangle, R. F. Hubbard, J. R. Peñano, and W. B. Mori, 2001, Phys. Rev. E **64**, 046404.
Hamster, H., A. Sullivan, S. Gordon, W. White, and R. W. Falcone, 1993, Phys. Rev. Lett. **71**(17), 2725.
Hemker, R. G., K.-C. Tzeng, W. B. Mori, C. E. Clayton, and T. Katsouleas, 1998, Phys. Rev. E **57**(5), 5920.
Hogan, M. J., R. Assmann, F. Decker, R. Iverson, P. Raimondi, S. Rokni, R. H. Siemann, D. Walz, D. Whittum, B. Blue, C. E. Clayton, E. Dodd, *et al.*, 2000, Phys. Plasmas **7**(5), 2241.
Hogan, M. J., C. D. Barnes, C. E. Clayton, F. J. Decker, S. Deng, P. Emma, C. Huang, R. H. Iverson, D. K. Johnson, C. Joshi, T. Katsouleas, P. Krejcik, *et al.*, 2005, Phys. Rev. Lett. **95**(5), 054802.
Hooker, S. M., D. J. Spence, and R. A. Smith, 2000, J. Opt. Soc. Am. B **17**(1), 90.
Horton, W., and T. Tajima, 1986, Phys. Rev. A **34**(5), 4110.
Hosokai, T., M. Kando, H. Dewa, H. Kotaki, S. Kondo, N. Hasegawa, K. Nakajima, and K. Horioka, 2000, Opt. Lett. **25**(1), 10.
Huang, Y. C., and R. L. Byer, 1996, Appl. Phys. Lett. **69**(15), 2175.
Johnson, L. C., and T. K. Chu, 1974, Phys. Rev. Lett. **32**(10), 517.
Joshi, C., C. E. Clayton, and F. F. Chen, 1982, Phys. Rev. Lett. **48**(13), 874.
Joshi, C., W. B. Mori, T. Katsouleas, J. M. Dawson, J. M. Kindel, and D. W. Forslund, 1984, Nature **311**, 525.
Joshi, C., T. Tajima, J. M. Dawson, H. A. Baldis, and N. A. Ebrahim, 1981, Phys. Rev. Lett. **47**(18), 1285.
Katsouleas, T., and J. M. Dawson, 1983, Phys. Rev. Lett. **51**(5), 392.
Katsouleas, T., and W. B. Mori, 1989, Phys. Rev. Lett. **61**(1),

90.
Katsouleas, T., S. Wilks, P. Chen, J. M. Dawson, and J. J. Su, 1987, Part. Accel. **22**(1), 81.
Keinings, R., and M. E. Jones, 1987, Phys. Fluids **30**, 252.
Kim, J. U., N. Hafz, and H. Suk, 2004, Phys. Rev. E **69**(02), 026409.
Kimura, W. D., N. E. Andreev, M. Babzien, I. Ben-Zvi, D. B. Cline, C. E. Dilley, S. C. Gottschalk, S. M. Hooker, K. P. Kusche, S. V. Kuznetsov, I. V. Pavlishin, I. V. Pogorelsky, *et al.*, 2005, IEEE Trans. Plasma Sci. **33**(1), 3.
Kimura, W. D., G. H. Kim, R. D. Romea, L. C. Steinhauer, I. V. Pogorelsky, K. P. Kusche, R. C. Fernow, X. Wang, and Y. Liu, 1995, Phys. Rev. Lett. **74**(4), 546.
Kimura, W. D., A. van Steenbergen, M. Babzien, I. Ben-Zvi, L. P. Campbell, D. B. Cline, C. E. Dilley, J. C. Gallardo, S. C. Gottschalk, P. He, K. P. Kusche, Y. Liu, *et al.*, 2001, Phys. Rev, Lett. **86**(18), 4041.
Kitagawa, Y., T. Matsumoto, T. Minamihata, K. Sawai, K. Matsuo, K. Mima, K. Nishihara, H. Azechi, K. A. Tanaka, H. Takabe, and S. Nakai, 1992, Phys. Rev. Lett. **68**(1), 48.
Kitagawa, Y., Y. Sentoku, S. Akamatsu, W. Sakamoto, R. Kodama, K. A. Tanaka, K. Azumi, T. Norimatsu, T. Matsuoka, H. Fujita, and H. Yoshida, 2004, Phys. Rev. Lett. **92**(20), 205002.
Kotaki, H., 2007, Colliding pulse injection.
Kotaki, H., M. Kando, T. Oketa, S. Masuda, J. K. Koga, S. Kondo, S. Kanazawa, T. Yokoyama, T. Matoba, and K. Nakajima, 2002, Phys. Plasmas **9**(4), 1392.
Kotaki, H., S. Masuda, M. Kando, J. K. Koga, and K. Nakajima, 2004, Phys. Plasmas **11**(6), 3296.
Krall, J., E. Esarey, P. Sprangle, and G. Joyce, 1994, Phys. Plasmas **1**(5), 1738.
Krall, J., A. Ting, E. Esarey, and P. Sprangle, 1993, Phys. Rev. E **48**(3), 2157.
Kruer, W. L., 1988, *The Physics of Laser Plasma Interactions* (Addison-Wesley, Redwood City).
Krushelnick, K., C. I. Moore, A. Ting, and H. R. Burris, 1998, Phys. Rev. Lett. **58**(3), 4030.
Krushelnick, K., A. Ting, C. I. Moore, H. R. Burris, E. Esarey, P. Sprangle, and M. Baine, 1997, Phys. Rev. Lett. **78**, 4047.
Kumarappan, V., K. Y. Kim, and H. M. Milchberg, 2005, Phys. Rev. Lett. **94**(20), 205004.
Kurki-Suonio, T., P. J. Morrison, and T. Tajima, 1989a, Phys. Rev. A **40**(6), 3230.
Kurki-Suonio, T., P. J. Morrison, and T. Tajima, 1989b, Phys. Rev. A **40**(6), 3230.
Lawson, J. D., 1979, IEEE Trans. Nucl. Sci, **NS-26**(3), 4217.
Le Blanc, S. P., , M. C. Downer, R. Wagner, S. Y. Chen, A. Maksimchuk, G. Mourou, and D. Umstadter, 1996, Phys. Rev. Lett. **77**(27), 5381.
Ledingham, K., P. McKenna, and R. P. Singhal, 2003, Science **300**, 1107.
Leemans, W., S. Chattopadhyay, E.Esarey, A. Zholents, M. Zolotorev, A. Chin, R. Schoenlein, and C. Shank, 2000, Comptes Rendus de l'Academie des Sciences Serie IV Physique Astrophysique **1**, 279.
Leemans, W. P., 2004, in *Advanced Accelerator Concepts*, edited by V. Yakimenko (AIP, New York), volume 737, pp. 11–28.
Leemans, W. P., P. Catravas, E. Esarey, C. G. R. Geddes, C. Toth, R. Trines, C. B. Schroeder, B. A. Shadwick, J. van Tilborg, and J. Faure, 2002, Phys. Rev. Lett. **89**(17), 174802.
Leemans, W. P., C. E. Clayton, K. A. Marsh, and C. Joshi, 1991, Phys. Rev. Lett. **67**, 1434.
Leemans, W. P., C. E. Clayton, W. B. Mori, K. A. Marsh, P. K. Kaw, A. Dyson, C. Joshi, and J. M. Wallace, 1992, Phys. Rev. A **46**, 1091.
Leemans, W. P., C. G. R. Geddes, J. Faure, C. Tóth, J. van Tilborg, C. B. Schroeder, E. Esarey, G. Fubiani, D. Auerbach, B. Marcelis, M. A. Carnahan, R. A. Kaindl, *et al.*, 2003, Phys. Rev. Lett. **91**(7), 074802.
Leemans, W. P., B. Nagler, A. J. Gonsalves, C. Tóth, K. Nakamura, C. G. R. Geddes, E. Esarey, C. B. Schroeder, and S. M. Hooker, 2006, Nature Phys. **2**, 696.
Leemans, W. P., D. Rodgers, P. E. Catravas, C. G. R. Geddes, G. Fubiani, E. Esarey, B. A. Shadwick, R. Donahue, and A. Smith, 2001, Phys. Plasmas **8**(5), 2510.
Leemans, W. P., C. W. Siders, E. Esarey, N. E. Andreev, G. Shvets, and W. B. Mori, 1996, IEEE Trans. Plasma Sci. **24**, 331.
Lindberg, R. R., A. E. Charman, J. S. Wurtele, and L. Friedland, 2004, Physical Review Letters **93**(5), 055001.
Lindberg, R. R., A. E. Charman, J. S. Wurtele, L. Friedland, and B. A. Shadwick, 2006, Physics of Plasmas **13**(12), 123103.
Litvak, A. G., 1969, Zh. Eksp. Teor. Fiz. **57**(2), 629.
Liu, X., R. Wagner, A. Maksimchuk, E. Goodman, J. Workman, U. D, and A. Migus, 1995, Opt. Lett. **20**(10), 1163.
Liu, Y., X. J. Wang, D. B. Cline, M. Babzien, J. M. Fang, J. Gallardo, K. Kusche, I. Pogorelsky, J. Skaritka, and A. van Steenbergen, 1998, Phys. Rev. Lett. **80**(20), 4418.
Lu, W., C. Huang, M. Zhou, M. Tzoufras, F. S. Tsung, W. B. Mori, and T. Katsouleas, 2006, Phys. Plasmas **13**(5), 056709.
Lu, W., C. Huang, M. M. Zhou, W. B. Mori, and T. Katsouleas, 2005, Phys. Plasmas **12**(6), 063101.
Luther, B. M., Y. Wang, M. C. Marconi, J. L. A. Chilla, M. A. Larotonda, and J. J. Rocca, 2004, Phys. Rev. Lett. **92**(23), 235002.
Maine, P., D. Strickland, P. Bado, M. Pessot, and G. Mourou, 1988, IEEE J. Quantum Electron. **QE-24**, 398.
Malka, G., E. Lefebvre, and J. L. Miquel, 1997, Phys. Rev. Lett. **78**(17), 3314.
Malka, V., J. Faure, Y. Glinec, A. Pukhov, and J. Rousseau, 2005, Phys. Plasmas **12**(5), 056702.
Malka, V., J. Faure, J. R. Marquès, F. Amiranoff, J. P. Rousseau, S. Ranc, J. P. Chambaret, Z. Najmudin, B. Walton, P. Mora, and A. Solodov, 2001, Phys. Plasmas **8**(6), 2605.
Malka, V., S. Fritzler, E. Lefebvre, M.-M. Aleonard, F. Burgy, J.-P. Chambaret, J.-F. Chemin, K. Krushelnick, G. Malka, S. P. D. Mangles, Z. Najmudin, M. Pittman, *et al.*, 2002, Science **298**, 1596.
Mangles, S. P. D., C. D. Murphy, Z. Najmudin, A. G. R. Thomas, J. L. Collier, A. E. Dangor, E. J. Divall, P. S. Foster, J. G. Gallacher, C. J. Hooker, D. A. Jaroszynski, A. J. Langley, *et al.*, 2004, Nature **431**(7008), 535.
Mangles, S. P. D., B. R. Walton, M. Tzoufras, Z. Najmudin, R. J. Clarke, A. E. Dangor, R. G. Evans, S. Fritzler, A. Gopal, C. Hernandez-Gomez, W. B. Mori, W. Rozmus, *et al.*, 2005, Phys. Rev. Lett. **94**(24), 245001.
Marquès, J. R., J. P. Geindre, F. Amiranoff, P. Audebert, J. C. Gauthier, A. Antonetti, and G. Grillon, 1996, Phys. Rev. Lett. **76**(19), 3566.
Max, C., J. Arons, and A. B. Langdon, 1974, Phys. Rev. Lett. **33**, 209.

McKinstrie, C. J., and R. Bingham, 1992, Phys. Fluids B **4**(8), 2626.
McKinstrie, C. J., and D. W. Forslund, 1987, Phys. Fluids **30**(3), 904.
Milchberg, H. M., T. R. Clark, C. G. Durfee III, and T. M. Antonsen, Jr., 1996, Phys. Plasmas **3**(5), 2149.
Modena, A., Z. Najmudin, A. E. Dangor, C. E. Clayton, K. A. Marsh, C. Joshi, V. Malka, C. B. Darrow, C. Danson, D. Neely, and F. N. Walsh, 1995, Nature **377**, 606.
Monot, P., T. Auguste, P. Gibbon, F. Jakober, G. Mainfray, A. Dulieu, M. Louis-Jacquet, G. Malka, and J. L. Miquel, 1995, Phys. Rev. Lett. **74**(15), 2953.
Moore, C. I., A. Ting, K. Krushelnick, E. Esarey, R. F. Hubbard, B. Hafizi, H. R. Burris, C. Manka, and P. Sprangle, 1997, Phys. Rev. Lett. **79**(20), 3909.
Moore, C. I., A. Ting, S. J. McNaught, J. Qiu, H. R. Burris, and P. Sprangle, 1999, Phys. Rev. Lett. **82**(8), 1688.
Mora, P., 1992, Phys. Fluids B **4**(6), 1630.
Mora, P., and T. M. Antonsen, Jr., 1996, Phys. Rev E **53**(3), R2068.
Mora, P., and T. M. Antonsen, Jr., 1997, Phys. Plasmas **4**(1), 217.
Mori, W. B., 1997, IEEE J. Quantum Electron. **33**(11), 1942.
Mori, W. B., C. D. Decker, D. E. Hinkel, and T. Katsouleas, 1994, Phys. Rev. Lett. **72**, 1482.
Mori, W. B., C. Joshi, J. M. Dawson, D. W. Forslund, and J. M. Kindel, 1988, Phys. Rev. Lett. **60**(13), 1298.
Mori, W. B., and T. Katsouleas, 1992, Phys. Rev. Lett. **69**(24), 3495.
Mourou, G., and D. Umstadter, 1992, Phys. Fluids B **4**, 2315.
Musumeci, P., S. Y. Tochitsky, S. Boucher, C. E. Clayton, A. Doyuran, R. J. England, C. Joshi, C. Pellegrini, J. E. Ralph, J. B. Rosenzweig, C. Sung, S. Tolmachev, *et al.*, 2005, Phys. Rev. Lett. **94**(15), 154801.
Nakajima, K., 1992, Phys. Rev. A **45**(2), 1149.
Nakajima, K., D. Fisher, T. Kawakubo, H. Nakanishi, A. Ogata, Y. Kato, Y. Kitagawa, R. Kodama, K. Mima, H. Shiraga, K. Suzuki, K. Yamakawa, *et al.*, 1995, Phys. Rev. Lett. **74**, 4428.
Nakamura, K., G. Fubiani, C. G. R. Geddes, P. Michel, J. van Tilborg, C. Tóth, E. Esarey, C. B. Schroeder, and W. P. Leemans, 2004, in *Advanced Accelerator Concepts*, edited by V. Yakimenko (AIP, New York), volume 737, pp. 901–906.
Nieter, C., and J. Cary, 2004, J. Comp. Phys. **196**, 448.
Palmer, R. B., 1980, Part. Accel. **11**(2), 81.
Pang, J., Y. K. Ho, X. Q. Yuan, N. Cao, Q. Kong, P. X. Wang, L. Shao, E. H. Esarey, and A. M. Sessler, 2002, Phys. Rev. E **66**(6), 066501.
Panofsky, W. K. H., and W. A. Wenzel, 1956, Rev. Sci. Instrum. **27**, 967.
Perry, M. D., and G. Mourou, 1994, Science **264**, 917.
Plettner, T., R. L. Byer, E. Colby, B. Cowan, C. M. S. Sears, J. E. Spencer, and R. H. Siemann, 2005, Phys. Rev. Lett. **95**(13), 134801.
Pukhov, A., and J. Meyer-ter-Vehn, 1996, Phys. Rev. Lett. **76**(21), 3975.
Pukhov, A., and J. Meyer-ter-Vehn, 2002, Appl. Phys. B **74**, 355.
Pukhov, A., Z.-M. Sheng, and J. Meyer-ter-Vehn, 1999, Phys. Plasmas **6**(7), 2847.
Quesnel, B., and P. Mora, 1998, Phys. Rev. E **58**(3), 3719.
Rankin, R., C. E. Capjack, N. H. Burnett, and P. B. Corkum, 1991, Optics Letters **16**, 835.
Reitsma, A. J. W., W. P. Leemans, E. Esarey, C. B. Schroeder, L. P. J. Kamp, and T. J. Schep, 2002, Phys. Rev. ST Accel. Beams **5**(5), 051301.
Ren, C., R. G. Hemker, R. A. Fonseca, B. J. Duda, and W. B. Mori, 2000, Phys. Rev. Lett. **85**(10), 2124.
Rosenbluth, M. N., and C. S. Liu, 1972, Phys. Rev. Lett. **29**(11), 701.
Rosenzweig, J. B., 1988, Phys. Rev. A **38**(7), 3634.
Rosenzweig, J. B., B. Breizman, T. Katsouleas, and J. J. Su, 1991, Phys. Rev. E **44**(10), R6189.
Rousse, A., K. Phuoc, R. Shah, A. Pukhov, E. Lefebvre, V. Malka, S. Kiselev, F. Burgy, J. Rousseau, D. Umstadter, and D. Hulin, 2004, Phys. Rev. Lett. **93**(13), 135005.
Rousseaux, C., G. Malka, J. L. Miquel, F. Amiranoff, S. D. Baton, and P. Mounaix, 1995, Phys. Rev. Lett. **74**(23), 4655.
Ruhl, H., 2000, *Collective Super-Intense Laser-Plasma Interactions*, Habilitationsschrift, Technischen Universität Darmstadt.
Sakharov, A. S., and V. I. Kirsanov, 1994, Phys. Rev. E **49**(4), 3274.
Santala, M. I. K., Z. Najmudin, E. L. Clark, M. Tatarakis, K. Krushelnick, A. E. Dangor, V. Malka, J. Faure, R. Allott, and R. J. Clarke, 2001a, Phys. Rev. Lett. **86**(7), 1227.
Santala, M. I. K., M. Zepf, F. N. Beg, E. L. Clark, A. E. Dangor, K. Krushelnick, M. Tatarakis, I. Watts, K. W. D. Ledingham, T. McCanny, I. Spencer, A. C. Machacek, *et al.*, 2001b, Appl. Phys. Lett. **78**(1), 19.
Schroeder, C. B., E. Esarey, C. G. R. Geddes, C. Tóth, B. A. Shadwick, J. van Tilborg, J. Faure, and W. P. Leemans, 2003a, Phys. Plasmas **10**(5), 2039.
Schroeder, C. B., E. Esarey, and B. A. Shadwick, 2005, Phys. Rev. E **72**(5), 055401.
Schroeder, C. B., E. Esarey, B. A. Shadwick, and W. P. Leemans, 2003b, Phys. Plasmas **10**(1), 285.
Schroeder, C. B., E. Esarey, B. A. Shadwick, and W. P. Leemans, 2006, Phys. Plasmas **13**(3), 033103.
Schroeder, C. B., E. Esarey, J. van Tilborg, and W. P. Leemans, 2004, Phys. Rev. E **69**(1), 016501.
Schroeder, C. B., P. B. Lee, J. S. Wurtele, E. Esarey, and W. P. Leemans, 1999a, Phys. Rev. E **59**(5), 6037.
Schroeder, C. B., J. S. Wurtele, and D. H. Whittum, 1999b, Phys. Rev. Lett. **82**(6), 1177.
Shadwick, B. A., G. M. Tarkenton, and E. H. Esarey, 2004, Phys. Rev. Lett. **93**(17), 175002.
Shadwick, B. A., G. M. Tarkenton, E. H. Esarey, and W. P. Leemans, 2002, IEEE Trans. Plasma Sci. **30**, 38.
Shadwick, B. A., G. M. Tarkenton, E. H. Esarey, and C. B. Schroeder, 2005, Phys. Plasmas **12**, 056710.
Shvets, G., N. J. Fisch, and A. Pukhov, 2002, Phys. Plasmas **9**(5), 2383.
Shvets, G., N. J. Fisch, A. Pukhov, and J. Meyer-ter Vehn, 1999, Phys. Rev. E **60**(2), 2218.
Shvets, G., and X. Li, 1999, Phys. of Plasmas **6**(2), 591.
Shvets, G., and J. S. Wurtele, 1994, Phys. Rev. Lett. **73**(26), 3540.
Shvets, G., J. S. Wurtele, T. C. Chiou, and T. C. Katsouleas, 1996, IEEE Trans. Plasma Sci. **24**(2), 351.
Shvets, G., J. S. Wurtele, and B. A. Shadwick, 1997, Phys. Plasmas **4**(5), 1872.
Siders, C. W., S. P. Le Blanc, D. Fisher, T. Tajima, M. C. Downer, A. Babine, A. Stepanov, and A. Sergeev, 1996, Phys. Rev. Lett. **76**(19), 3570.
Spence, D. J., and S. M. Hooker, 2001, Phys. Rev. E **63**(1),

015401.
Sprangle, P., and E. Esarey, 1992, Phys. Fluids B **4**, 2241.
Sprangle, P., E. Esarey, and J. Krall, 1996a, Phys. Plasmas **3**, 2183.
Sprangle, P., E. Esarey, and J. Krall, 1996b, Phys. Rev. E **54**, 4211.
Sprangle, P., E. Esarey, J. Krall, and G. Joyce, 1992, Phys. Rev. Lett. **69**(15), 2200.
Sprangle, P., E. Esarey, and A. Ting, 1990a, Phys. Rev. A **41**, 4463.
Sprangle, P., E. Esarey, and A. Ting, 1990b, Phys. Rev. Lett. **64**, 2011.
Sprangle, P., E. Esarey, A. Ting, and G. Joyce, 1988, Appl. Phys. Lett. **53**, 2146.
Sprangle, P., B. Hafizi, J. R. Peñano, R. F. Hubbard, A. Ting, C. I. Moore, D. F. Gordon, A. Zigler, D. Kaganovich, and T. M. Antonsen, Jr., 2001, Phys. Rev. E **63**(5), 056405.
Sprangle, P., J. Krall, and E. Esarey, 1994, Phys. Rev. Lett. **73**, 3544.
Sprangle, P., C. M. Tang, and E. Esarey, 1987a, IEEE Trans. Plasma Sci. **PS-15**, 145.
Sprangle, P., A. Ting, and C. M. Tang, 1987b, Phys. Rev. A **36**, 2773.
Sprangle, P., A. Zigler, and E. Esarey, 1991, Appl. Phys. Lett. **58**, 346.
Steinhauer, L. C., and H. G. Ahlstrom, 1971, Phys. Fluids **14**(6), 1109.
Strickland, D., and G. Mourou, 1985, Opt. Commun. **56**, 219.
Stupakov, G. V., and M. S. Zolotorev, 2001, Phys. Rev. Lett. **86**(23), 5274.
Suk, H., N. Barov, J. B. Rosenzweig, and E. Esarey, 2001, Phys. Rev. Lett. **86**(6), 1011.
Sun, G. Z., E. Ott, Y. C. Lee, and P. Guzdar, 1987, Phys. Fluids **30**, 526.
Tajima, T., and J. M. Dawson, 1979, Phys. Rev. Lett. **43**(4), 267.
Tang, C. M., P. Sprangle, and R. N. Sudan, 1985, Phys. Fluids **28**(6), 1974.
Teychenné, D., G. Bonnaud, and J. Bobin, 1993, Phys. Rev. E **48**(5), R3248.
Teychenné, D., G. Bonnaud, and J.-L. Bobin, 1994a, Phys. Plasmas **1**(6), 1771.
Teychenné, D., G. Bonnaud, and J.-L. Bobin, 1994b, Phys. Rev. E **49**(4), 3253.
Ting, A., E. Esarey, and P. Sprangle, 1990, Phys. Fluids B **2**, 1390.
Ting, A., D. Kaganovich, D. F. Gordon, R. F. Hubbard, and P. Sprangle, 2005, Phys. Plasmas **12**(1), 010701.
Ting, A., K. Krushelnick, C. I. Moore, H. R. Burris, E. Esarey, J. Krall, and P. Sprangle, 1996, Phys. Rev. Lett. **77**(27), 5377.
Ting, A., C. I. Moore, K. Krushelnick, C. Manka, E. Esarey, P. Sprangle, R. Hubbard, H. R. Burris, R. Fischer, and M. Baine, 1997, Phys. Plasmas **4**(5), 1889.
Tochitsky, S., R. Narang, C. V. Filip, P. Musumeci, C. E. Clayton, R. B. Yoder, K. A. Marsh, J. B. Rosenzweig, C. Pellegrini, and C. Joshi, 2005, Phys. Rev. Lett. **92**(9), 095004.
Tomassini, P., M. Galimberti, A. Giulietti, D. Giulietti, L. A. Gizzi, L. Labate, and F. Pegoraro, 2003, Phys. Rev. ST Accel. Beams **6**(12), 121301.
Tsung, F. S., R. Narang, W. B. Mori, C. Joshi, R. A. Fonseca, and L. O. Silva, 2004, Phys. Rev. Lett. **93**(18), 185002.
Tzeng, K.-C., W. B. Mori, and C. D. Decker, 1996, Phys. Rev, Lett. **76**(18), 3332.
Tzeng, K.-C., W. B. Mori, and T. Katsouleas, 1997, Phys. Rev. Lett. **79**(26), 5258.
Umstadter, D., S.-Y. Chen, A. Maksimchuk, G. Mourou, and R. Wagner, 1996a, Science **273**(5274), 472.
Umstadter, D., E. Esarey, and J. Kim, 1994, Phys. Rev. Lett. **72**(8), 1224.
Umstadter, D., J. Kim, E. Esarey, E. Dodd, and T. Neubert, 1995, Phys. Rev. E **51**(4), 3484.
Umstadter, D., J. K. Kim, and E. Dodd, 1996b, Phys. Rev. Lett. **76**(12), 2073.
van Tilborg, J., C. B. Schroeder, C. V. Filip, C. Tóth, C. G. R. Geddes, G. Fubiani, R. Huber, R. A. Kaindl, E. Esarey, and W. P. Leemans, 2006, Phys. Rev. Lett. **96**, 014801.
Volfbeyn, P., E. Esarey, and W. Leemans, 1999, Phys. Plasmas **6**, 2269.
Wagner, R., S.-Y. Chen, A. Maksimchuk, and D. Umstadter, 1997, Phys. Rev. Lett. **78**(16), 3125.
Whittum, D. H., A. M. Sessler, and J. M. Dawson, 1990, Phys. Rev. Lett. **64**(21), 2511.
Wilks, S. C., J. M. Dawson, W. B. Mori, T. Katsouleas, and M. E. Jones, 1989, Phys. Rev. Lett. **62**(22), 2600.
Woodward, P. M., 1947, J. Inst. Electr. Eng. **93**(IIIA), 1554.
Young, P. E., M. E. Foord, J. H. Hammer, W. L. Kruer, M. Tabak, and S. C. Wilks, 1995, Phys. Rev. Lett. **75**(6), 1082.
Zigler, A., Y. Ehrlich, C. Cohen, J. Krall, and P. Sprangle, 1996, J. Opt. Soc. Am. B. **13**, 68.

FIGURES

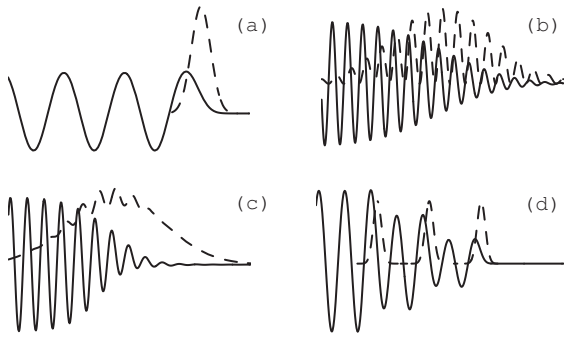

FIG. 1 Schematic of laser-driven plasma-based accelerators: (a) laser wakefield accelerator (LWFA), (b) plasma beat wave accelerator (PBWA), (c) self-modulated laser wakefield accelerator (SM-LWFA), and (d) resonant laser pulse train. Shown are the excited plasma wave potentials (solid lines) and right-moving laser intensity envelopes (dashed lines).

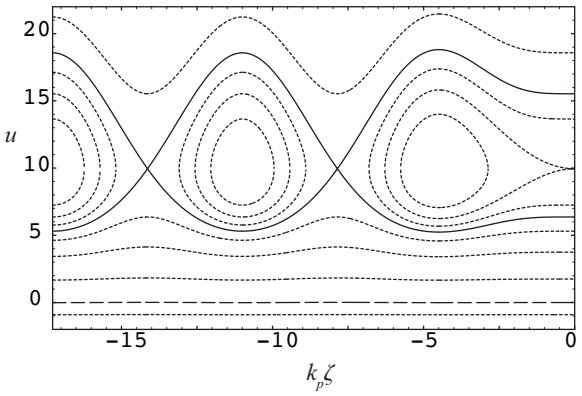

FIG. 2 Single particle orbits in phase space $(u, k_p\zeta)$ for an electron in a small amplitude, sinusoidal plasma wave with a normalized potential given by $\phi = \phi_0 \cos\psi$, with $\gamma_\varphi = 10$ and $\phi_0 = 10^{-2}$. Solid curve is separatrix. Dashed curve is the cold fluid orbit. Excitation of the plasma wave by a laser pulse with a half-sine envelope of length $\lambda_p/2$ (head at $k_p\zeta = 0$) is assumed.

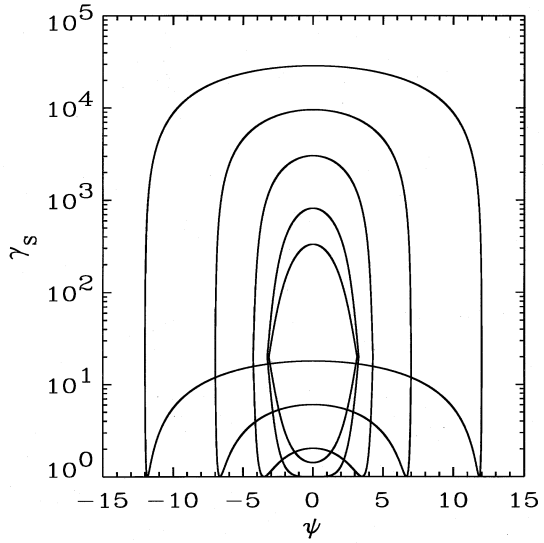

FIG. 3 Phase-space separatrix $\gamma_s(\psi)$ plotted for several values of the plasma wave amplitude $\epsilon = 0.03$, 0.04, 0.1, 0.3, and 0.9 ($\epsilon = 1$ corresponds to the cold wavebreaking limit), with $\gamma_p = 20$. The value $\epsilon = 0.03$ corresponds to the innermost curve and $\epsilon = 0.9$ corresponds to the outermost curve.

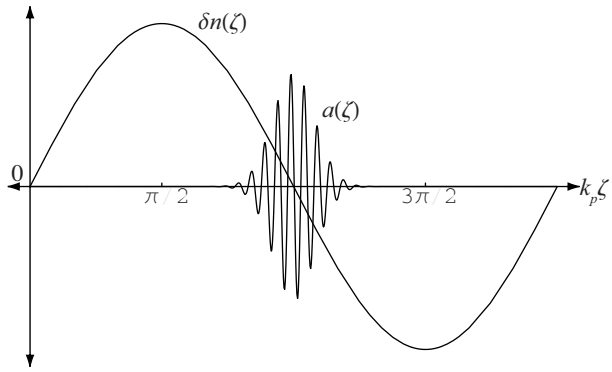

FIG. 4 Schematic of laser pulse frequency upshifting by a plasma wave with $v_p \simeq v_g \simeq c$ (pulse moving to the right). Positive frequency shifts require the laser pulse a to be centered about regions of the plasma wave ($\delta n = n - n_0$) with a decreasing density.

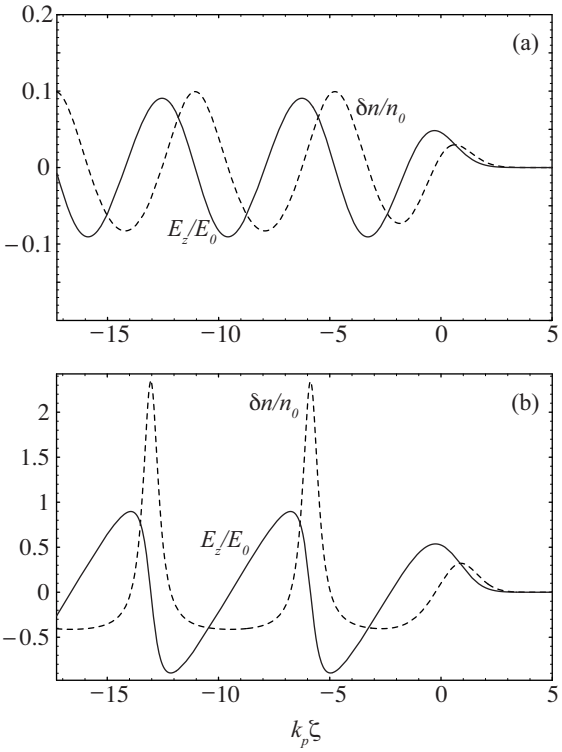

FIG. 5 Density variation $\delta n/n_0$ (dashed curve) and axial electric field E_z/E_0 (solid curve) in an LWFA driven by a Gaussian laser pulse (pulse is moving to the right, centered at $k_p\zeta = 0$ with rms intensity duration k_p^{-1}), for (a) $a_0 = 0.5$ and (b) $a_0 = 2.0$.

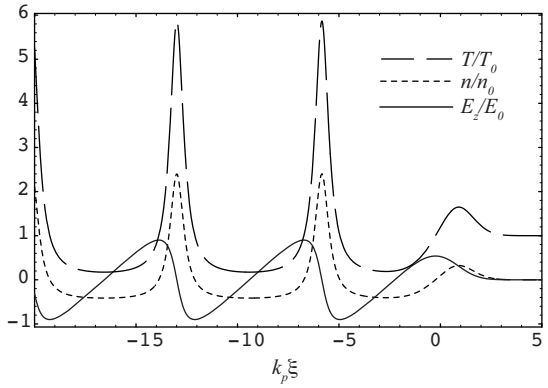

FIG. 6 Plasma density n/n_0 (dotted curve), plasma wave electric field E_z/E_0 (solid curve), and plasma temperature T/T_0 (dashed curve) excited by a Gaussian laser pulse with normalized intensity $a = 2$ and RMS length $k_pL_{\rm RMS} = 1$ (centered at $k_p\xi = 0$).

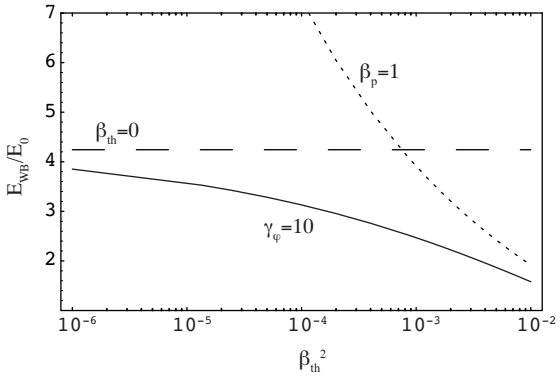

FIG. 7 Maximum plasma wave electric field amplitude $\hat{E}_{\rm max} = E_{\rm max}/E_0$ [Eq. (22)] versus initial temperature $\beta_{\rm th}^2$ with $\gamma_\varphi = 10$ and $\gamma_\perp = 1$. The dotted curve is the ultra-relativistic result $\beta_\varphi = 1$, and the dashed line is the cold limit.

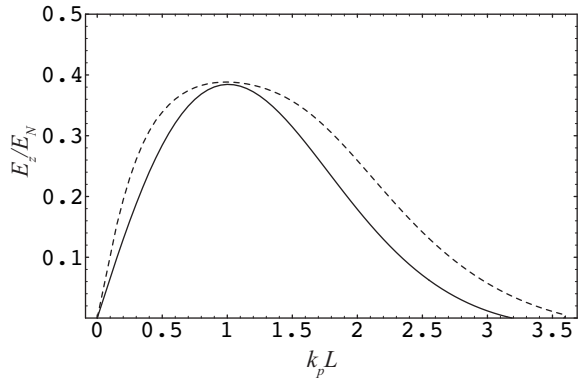

FIG. 8 Amplitude of axial electric field E_z [normalized to the maximum amplitude of a flat-top pulse $E_N = a_0^2/(1 + a_0^2/2)^{1/2}$] plotted as a function of laser pulse length k_pL for the LWFA examples shown in Fig. 5: $a_0 = 0.5$ (solid curve) and $a_0 = 2.0$ (dashed curve). The laser pulse envelope is given by $a = a_0 \exp(-\zeta^2/4L)$ such that L is the rms of the laser intensity.

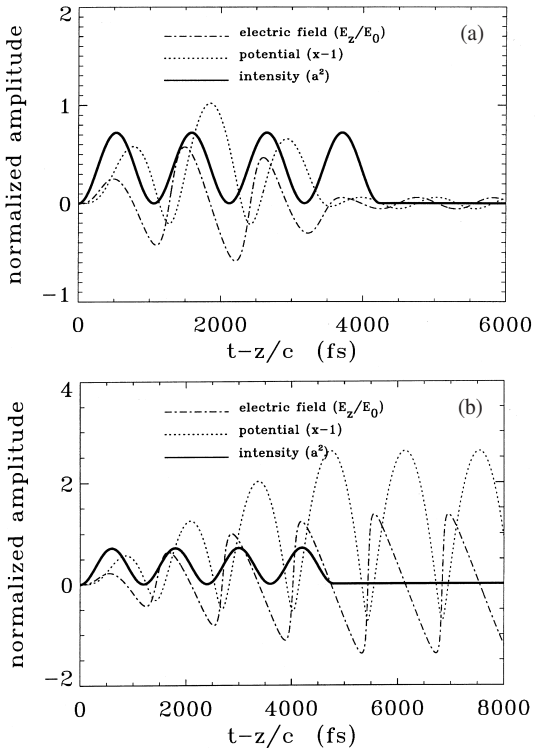

FIG. 9 Examples of PBWA consisting of four beat pulses with $a_0 = 1.2$ in a plasma of density $n_0 = 10^{16}$ cm^{-3}: (a) without optimization $\Delta\omega = \omega_p$, showing the effects of detuning, and (b) with optimization $\Delta\omega < \omega_p$. Normalized intensity profile a^2 (solid curve), wake potential ϕ (dotted curve), and axial field E_z/E_0 (dashed curve) versus $t - z/c$. Pulses are linearly polarized (moving to the left).

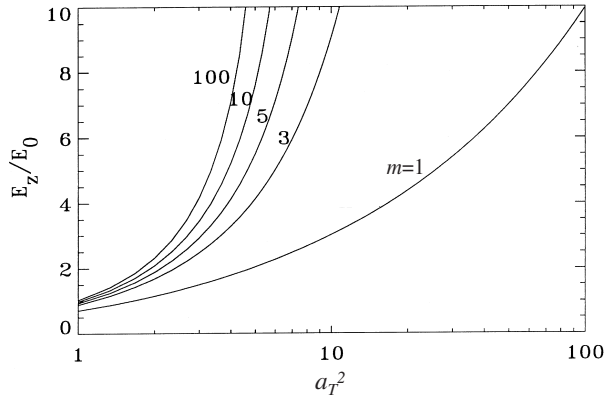

FIG. 10 Maximum electric field amplitude E_z/E_0 versus $a_T^2 = ma_0^2$, for $m = 1$, 3, 5, 10, and 100 optimized square laser pulses with $a_0 = 1$.

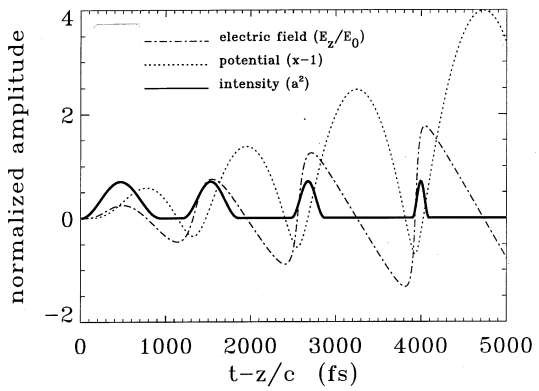

FIG. 11 Laser pulse train consisting of four optimized sine-shaped laser pulses with $a_0 = 1.2$ and $n_0 = 10^{16}$ cm^{-3}. Normalized intensity profile a^2 (solid curve), wake potential ϕ (dotted curve), and axial field E_z/E_0 (dashed curve) are plotted versus the comoving variable $t - z/c$. Pulses are linearly polarized (moving to the left).

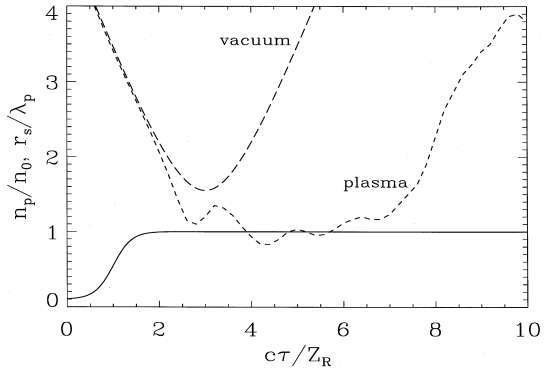

FIG. 12 Ambient plasma density n_p/n_0 (solid curve) and spot size r_s/λ_p (dashed curve) versus normalized propagation distance $c\tau/Z_R$ for a self-modulated LWFA with $n_0 = 2.8 \times 10^{18}$ cm^{-3}. Laser is initially converging such that the minimum spot size in vacuum is reached at $c\tau = 3Z_R$.

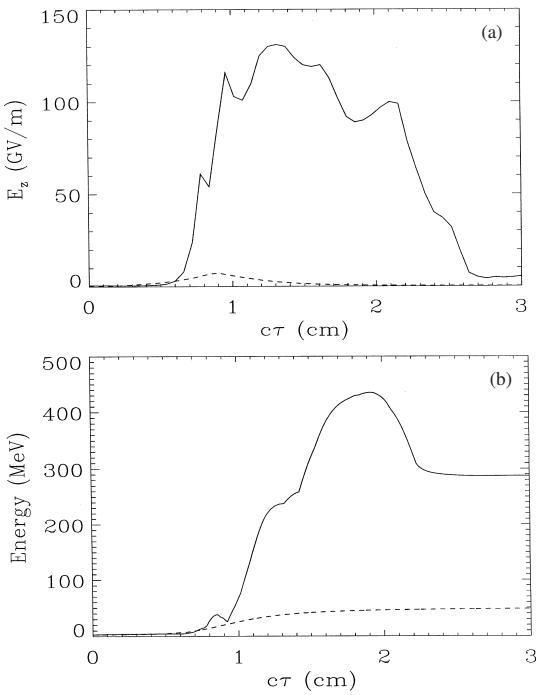

FIG. 13 (a) Peak accelerating field and (b) peak energy of the injected particles versus propagation distance $c\tau$ for the standard LWFA (dashed curve) with $n_0 = 1.4 \times 10^{17}$ cm^{-3} and the self-modulated LWFA (solid curve) with $n_0 = 2.8 \times 10^{18}$ cm^{-3}.

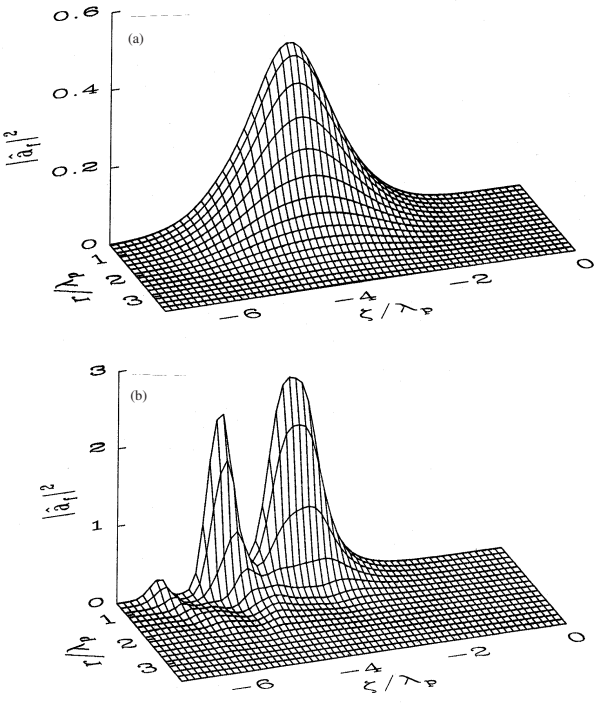

FIG. 14 Normalized laser intensity $|a|^2$ for the self-modulated LWFA case at (a) $c\tau = 2Z_R$ and (b) $c\tau = 3.2Z_R$. Laser pulse is moving to the right.

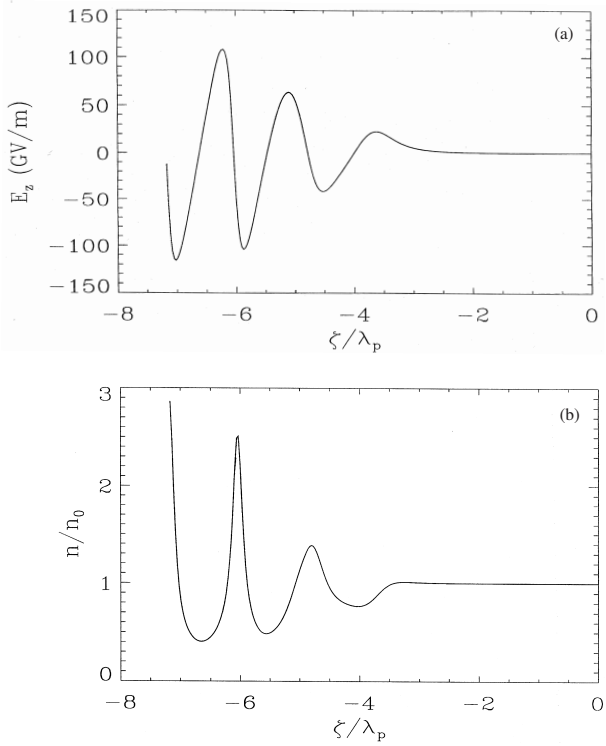

FIG. 15 (a) Axial electric field E_z and (b) normalized plasma electron density n/n_0 versus ζ at $c\tau = 3.2Z_R$ for the self-modulated LWFA case.

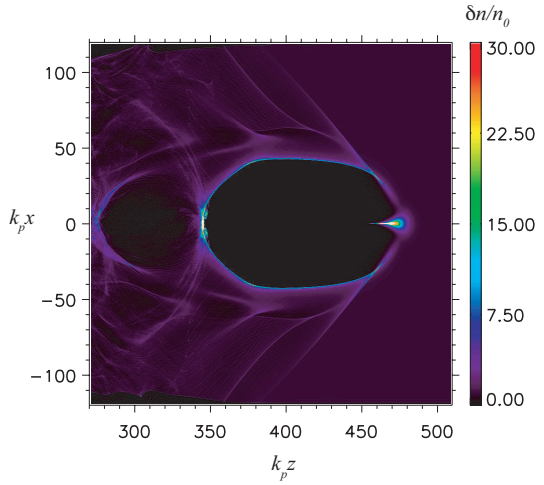

FIG. 16 Electron density wake from an electron beam with energy 0.5 GeV, density $n_b = 10n_0$, rms longitudinal beam size $k_p^2\sigma_z^2 = 2$ (Gaussian longitudinal profile), and rms transverse beam size $k_p^2\sigma_x^2 = 2$ (Gaussian transverse profile). The electron beam is moving toward the right with its center located at $k_p z = 454$ in a plasma of density $n_0 = 5 \times 10^{17}$ cm^{-3}. Numerical parameters: 25 particles per cell and a transverse and longitudinal cell size of 0.33 μm.

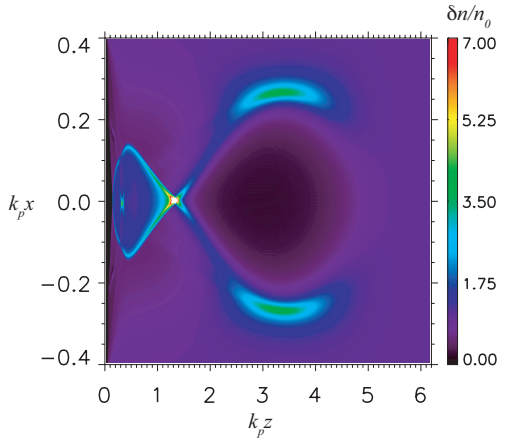

FIG. 17 Electron density wake from a laser pulse with $a_0 = 0.35$, rms length 100 μm (half-sine longitudinal profile), spot size $r_0 = 10$ μm (Gaussian transverse profile), and wavelength $\lambda = 0.8$ μm. The laser is moving toward the right (peak located at $k_p z = 4.9$) in a plasma of density $n_0 = 8 \times 10^{15}$ cm^{-3} ($\lambda_p = 300$ μm). Numerical parameters: 4 particles per cell, 24 cells per laser wavelength longitudinally, and 6 cells per laser wavelength transversely.

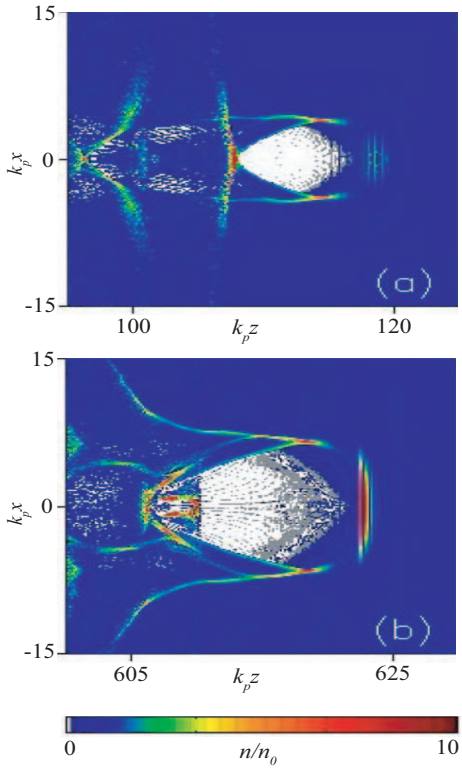

FIG. 18 Electron density wake at (a) $\omega_p t = 127$ and (b) $\omega_p t = 633$ driven by a laser pulse with an initial envelope $a = a_0 \exp(-z^2/L^2)\exp(-x^2/r_0^2)$ with $a_0 = 5$, $L = 6$ μm, $r_0 = 9$ μm and $\lambda = 0.8$ μm. The laser is propagating to the right in a plasma of density density $n_0 = 7 \times 10^{18}$ cm^{-3}. Numerical parameters: longitudinal cell size $dz = \lambda_0/50$, transverse cell size $dx = \lambda_0/3.2 = r_0/36 = \lambda_p/50$, and 9 particles per cell.

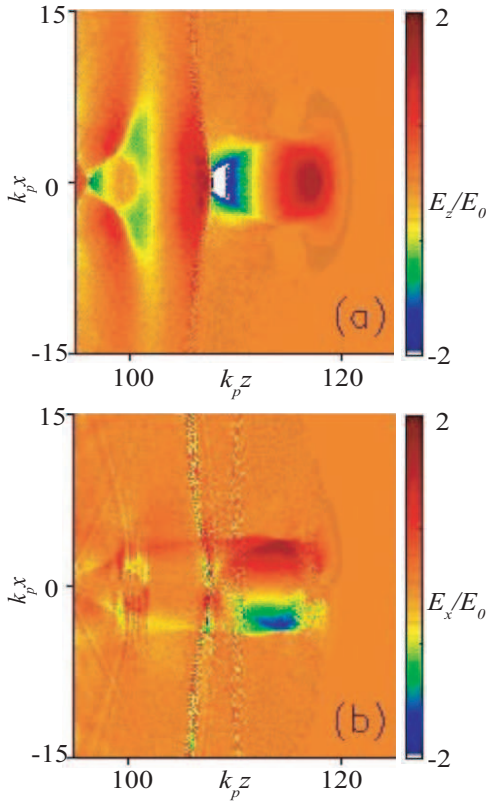

FIG. 19 (a) Longitudinal electric field and (b) transverse electric field, normalized to E_0, as a function of $k_p z$ and $k_p x$, for the parameters of Fig. 18(a) at $\omega_p t = 127$.

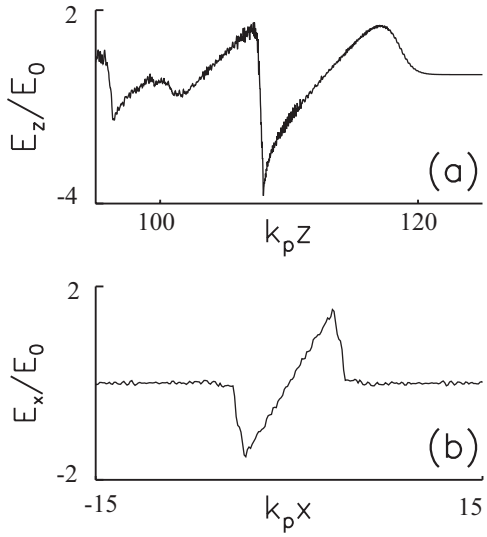

FIG. 20 Lineouts of (a) longitudinal electric field on axis (b) and transverse electric field at $k_p dz = 113$, for the parameters of Fig. 18(a) at $\omega_p t = 127$.

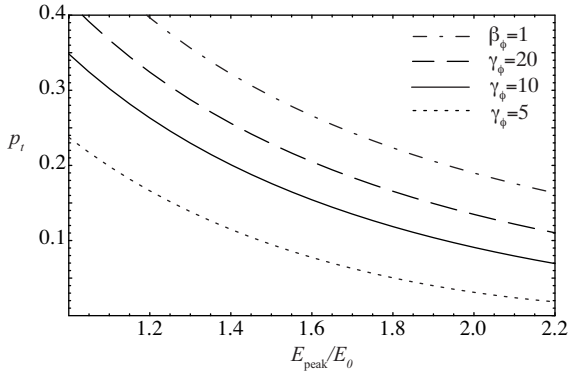

FIG. 21 Initial electron momentum $\tilde{p}_t$ required to be trapped by a plasma wave with field amplitude $E_{\rm peak}/E_0$ and phase velocity $\gamma_\varphi = 5$ (dotted curve), $\gamma_\varphi = 10$ (solid curve), $\gamma_\varphi = 20$ (dashed curve), and $\beta_\varphi = 1$ (dash-dotted curve), assuming an initial plasma temperature $\beta_{\rm th} = 10^{-2}$.

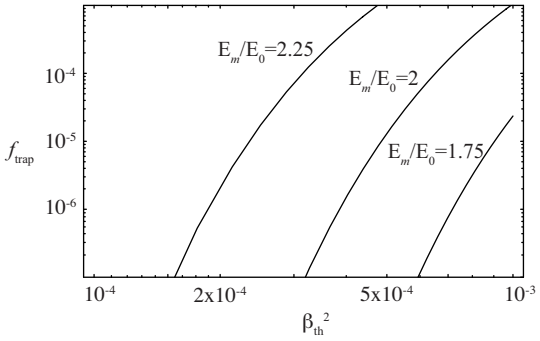

FIG. 22 Fraction of trapped electrons $f_{\rm trap}$ [Eq. (55)] versus the initial temperature of a Gaussian plasma electron distribution $\beta_{\rm th}^2 = k_{\rm B}T_0/mc^2$ for three different nonlinear plasma wave amplitudes driven by a laser with $k_pL_{\rm RMS} = 1$ and $a_0 = 3.65$ ($\hat{E}_m \simeq 1.75$), $a_0 = 4.15$ ($\hat{E}_m \simeq 2$), and $a_0 = 4.75$ ($\hat{E}_m \simeq 2.25$), with $\gamma_\varphi = 10$.

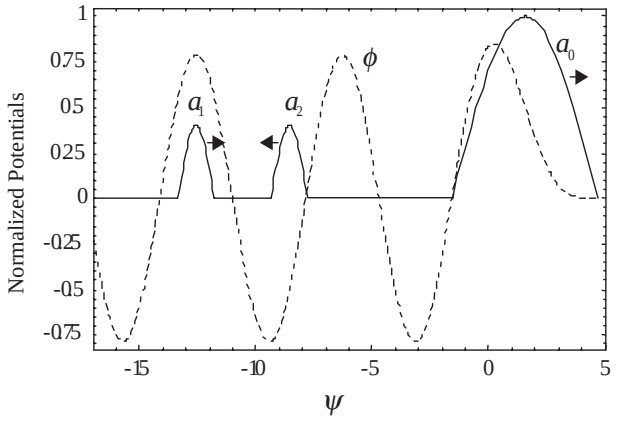

FIG. 23 Profiles of the pump laser pulse a_0, the wake ϕ, and the forward a_1 injection pulse, all of which are stationary in the $\psi = k_p(z - v_pt)$ frame, and the backward injection pulse a_2, which moves to the left at $\simeq 2c$.

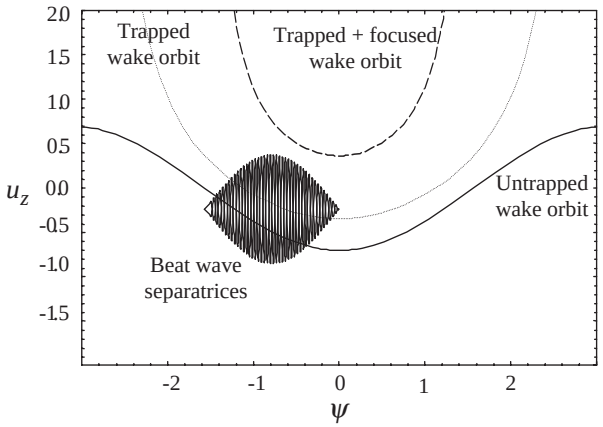

FIG. 24 Longitudinal phase space showing beat wave separatrices, an untrapped plasma wave orbit (solid line), a trapped plasma wave orbit (dotted line), and a trapped and focused plasma wave orbit (dashed line).

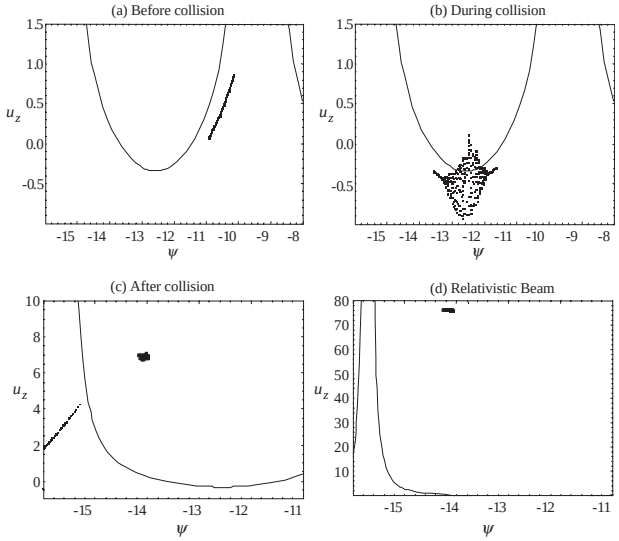

FIG. 25 Electron distribution in longitudinal (u_z, ψ) phase space (a) before injection pulse collision ($\omega_p\Delta t = 0$), (b) during collision ($\omega_p\Delta t = 3$), (c) just after collision ($\omega_p\Delta t = 14$), and (d) at $\omega_p\Delta t = 114$ (38 MeV electron bunch with 1 fs duration, 0.2% energy spread, and 0.9 mm-mrad normalized transverse emittance). The separatrix between trapped and untrapped wake orbits (solid line) is shown.

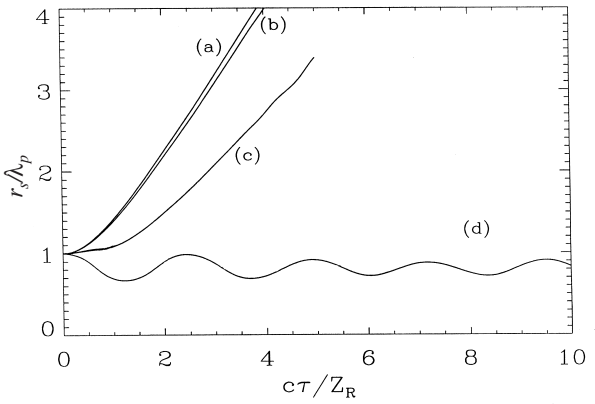

FIG. 26 Laser spot size r_s versus normalized propagation distance $c\tau/Z_R$ for (a) vacuum diffraction, (b) $L = \lambda_p/4$, and (c) $L = \lambda_p$, with parameters $P = P_c$, $a_0 = 0.9$, and $\lambda_p = 0.03$ cm. (d) Guiding of $L = \lambda_p$ pulse in a preformed parabolic plasma density channel with $\Delta n = 1/(\pi r_e r_s^2)$.

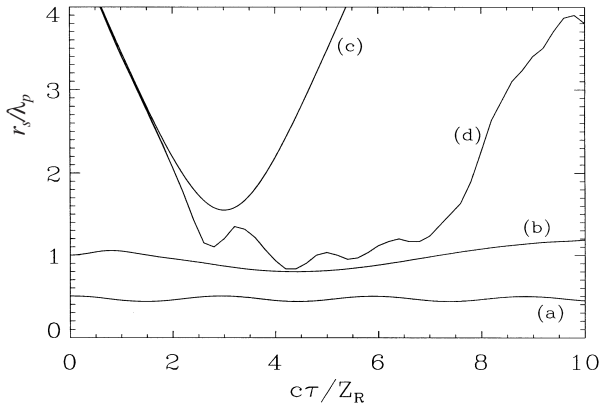

FIG. 27 Laser spot size r_s versus propagation distance $c\tau$ for (a) a channel-guided LWFA, (b) a tailored-pulse LWFA, (c) vacuum diffraction, and (d) the self-modulated LWFA shown in Figs. 13–15.

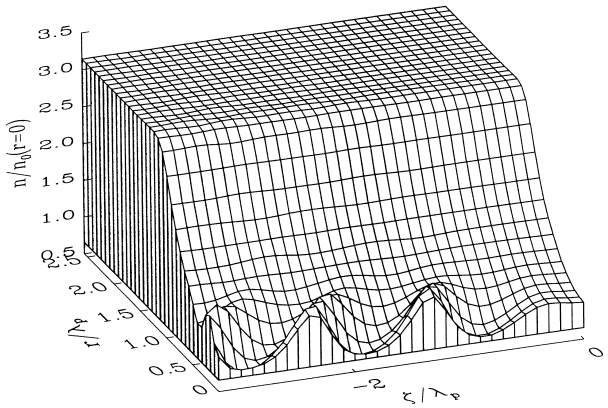

FIG. 28 Plasma electron density n/n_0 at $c\tau = 20Z_R$ for a channel-guided LWFA. Initial density profile is parabolic with a depth $\Delta n = \Delta n_c = 1/(\pi r_e r_0^2)$.

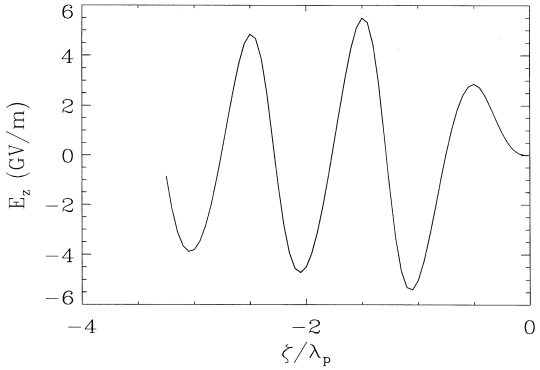

FIG. 29 Axial electric field E_z on axis at $c\tau = 20Z_R$ for channel-guided LWFA shown in Fig. 28.

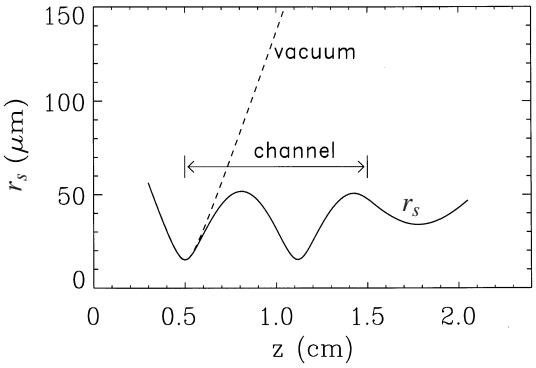

FIG. 30 Laser spot size versus propagation distance $z = c\tau$ in vacuum (dashed curve) and in a plasma channel (solid curve) located at 0.5 cm $< z <$ 1.5 cm for a low-power $P \ll P_c$ mismatched pulse.

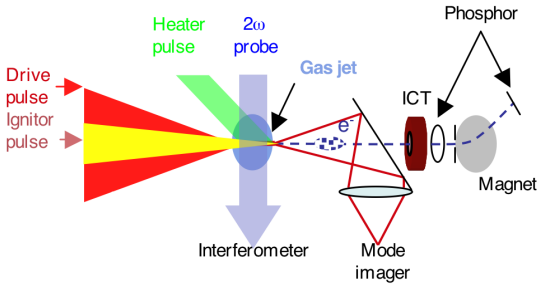

FIG. 31 Schematic of a generic experimental setup used in laser-plasma-based accelerators. The laser beams are usually produced by a CPA-based laser system. Plasma density profiles can be measured using a frequency-doubled probe beam that comes orthogonal to the main drive beam. For single beam experiments only the "main" or drive beam is used. Guiding experiments based on formation of preformed channels via the ignitor-heater method use two additional laser beams. One beam that co-propagates with the main drive beam to ionize the gas emerging from the pulsed gas jet (ignitor beam) and a second to rapidly heat the plasma filament via inverse Bremsstrahlung heating. The high peak power laser beams are focused, using off-axis parabolic mirrors, onto a high pressure pulsed gas jet, operating with a specific backing pressure that can be varied to control the plasma density. An integrating current transformer (ICT) is typically used to measure the charge per bunch of the electron beam. A dipole magnet permits electron beam energy distribution measurements. Various optical and other types of detectors are used to monitor laser beam, plasma, and secondary radiation (e.g., THz radiation, γ-rays, and neutrons).

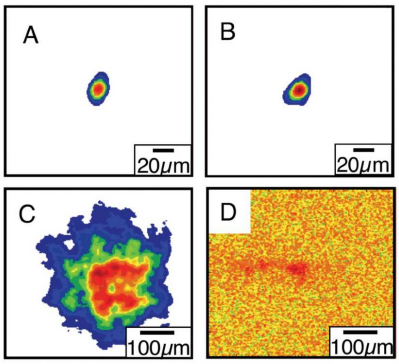

FIG. 32 Mode images of laser propagation at 4 TW, or twice the critical power for self focusing. The guided output mode after 2.5 mm ($> 10Z_R$) of propagation (b) is indistinguishable from the input mode (a). The effect of the channel can be seen by comparison to vacuum propagation over the same distance where the output mode is severely diffracted (c). Self guiding also does not maintain the spot over this distance due to instability, and the output mode with gas jet on but without the guide displays enhanced diffraction (d). Note enlarged scale in (c) and (d).

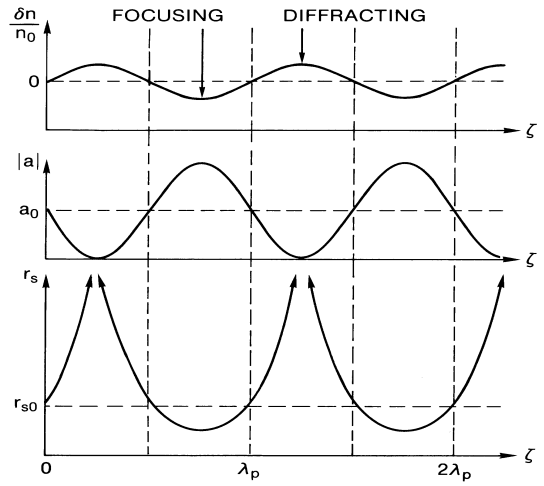

FIG. 33 Schematic of focusing effects of an externally generated plasma wave on an initially uniform low-intensity laser pulse.

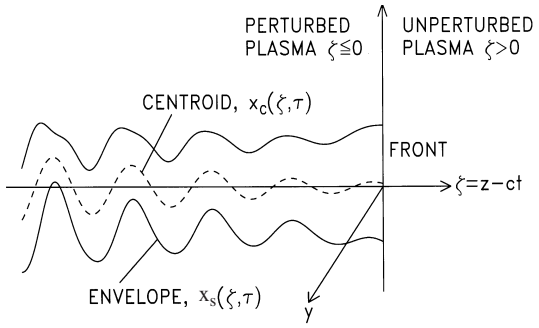

FIG. 34 Schematic of the hose-modulation instability showing the laser pulse centroid x_c and spot size x_s.

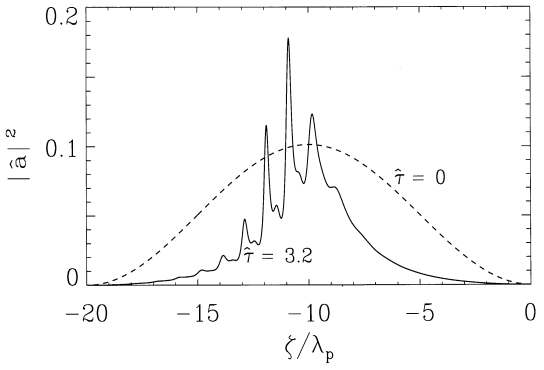

FIG. 35 Normalized laser intensity $|a|^2$ versus ζ/λ_p at $c\tau = 0$ (dashed curve) and $c\tau = 3.2Z_R$ (solid curve) for the parameters $\lambda_p = r_0/2 = 30$ μm. Laser is moving to the right.

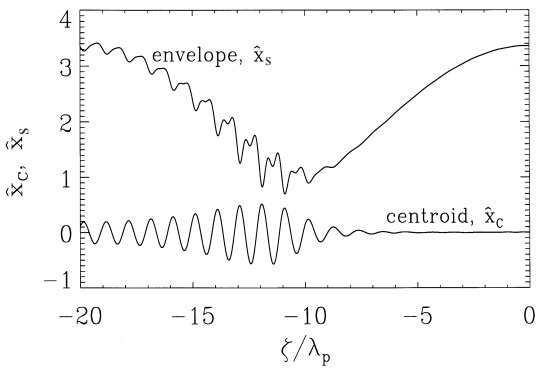

FIG. 36 Laser envelope x_s (upper curve) and centroid x_c (lower curve) versus ζ/λ_p at $c\tau = 3.2Z_R$ for an initial perturbation of 1% in x_c. Perturbations grow at $\lambda_p = r_0/2 = 30\ \mu$m.

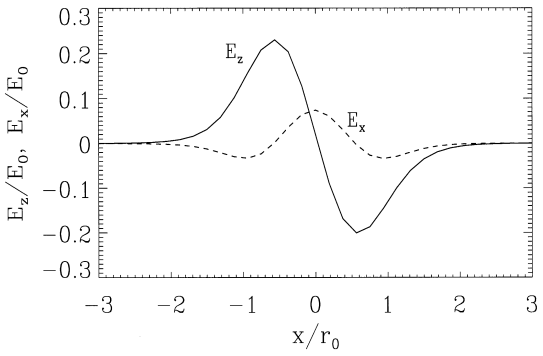

FIG. 37 Transverse profiles of the axial wakefield E_z/E_0 (solid curve) and the transverse wakefield E_x/E_0 (dashed curve) at $c\tau = 1.8Z_R$ and $\zeta = -18\lambda_p$ for a hose-dominated case.

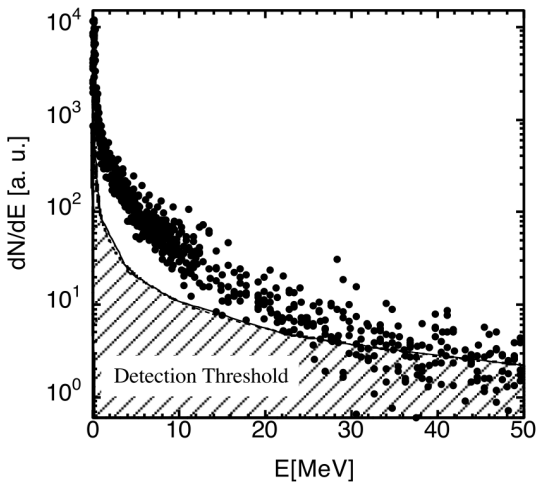

FIG. 38 Electron energy spectrum dN/dE measured using a double focusing imaging magnetic spectrometer. The spectrum was obtained by scanning the excitation current in the magnet and measuring the intensity on a phosphor screen. Each data point represents 10 shots. The spectrum is reasonably well approximated by a Boltzmann distribution with an effective temperature of 4.6 MeV.

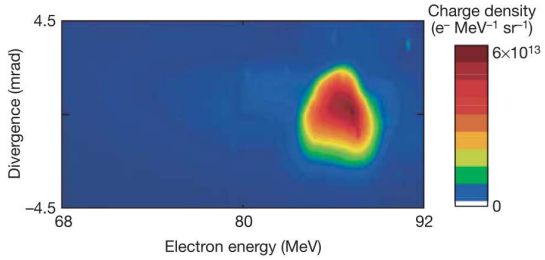

FIG. 39 Electron energy spectrum of a bunch produced by the channel guided accelerator. The spectrum was obtained by dispersing the electron beam with the 55° magnetic spectrometer and recording the beam image on a phosphor screen imaged with a high resolution CCD-camera. The energy range covered in this single shot is from 68–92 MeV and shows the appearance of mono-energetic features, here with 3×10^9 electrons in a bunch with energy spread of 4% FWHM at 78 MeV. In the vertical (non-dispersive) plane, the divergence was near 3 mrad FWHM for this bunch.

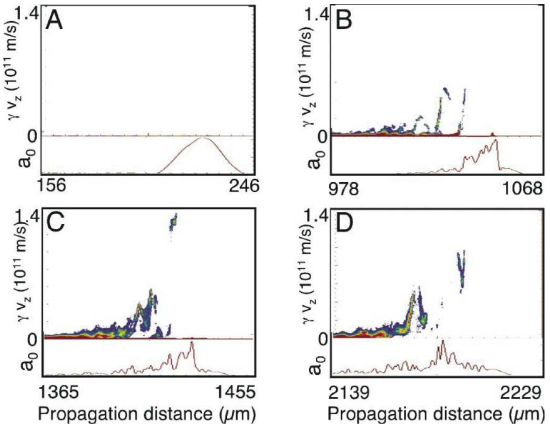

FIG. 40 Particle-in-cell simulation momentum phase space (top of each panel) and laser envelope (bottom of each panel) as a function of propagation distance. The laser enters the plasma (a), and is modulated by the plasma response, exciting a wake and trapping electrons (b). If trapping turns off after the initial bunch is loaded (see Fig. 41), the trapped electrons are concentrated in energy at the dephasing length, forming a high-energy, low-energy spread bunch (c) which dissipates with further propagation (d).

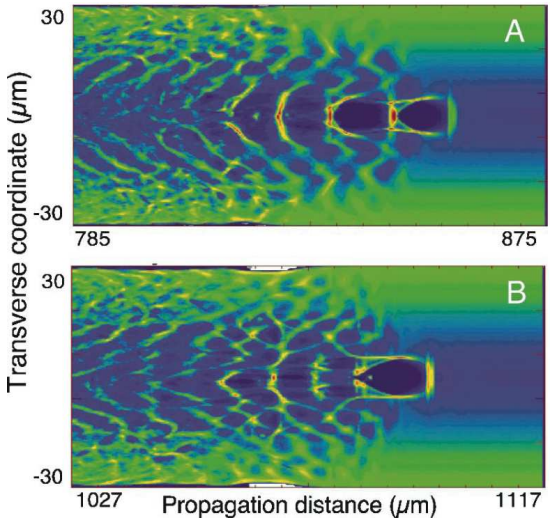

FIG. 41 Particle-in-cell simulation of electron density after laser propagation of 875 μm (a) and 1117 μm (b). Just before trapping in the first bucket behind the laser (a), the wake structure is undisturbed and large in amplitude, allowing self-trapping of electrons. When a bunch is trapped, the wake is damped, suppressing further trapping and hence isolating the initial bunch in phase space (b). The bunch is visible in (b) as a small isolated green dot in the center of the first bucket, with density comparable to the plasma density.

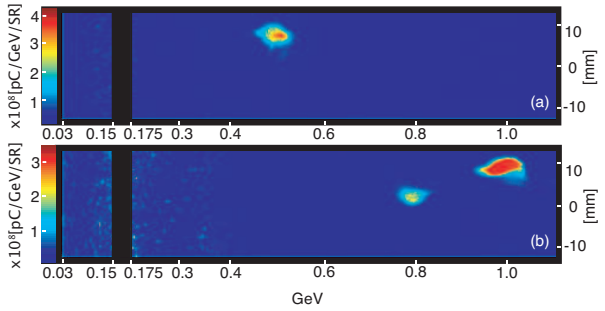

FIG. 42 Single-shot electron bunch spectra of the capillary-guided accelerator. The spectrometer did not utilize an input slit, but the angular acceptance was limited by the transport beam pipe. The uncertainty in central energy associated with the finite acceptance angle is indicated. Examples are shown of bunches at (a) $0.50^{+0.02}_{-0.015}$ GeV (5.6% rms energy spread, 2.0 mrad divergence rms, ~50 pC charge) and (b) $1.0^{+0.08}_{-0.05}$ GeV (2.5% rms energy spread, 1.6 mrad divergence rms, ~30 pC). The 0.5 GeV (1.0 GeV) bunch was obtained in the 225 (310) μm capillary with a density of 4.3×10^{18} (4.9×10^{18}) cm^{-3} and input laser power of 13 TW (38 TW). The black stripe denotes the energy range not measured by the spectrometer. In (b) a second bunch at 0.8 GeV is also visible. Note that the energy spread and divergence are obtained after including the imaging properties of the spectrometer. The energy spread at 1 GeV may be less due limitations on energy resolution at 1 GeV and the slight saturation of the image.

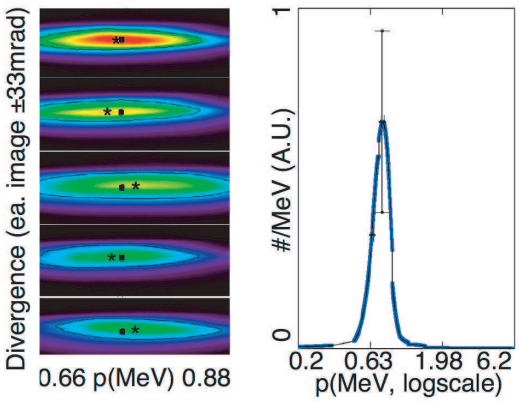

FIG. 43 Momentum distributions obtained from a magnetic spectrometer for electron bunches produced by a laser focused in the plasma density downramp, showing stable bunches at 0.76 MeV/c with ±10% momentum spread and ±3% momentum stability. Sequential single shot images are shown on the left with the centroid (*) indicated with respect to the average (square) over 48 shots. Integrated magnetic spectrum is shown on the right (vertical bar denotes the RMS charge error) with the data points (blue) connected by a black line.